New Physics at LHC

L. Bravina (UiO),

In collaboration with

A.B.Kaidalov, K. Boreskov, O.V. Kancheli,

J. Bleibel, G. Eyyubova, R.Kolevatov,

L. Malinina, M.S. Nilsson, E. Zabrodin

TORIC 2011, 07.09.2011, Candia Maris, Heraklion, Crete

PP PHYSICS AT LHC

Do pp collisions look similar to AA ?

M.Chojnacki

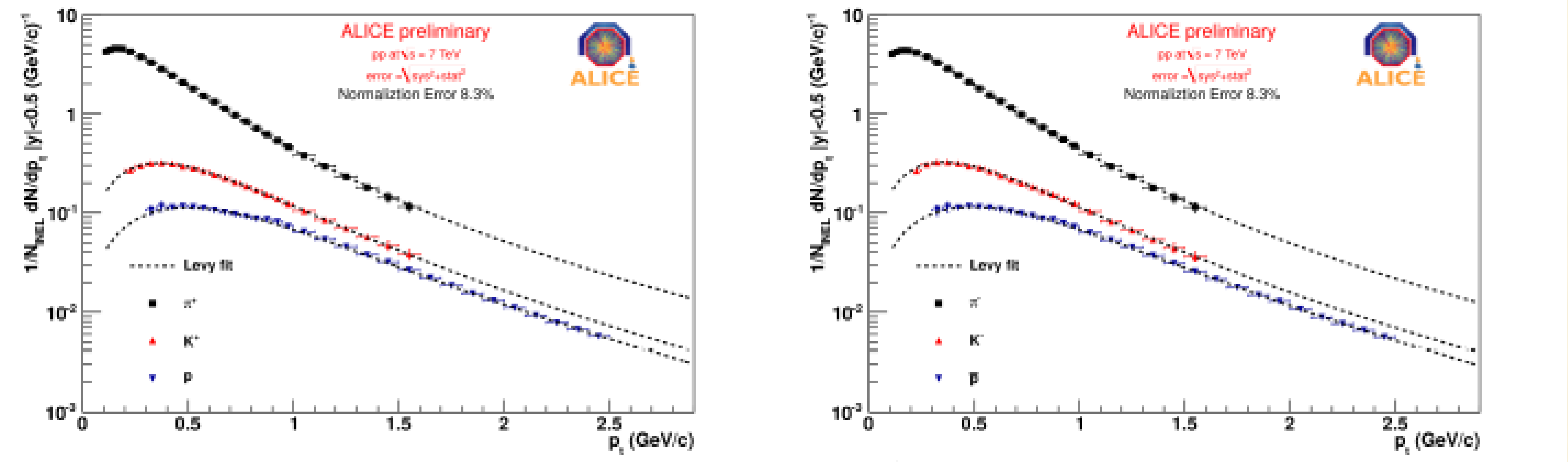

In high multiplicity events spectra show significant radial flow already at Tevatron energies. – Similar to AA.

COMPARISON TO RHIC (0-5% CENTRAL)

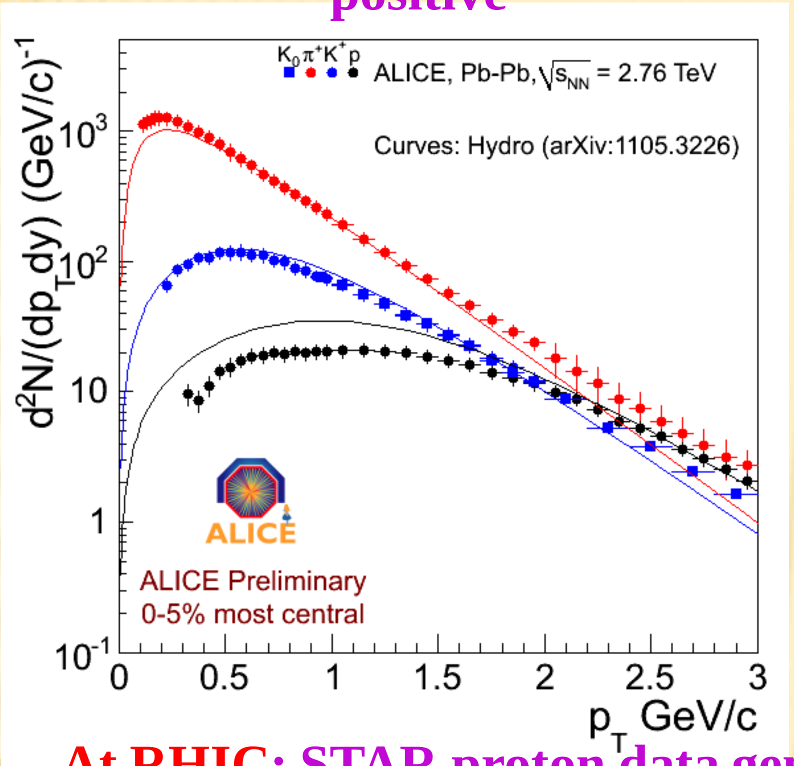

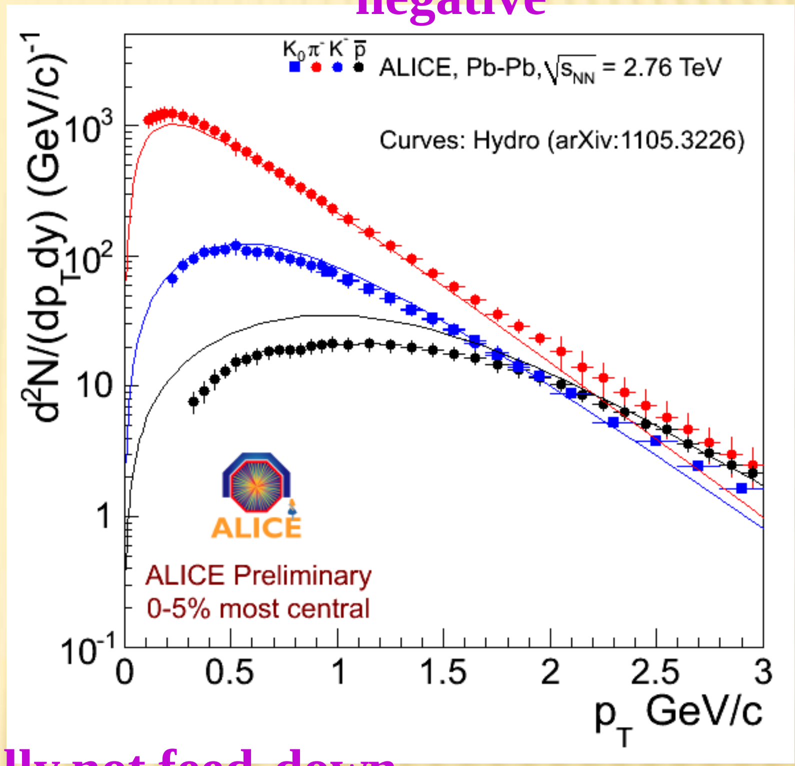

At RHIC: STAR proton data generally not feed-down corrected.

Large feed down correction

At LHC: ALICE spectra are feed-down corrected

→Consistent picture with feed-down corrected spectra

STAR, PRL 97, 152301 (2006)

STAR, PRC 79 , 034909 (2009)

PHENIX, PRC69, 03409 (2004)

- **Harder spectra, flatter p at low pt**
- **Strong push on the p due to radial flow?**

$K^0_s K^0_s$ correlations in 7 TeV *pp* collisions from the ALICE experiment at the LHC

T. J. Humanic for the ALICE Collaboration

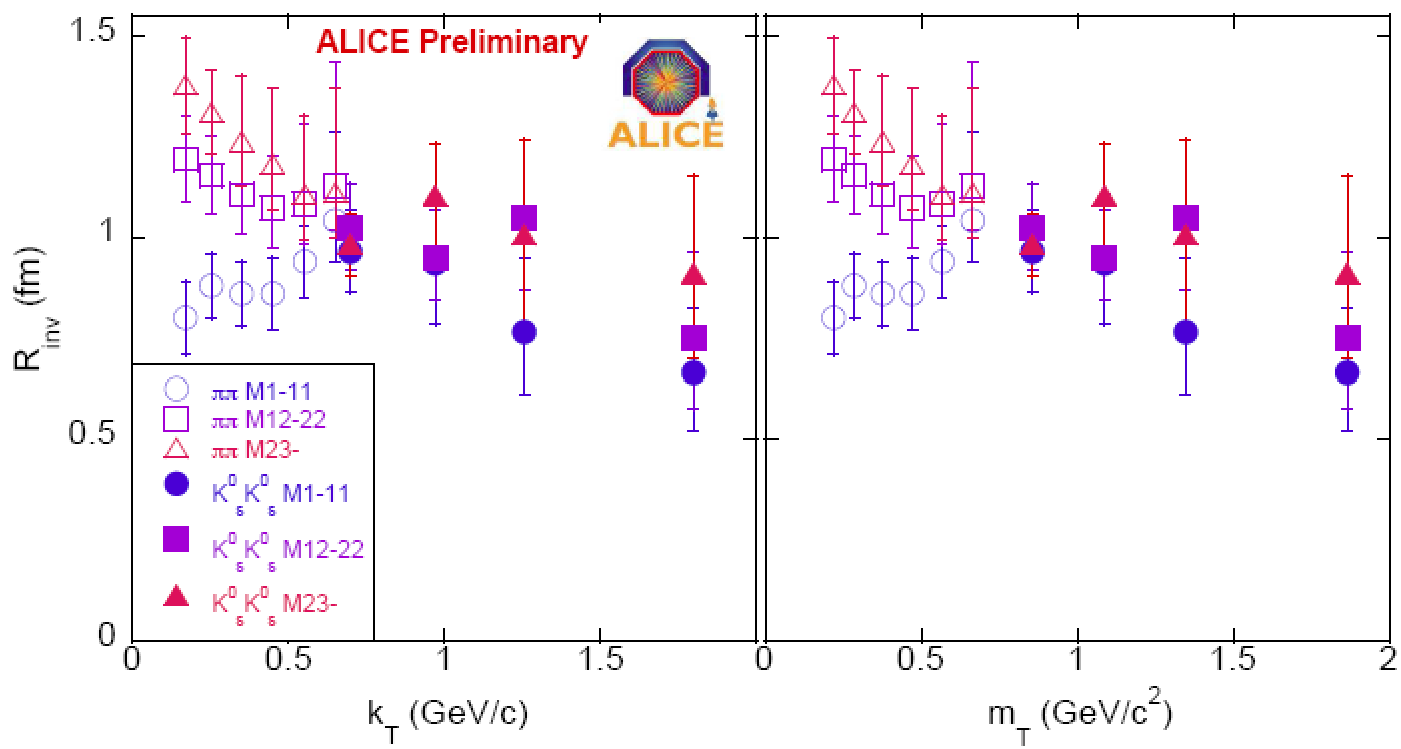

as seen in heavy-ion collisions. Also, $K^0_s K^0_s$ correlations are observed to smoothly extend this $\pi\pi$ R_{inv} behavior for the *pp* system up to about three times higher k_T than the k_T range measured in $\pi\pi$ correlations.

Observation of Long-Range, Near-Side Angular Correlations in Proton-Proton Collisions at the LHC

JHEP 1009:091,2010
Sep 2010. e-Print: **arXiv:1009.4122** [hep-ex]
CMS Collaboration,

okhtin,

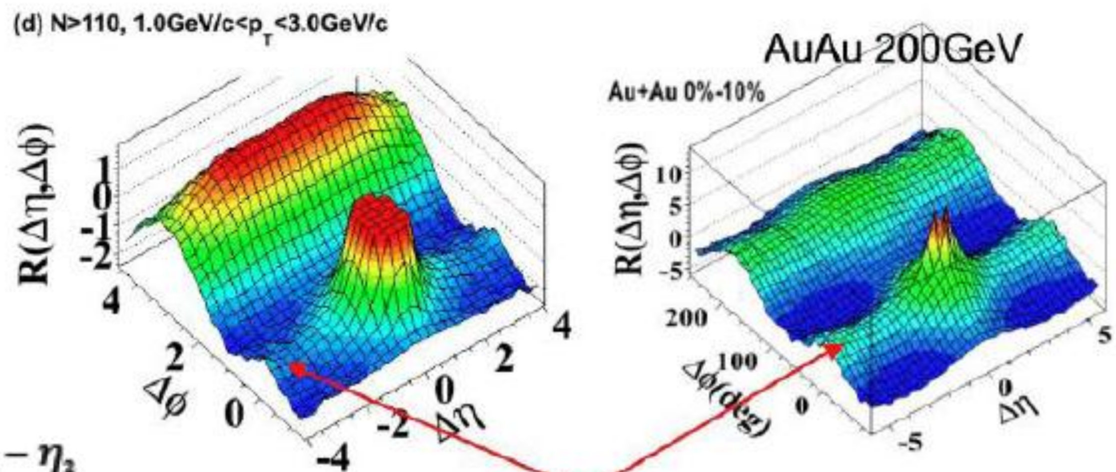

$\Delta\eta = \eta_1 - \eta_2$

$\Delta\varphi = \varphi_1 - \varphi_2$

Similar "ridge" in high multiplicity pp
(even similar p_T dependence)

Signal is observed at large difference |Δη| < 4.8, large multiplicity N > 90 and at medium particle transverse momentum 1 < pT < 3 GeV/c.

OSLO HEAVY-ION THEORY GROUP

1. Gluon shadowing

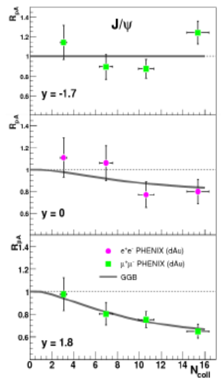

- shadowing in agreement with data at RHIC
- first signal of coherent HQ production?
- at LHC - strong IS effect!

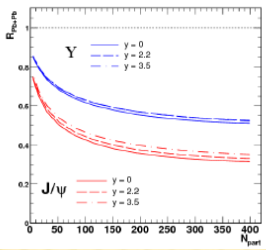

2. Elliptic flow

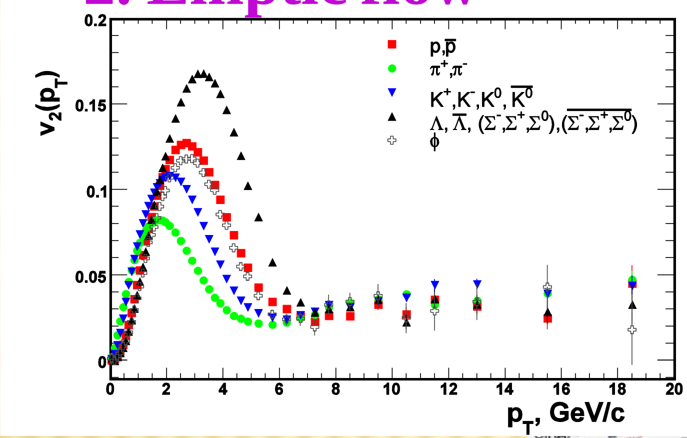

3. HYDJET++

- realistic nuclear geometry
- describes well RHIC data on high-p_T
- well suited for LHC energies
- basic MC tool for CMS HI analysis, also used by ALICE

4. Freeze-out

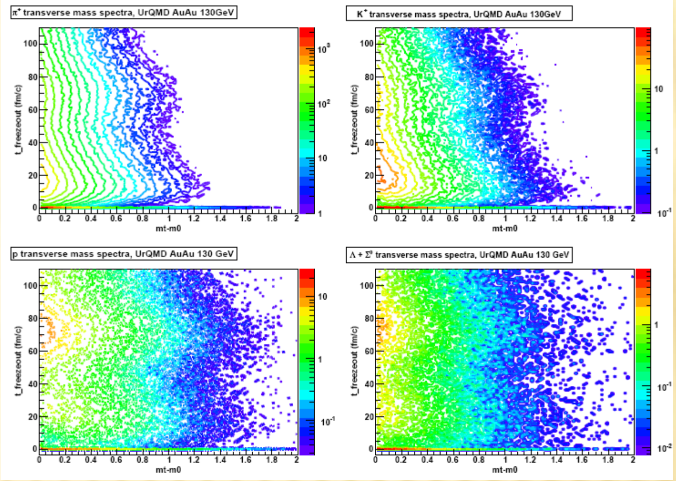

5. HBT correlations

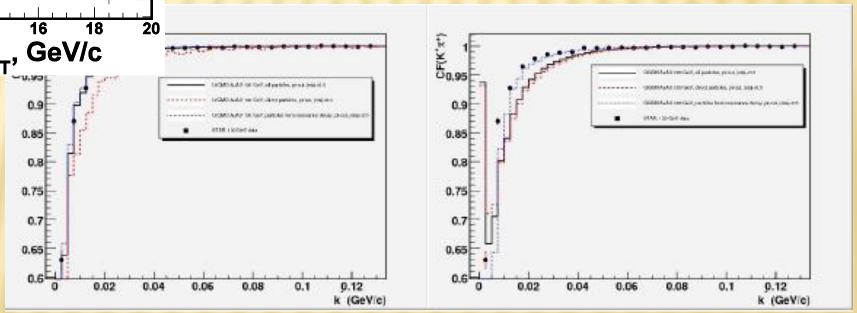

6. Equation of State

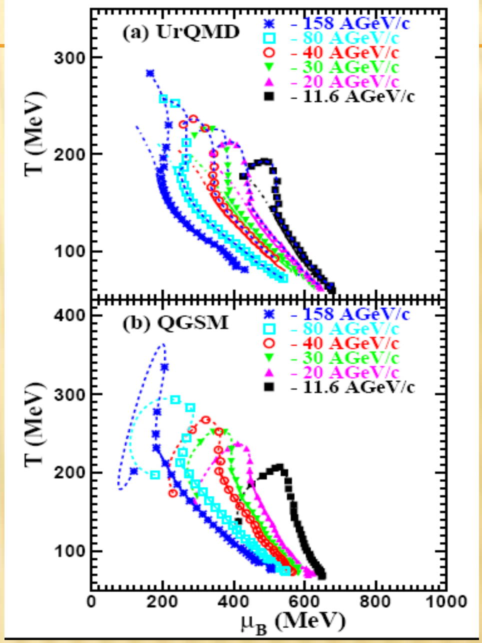

7. Predictions for pp

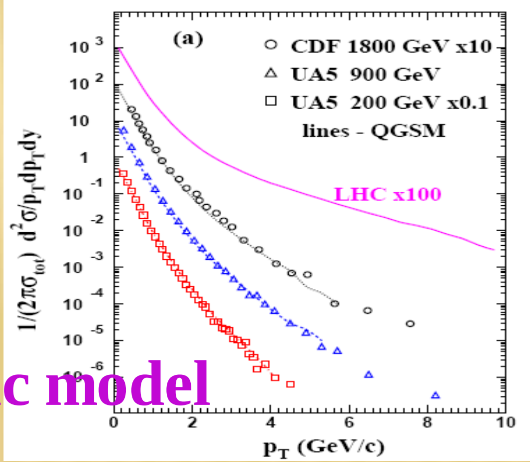

8. Flow in pp 9. Regge field theory and stochastic model

10. Di-hadron azimuthal correl. …

LHC results:

23.11.2009 – pp 900 GeV, first ALICE paper

First proton–proton collisions at the LHC as observed with the ALICE detector: measurement of the charged-particle pseudorapidity density at √s=900 GeV

Citation: Eur. Phys. J. C (2010) 65: 111-125

2010 - pp 2.36 TeV and pp 7 TeV

- **Charged-particle multiplicity measurement in proton proton collisions at √s=7 TeV with ALICE at LHC** Eur. Phys. J. C (2010) 68: 345–354
- **Charged-particle multiplicity measurement in proton–proton collisions at √s=0.9 and 2.36 TeV with ALICE at LHC** Eur. Phys. J. C (2010) 68: 89–108
- **Charged-particle multiplicity measurement in proton–proton collisions at √s=7 TeV with ALICE at LHC** Eur. Phys. J. C (2010) 68: 345–354
- **Midrapidity Antiproton-to-Proton Ratio in pp Collisons at √s=0.9 and 7 TeV Measured by the ALICE Experiment** Phys Rev Lett Vol.105, No.7, (2010)
- **Two-pion Bose-Einstein correlations in pp collisions at √s=900 GeV**

  Phys. Rev. D 82, 052001 (2010)
- **Transverse momentum spectra of charged particles in proton–proton collisions at √s=900 GeV with ALICE at the LHC** Physics Letters B 693 (2010) 53–68

8.11.2010 - Pb-Pb collisions at 2.76 ATeV

- Charged-particle multiplicity density at mid-rapidity in central Pb-Pb collisions at sqrt(sNN) = 2.76 TeV **arXiv:1011.3916v2** ***ALICE experiment***

The first measurement of the charged-particle multiplicity density at mid-rapidity in Pb–Pb collisions at a centre-of-mass energy per nucleon pair $\sqrt{s_{NN}} = 2.76$ TeV is presented. For an event sample corresponding to the most central 5% of the hadronic cross section the pseudo-rapidity density of primary charged particles at mid-rapidity is 1584 ± 4 (*stat.*) ± 76 (*sys.*), which corresponds to 8.3 ± 0.4 (*sys.*) per participating nucleon pair. This represents an increase of about a factor 1.9 relative to pp collisions at similar collision energies, and about a factor 2.2 to central Au–Au collisions at $\sqrt{s_{NN}} = 0.2$ TeV. This measurement provides the first experimental constraint for models of nucleus–nucleus collisions at LHC energies.

- **Charged-particle multiplicity density at mid-rapidity in central Pb-Pb collisions at sqrt(sNN) = 2.76 TeV** arXiv:1011.3916v2

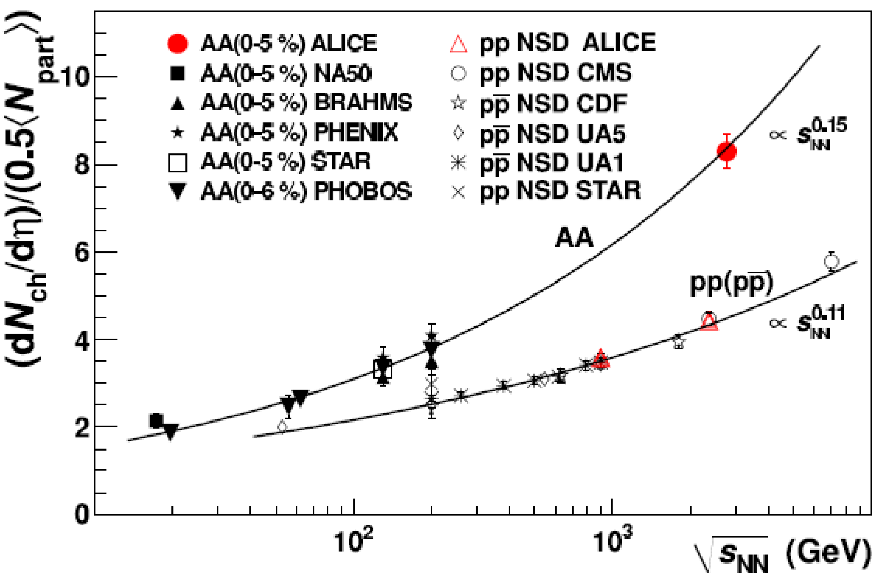

FIG. 3. Charged particle pseudo-rapidity density per participant pair for central nucleus–nucleus [16–24] and non-single diffractive pp/pp̄ collisions [25–31], as a function of $\sqrt{s_{NN}}$. The energy dependence can be described by $s_{NN}^{0.15}$ for nucleus–nucleus, and $s_{NN}^{0.11}$ for pp/pp̄collisions.

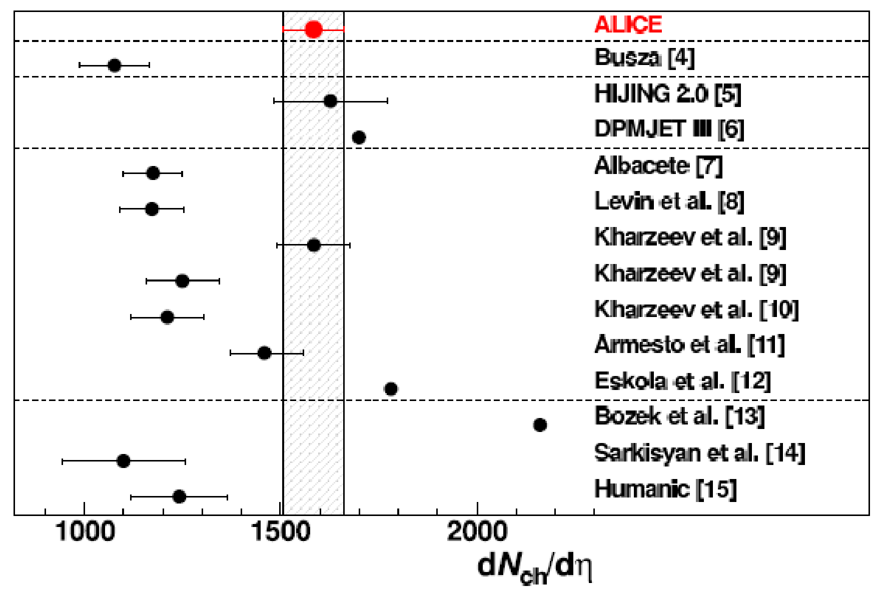

FIG. 4. Comparison of this measurement with model predictions. Dashed lines group similar theoretical approaches.

8.11.2010 - Pb-Pb collisions at 2.76 ATeV

Elliptic flow of charged particles in Pb-Pb collisions at 2.76 TeV arXiv:1011.3914v1

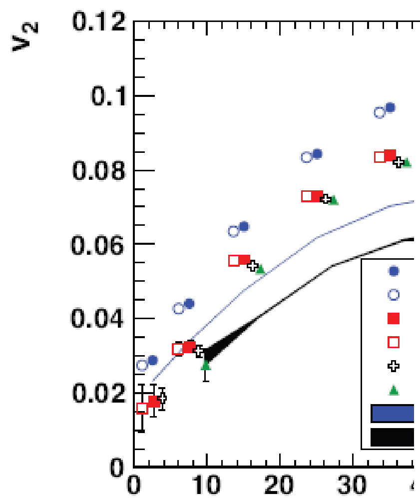

FIG. 3. (color online) Ellipti
range $0.2 < p_t < 5.0$ GeV/c,
trality, for the 2- and 4-particl
the distribution of the flow vec
method. For the cumulants the
all charged particles (full marke
(open markers). Data points ar
measurements for Au–Au at $\sqrt{s}$
plane $v_2\{EP\}$ and Lee-Yang Ze
area.

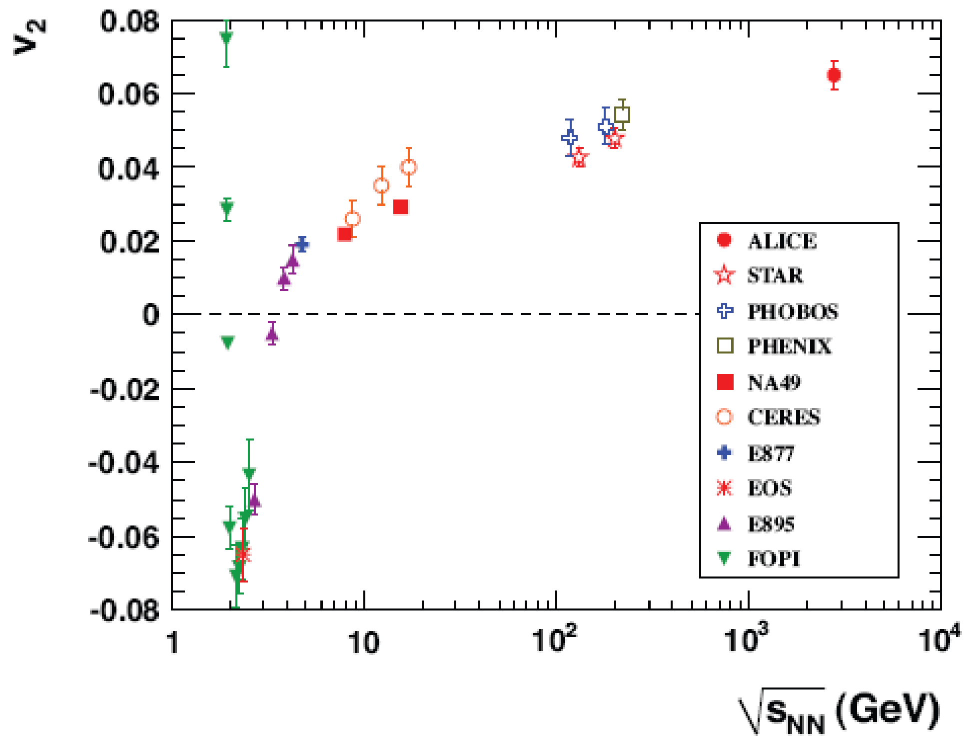

FIG. 4. (color online) Integrated elliptic flow at 2.76 TeV in Pb–Pb 20–30% centrality class compared with results from lower energies taken at similar centralities [35, 38].

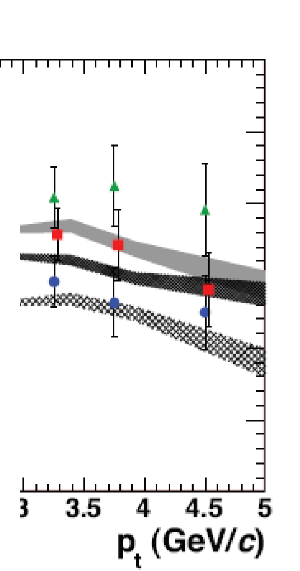

compared to STAR mea-
20–30% centrality bin are

PP@LHC

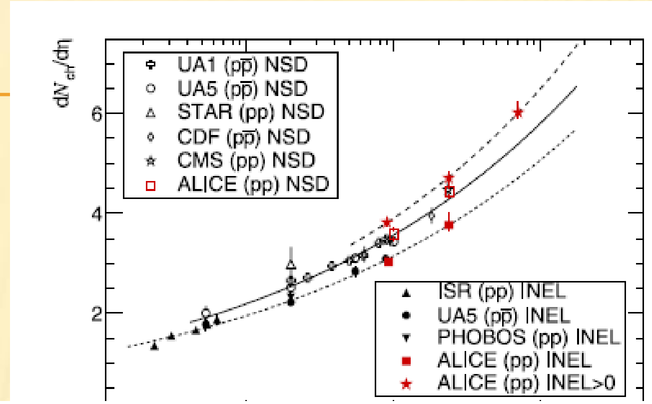

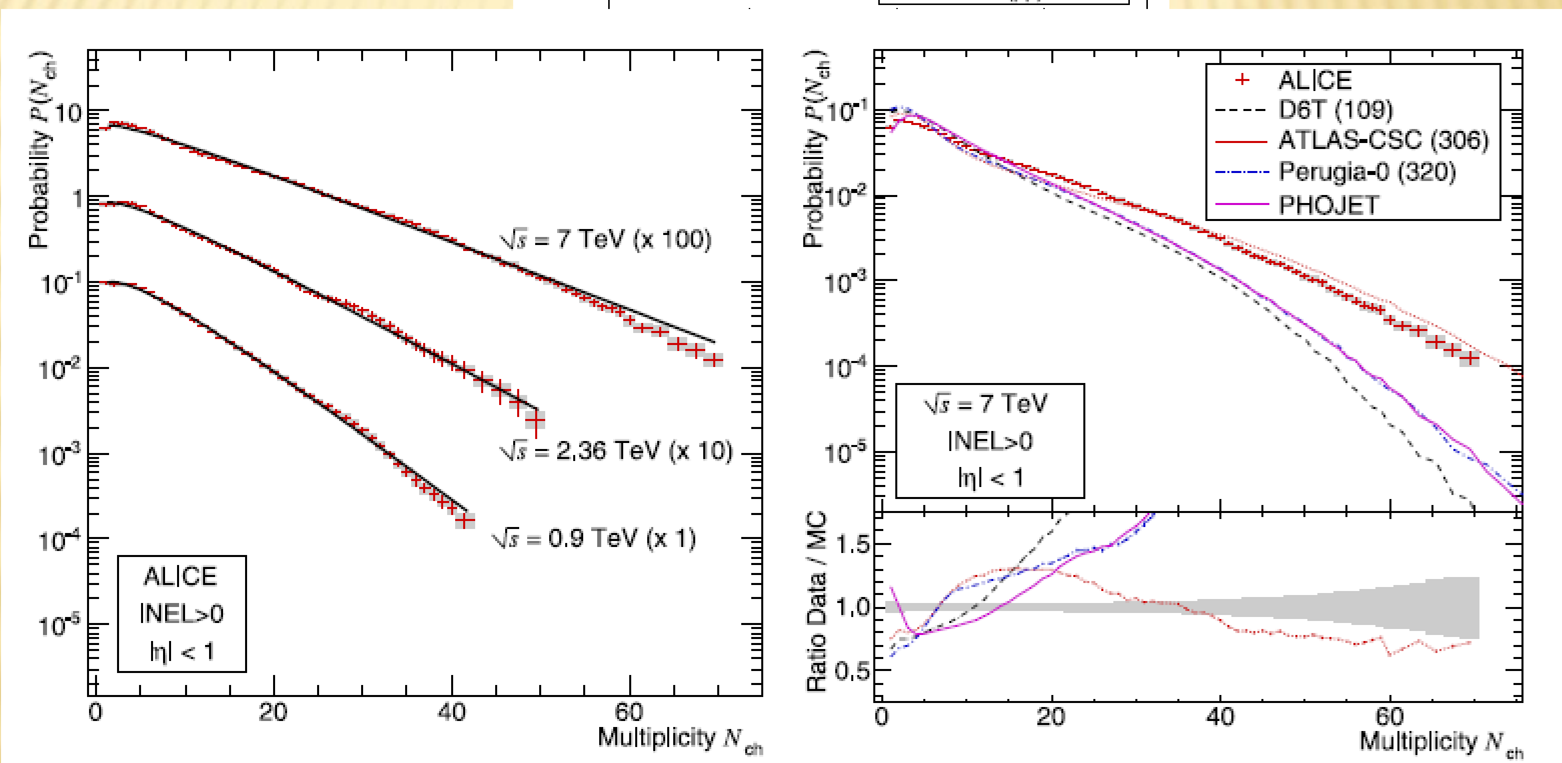

0.9–2.36	23.3 ± 0.4	17.3	17.6	17.3	15.4
0.9–7	$57.6 \pm 0.4^{+3.6}_{-1.8}$	43.0	47.6	43.3	33.4

PP AT LHC

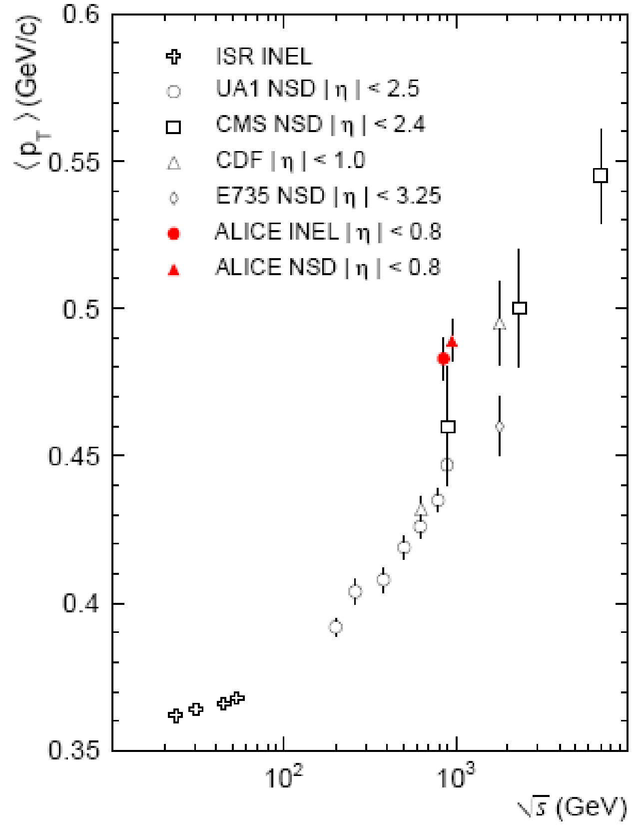

Figure 4: Energy dependence of the average transverse momentum of primary charged particles in pp and $p\bar{p}$ collisions. Data from other experiments are taken from [20, 21, 22, 23, 24, 25].

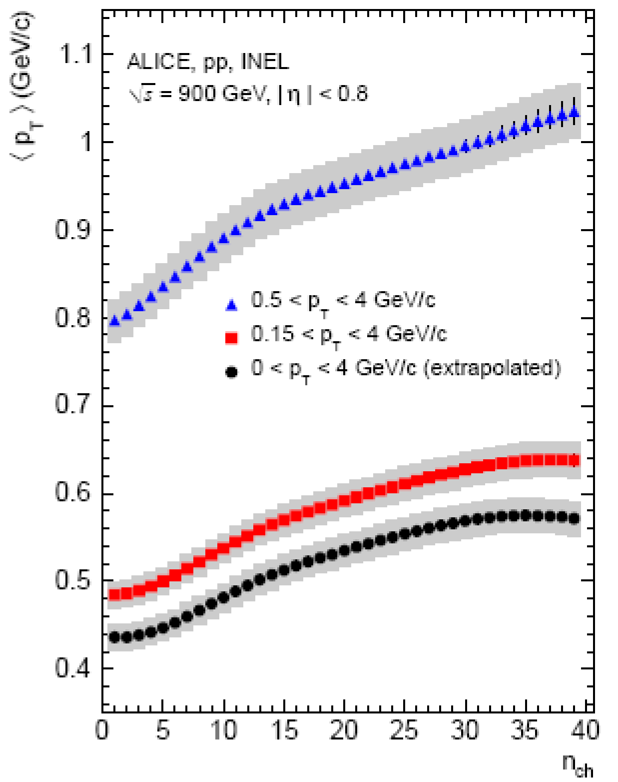

Observation of Long-Range, Near-Side Angular Correlations in Proton-Proton Collisions at the LHC

JHEP 1009:091,2010
Sep 2010. e-Print: **arXiv:1009.4122** [hep-ex]
CMS Collaboration,

.okhtin,

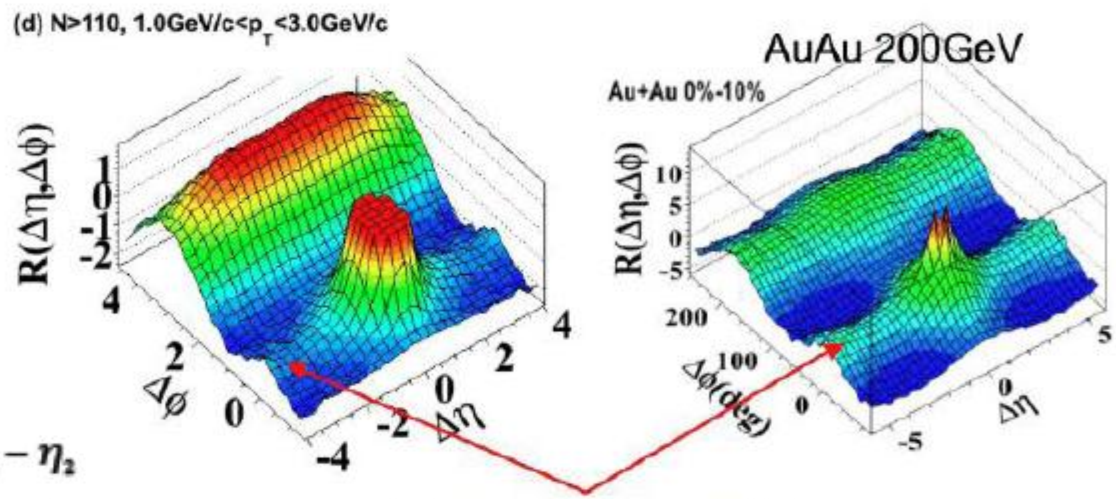

$\Delta\eta = \eta_1 - \eta_2$

$\Delta\varphi = \varphi_1 - \varphi_2$

Similar "ridge" in high multiplicity pp
(even similar p_T dependence)

Signal is observed at large difference $|\Delta\eta| < 4.8$, large multiplicity N > 90 and at medium particle transverse momentum $1 < pT < 3$ GeV/c.

FLOW & 2 PARTICLE CORRELATIONS

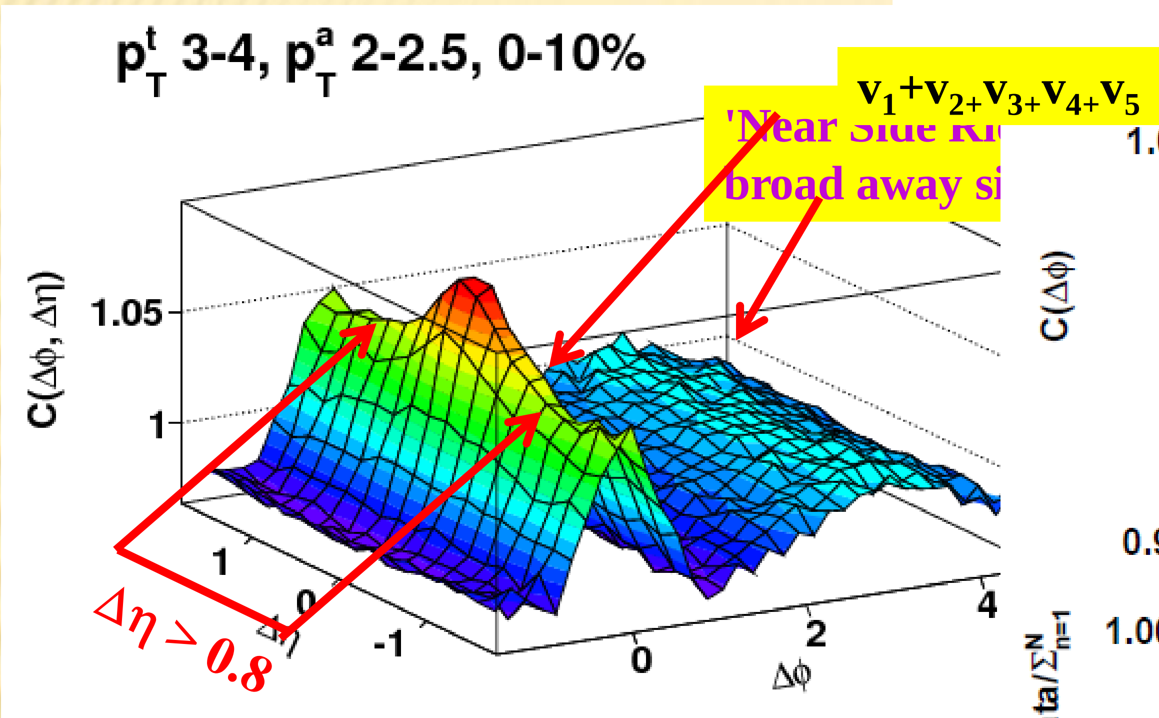

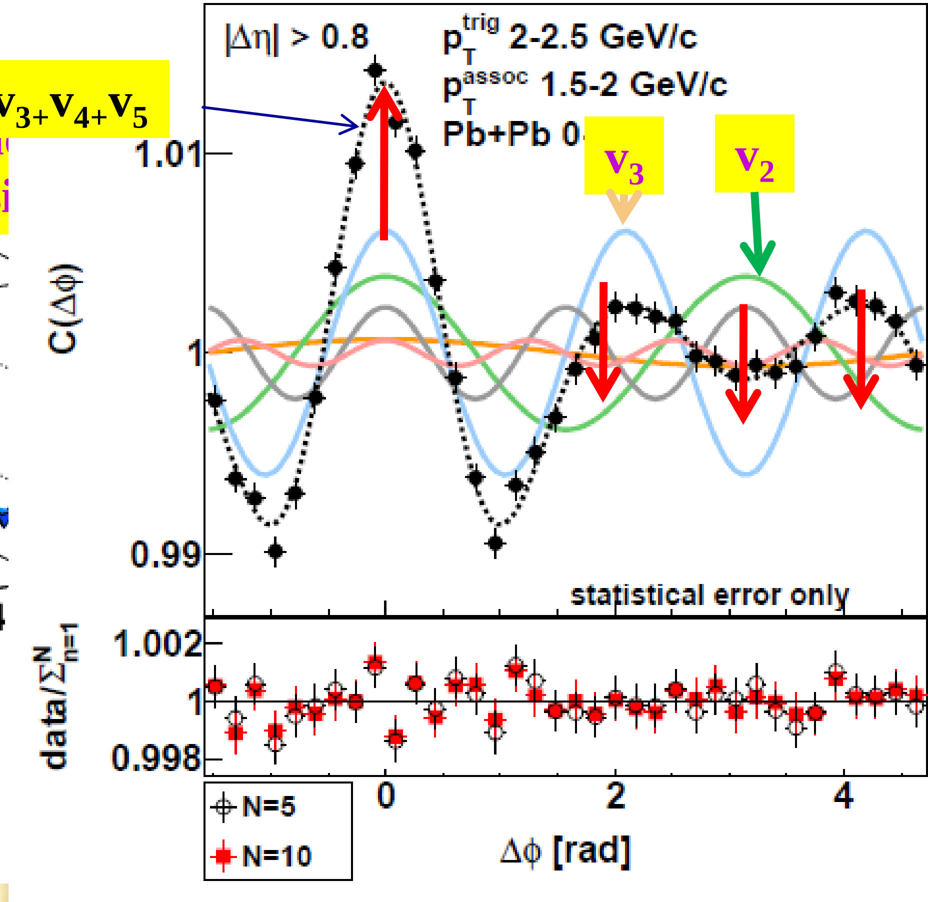

Projection on Δφ for Δη > 0.8

Clean double Hump (aka 'Mach Cone') appears for ultra-central

(without any flow subtraction !)

Full correlation structure described by Fourier Coefficients v_1,v_2, v_3, v_4,v_5 (for |η|>0.8)

v3 very visible, indeed, v3 ≈ v2 for very central

'Mach Cone' & 'Near Side Ridge' shapes evolve smooth with magnitude of v_2 and v_3

I.Alsybeev, G.Feofilov, A.Ivanov, V.Vechernin
SAINT-PETERSBURG STATE UNIVERSITY

Motivation(theory) Application of string model.

Investigations of the charged particles long-range multiplicity correlations, measured for well separated rapidity intervals, can give us information on the number of emitting centers and hence on the fusion of color strings[2,3].

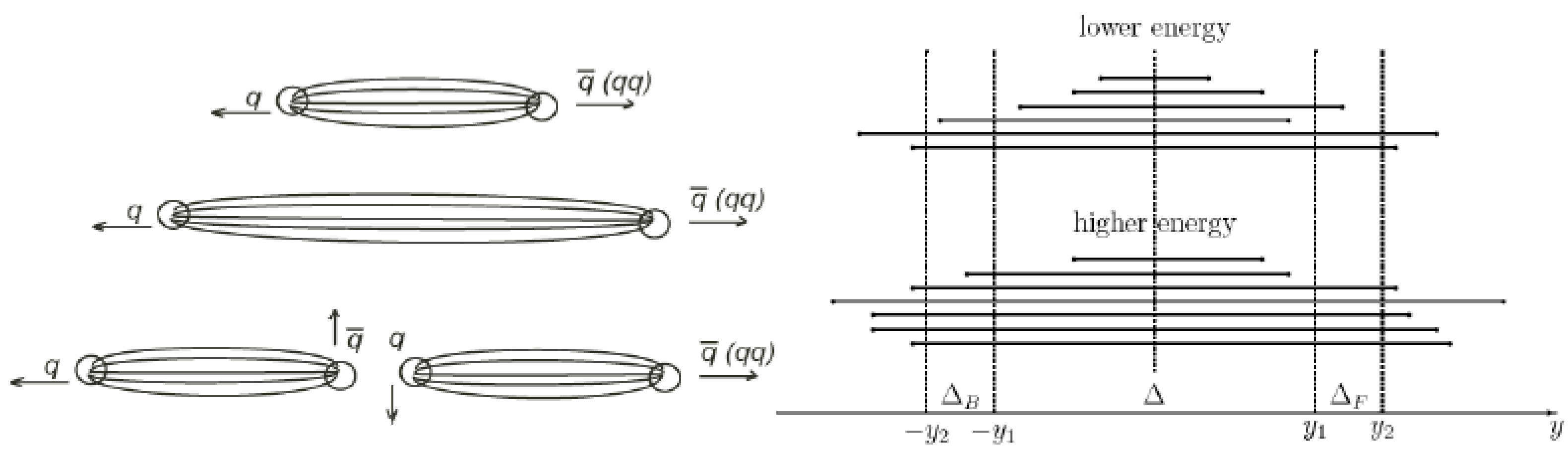

Fig.1. Quark-gluon strings and schematics for studies of Long-Range Correlations[2]

A.B.Kaidalov, Phys. Lett., **116B**(1982)459;
A.B.Kaidalov K.A.Ter-Martirosyan, Phys.Lett., **117B**(1982)247.
A.Capella, U.P.Sukhatme, C.--I.Tan and J.Tran Thanh Van, Phys. Lett. **B81** (1979) 68; Phys. Rep. 236 (1994) 225.
Abramovskii V. A., Gedalin E. V., Gurvich E. G., Kancheli O. V. , Long-range azimuthal correlations in multiple-production processes at high energies, JETP Lett., vol.47, 337-339 , 1988
M.A.Braun, C.Pajares and V.V.Vechernin, Low pT Distributions in the Central Region and the Fusion of Colour Strings, Internal Note/FMD ALICE-INT-2001-16

String fusion, centrality and low pt limit…

- Long-range part of multiplicity-multiplicity correlations in ALICE pp@7TeV is well described in the model with independent emitters (strings) but also we see nontrivial long-range Pt-Pt correlations that, in a field of string fusion model, require presence of string interaction.
- This means that in some events there are some emitters (string clusters) that have higher average Pt
- From this point of view "two main conditions to see near-side structure" means:
    1. **Centrality -** transverse string density must be sufficient to form string clusters with reasonable probability
    2. **Low Pt limit –** Low Pt limit (~0.8) rather high but it is still a soft process region. Such cut on Pt distribution can be a way to maximize contamination of particles coming form string clusters (sources having higher <Pt> than normal strings) in correlation function.

    Only combination of these two factors make near-side ridge structure visible.
- PtPt correlation is more sensible to string fusion effect than NN, so we are looking for a way to include Pt of both particles into $\Delta\eta$-$\Delta\varphi$ correlation function.

RIDGE IN HI AT RHIC

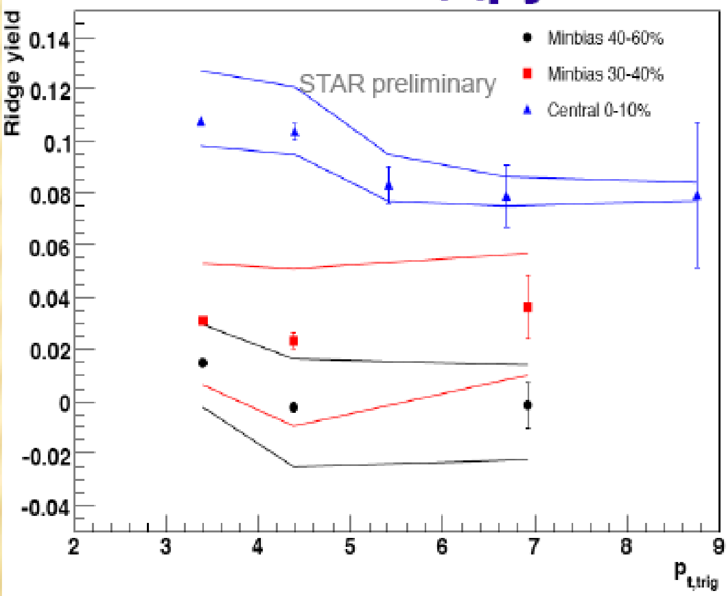

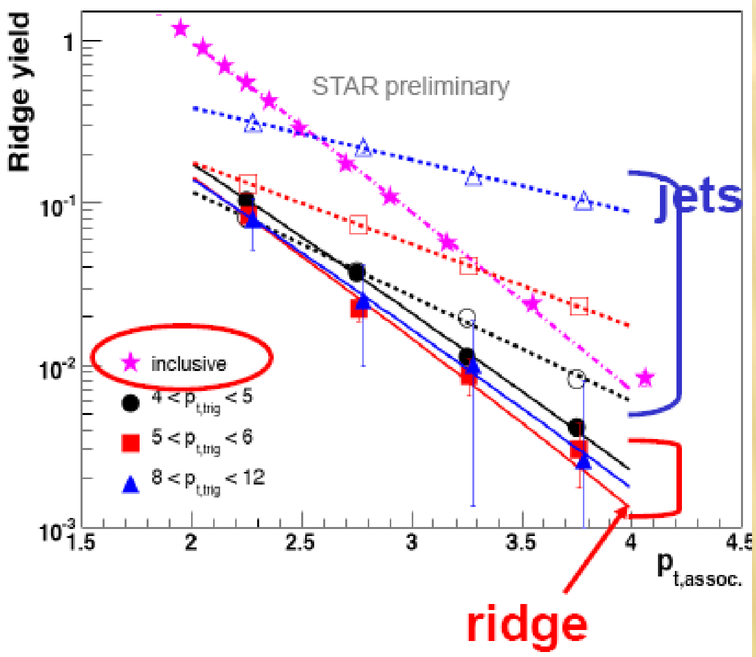

Ridge Independence to trigger momentum

Ridge momentm spectr is soft and very close to min bias

HI AT RHIC

STAR, Au-Au, 200 GeV

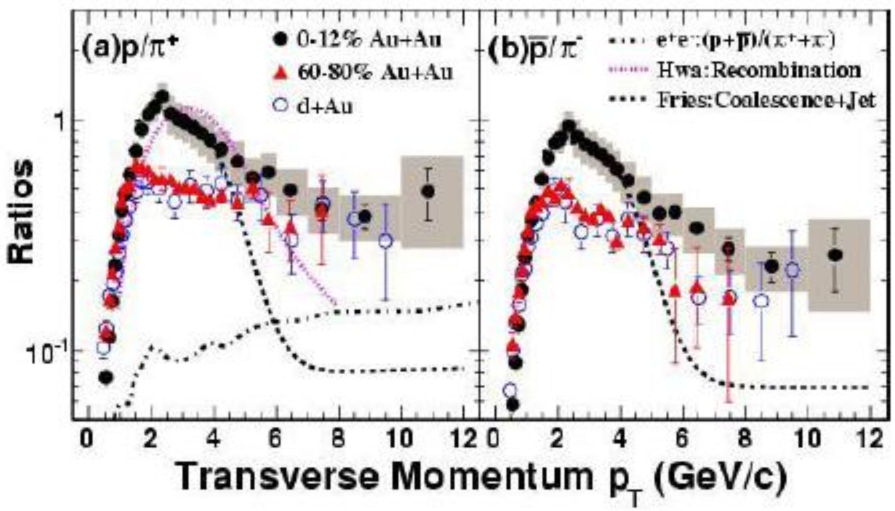

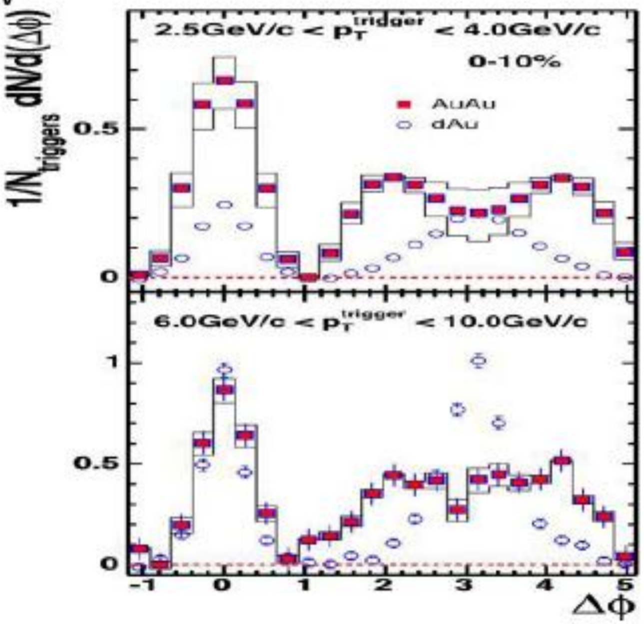

Anomal ratio barion/meson, larger then in p+p and e+e- in four times

Deformation away-side peak and two hump appearence

INTERPRETATION OF RIDGE IN PP

Physics of the ridge

Jet-Jet or Jet-proton remnant:

- Many questions about the role of jets
- Should predict ridge is always aligned with jet in ϕ

Hydrodynamic flow:

- Original motivation of the analysis
- Possible although degree of thermalization is hard to evaluate

Glasma tube from BNL group

- Glasma tube+radial flow -> ridge in HI
- Intrinsic ridge in pp even without radial flow
- Similar p_T dependence as the data

Wei Li, Oct 4, 2010, CMS QCD meeting

JET QUENCHING AT LHC?

arXiv:1011.6182v1 [hep-ex] 29 Nov 2010

Observation of a Centrality-Dependent Dijet Asymmetry in Lead-Lead Collisions at $\sqrt{s_{NN}} = 2.76$ TeV with the ATLAS Detector at the LHC

G. Aad *et al.* (The ATLAS Collaboration)*

Using the ATLAS detector, observations have been made of a centrality-dependent dijet asymmetry in the collisions of lead ions at the Large Hadron Collider. In a sample of lead-lead events with a per-nucleon center of mass energy of 2.76 TeV, selected with a minimum bias trigger, jets are reconstructed in fine-grained, longitudinally-segmented electromagnetic and hadronic calorimeters. The underlying event is measured and subtracted event-by-event, giving estimates of jet transverse energy above the ambient background. The transverse energies of dijets in opposite hemispheres is observed to become systematically more unbalanced with increasing event centrality leading to a large number of events which contain highly asymmetric dijets. This is the first observation of an enhancement of events with such large dijet asymmetries, not observed in proton-proton collisions, which may point to an interpretation in terms of strong jet energy loss in a hot, dense medium.

2

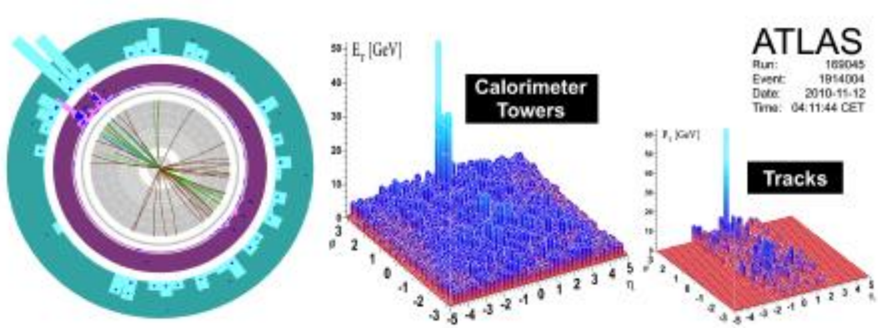

FIG. 1: Event display of a highly asymmetric dijet event, with one jet with $E_T > 100$ GeV and no evident recoiling jet, and with high energy calorimeter cell deposits distributed over a wide azimuthal region. By selecting tracks with $p_T > 2.6$ GeV and applying cell thresholds in the calorimeters ($E_T > 700$ MeV in the electromagnetic calorimeter, and $E > 1$ GeV in the hadronic calorimeter) the recoil can be seen dispersed widely over azimuth.

After event selection, the requirement of a leading jet with $E_T > 100$ GeV and $|\eta| < 2.8$ yields a sample of 1693 events. These are called the "jet selected events". The lead-lead data are also compared with a sample of 17 nb^{-1} of proton-proton collision data [13], which yields 6732 events.

$$A_J = \frac{E_{T1} - E_{T2}}{E_{T1} + E_{T2}}, \Delta\phi > \frac{\pi}{2}$$

where the first jet is required to have a transverse energy $E_{T1} > 100$ GeV, and the second jet is the highest transverse energy jet in the opposite hemisphere with $E_{T2} > 25$ GeV. The average contribution of the under-

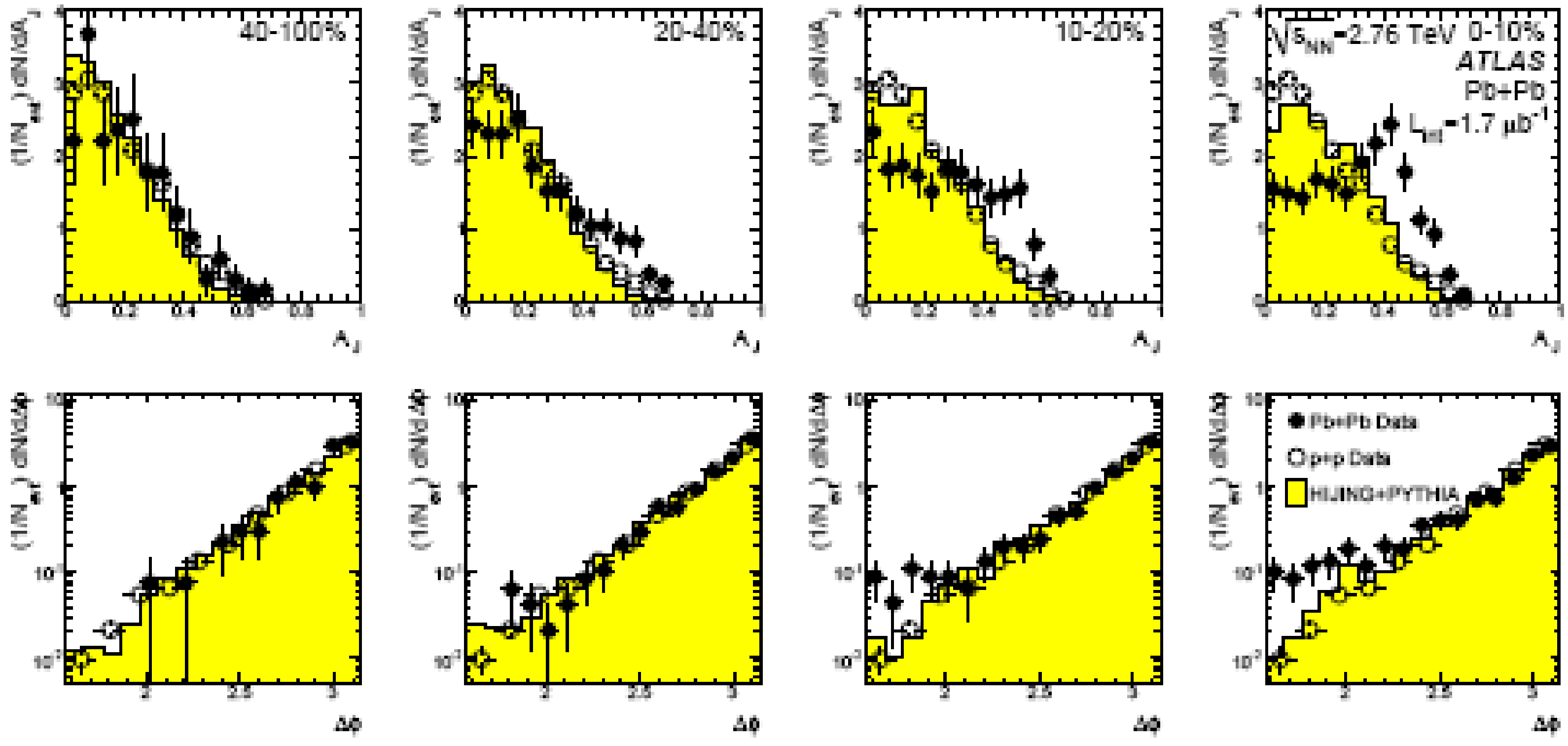

FIG. 3: (top) Dijet asymmetry distributions for data (points) and unquenched HIJING with superimposed PYTHIA dijets (solid yellow histograms), as a function of collision centrality (left to right from peripheral to central events). Proton-proton data from $\sqrt{s} = 7$ TeV, analyzed with the same jet selection, is shown as open circles. (bottom) Distribution of $\Delta\phi$, the azimuthal angle between the two jets, for data and HIJING+PYTHIA, also as a function of centrality.

Jet quenching observed by CMS in heavy-ion collisions – 271110

http://press.web.cern.ch/press/pressreleases/releases2010/pr23.10e.html

Pt=70 GeV

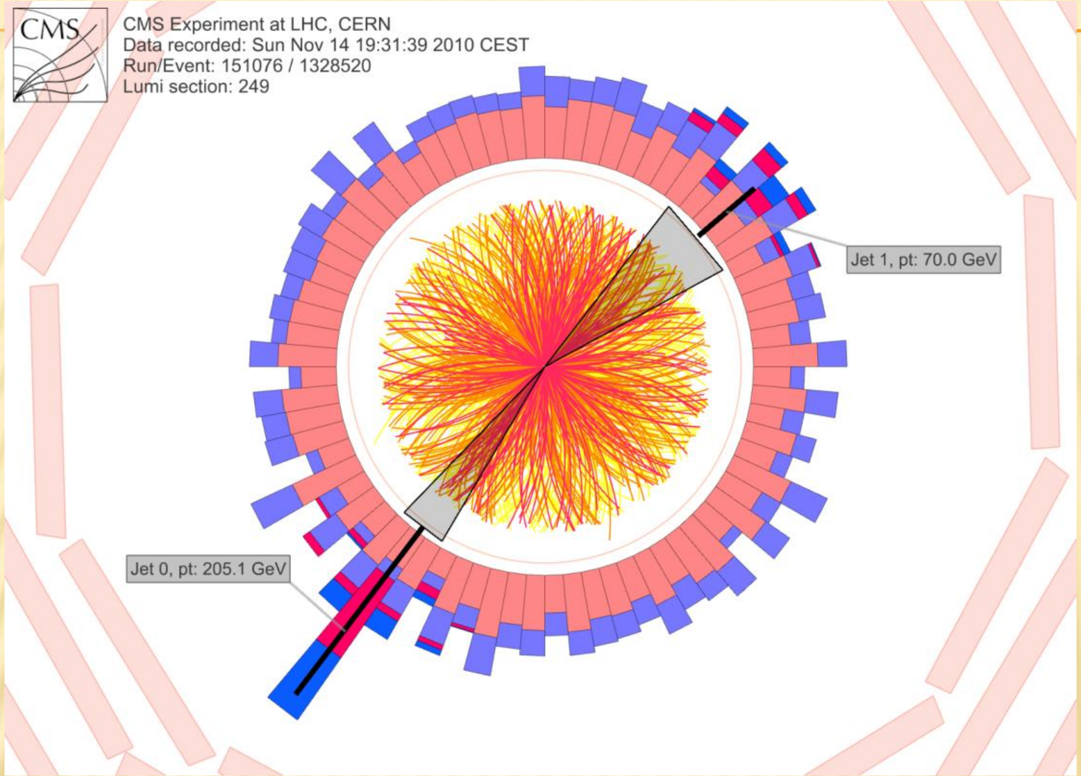

Pt=205 GeV

Figure 1 LHC lead-lead collision in the CMS detector showing particles (yellow and red tracks) radiating from the collision point. The particles deposit their energy in the calorimeters (salmon, mauve, red and blue towers, with a height proportional to energy). Two back-to-back jets are seen with a large energy asymmetry, as expected from the jet-quenching mechanism.

HI COLLISION - NUCLEAR MODIFICATION FACTOR R_{AA}

A+A

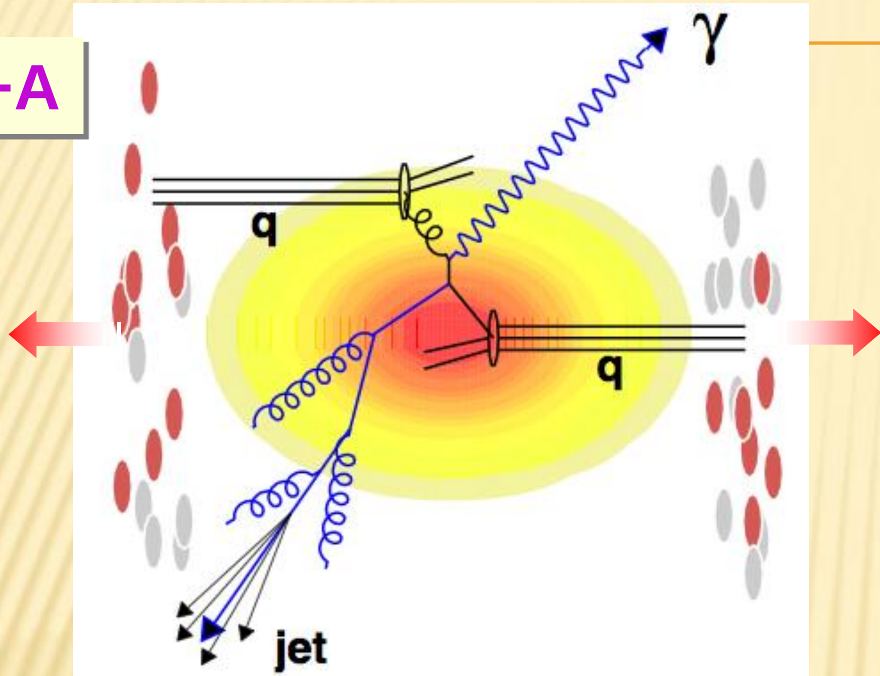

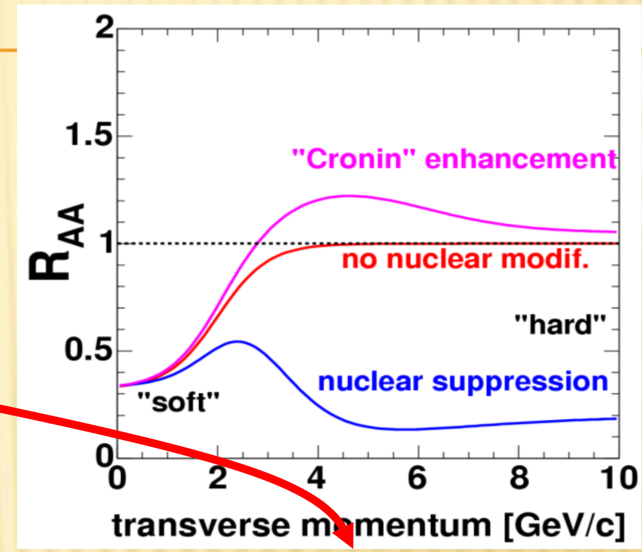

$$R_{AA}(p_T) = \frac{d^2N^{AA}/dp_T d\eta}{\langle N_{binary}\rangle d^2N^{pp}/dp_T d\eta}$$

p+p

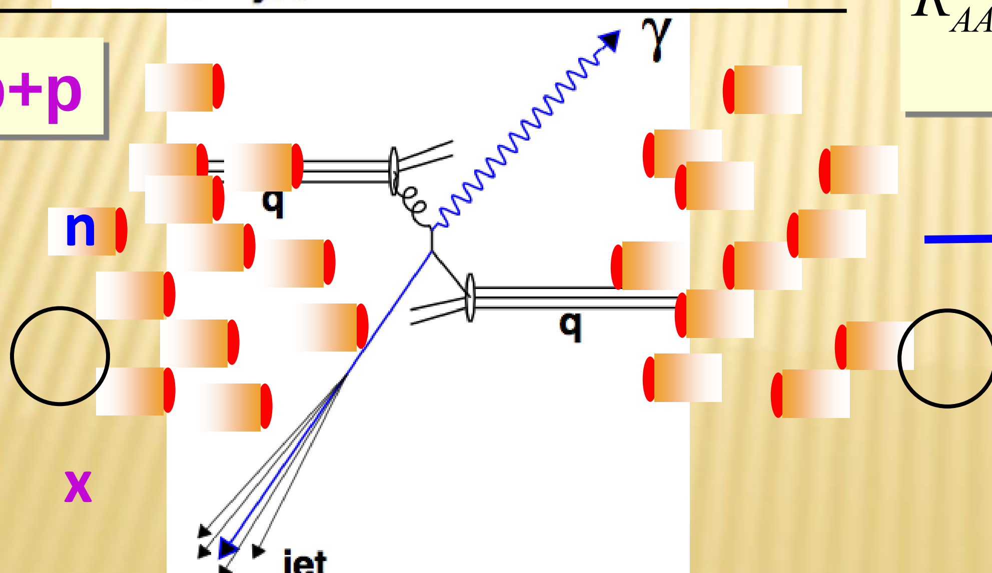

varies with impact parameter *b*

OSLO HEAVY-ION THEORY GROUP

1. Gluon shadowing

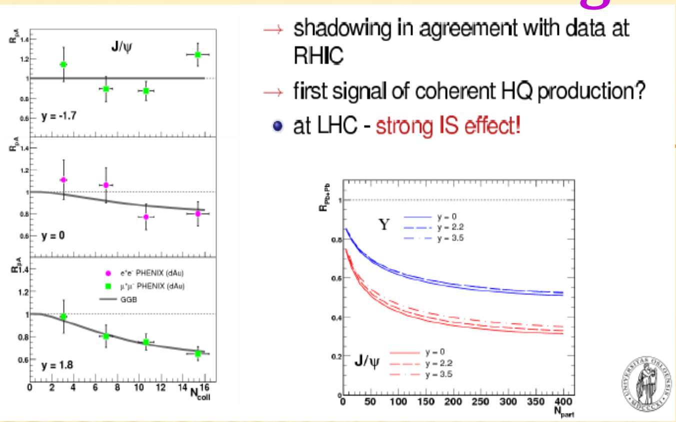

2. Elliptic flow

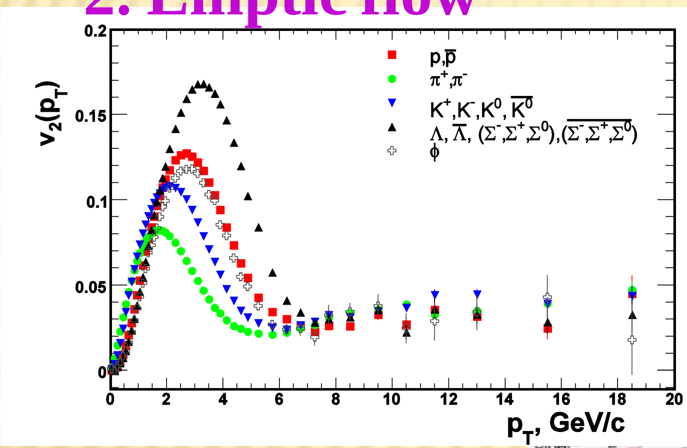

3. HYDJET++

- realistic nuclear geometry
- describes well RHIC data on high-p_T
- well suited for LHC energies
- basic MC tool for CMS HI analysis, also used by ALICE

4. Freeze-out

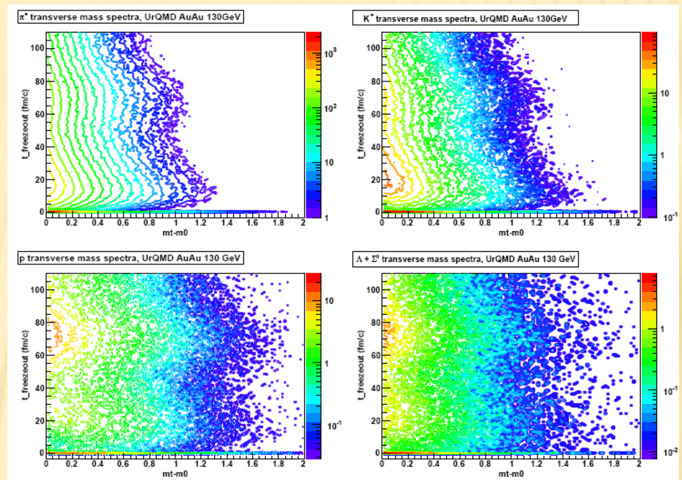

5. HBT correlations

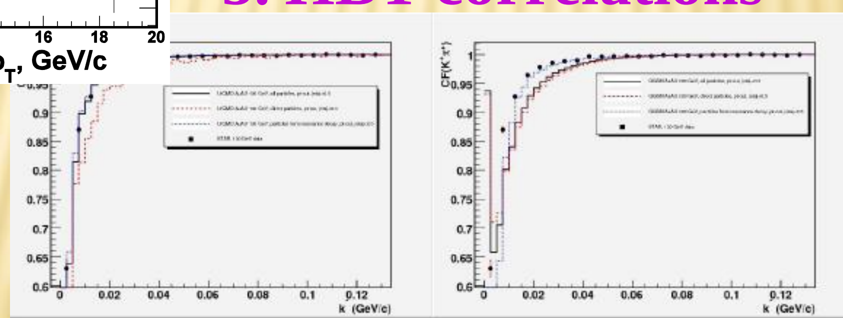

6. Equation of State

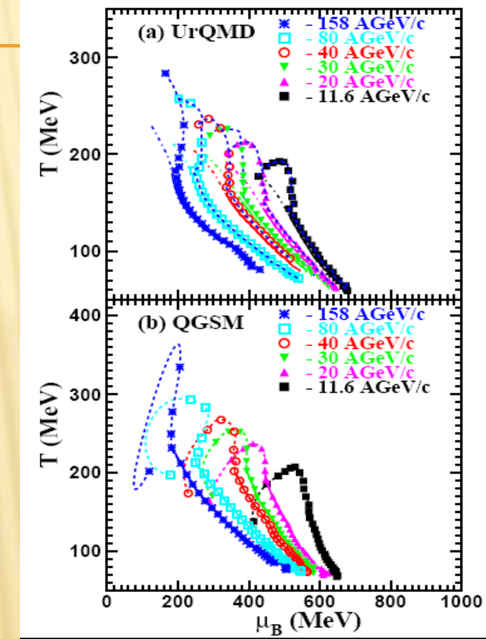

7. Predictions for pp

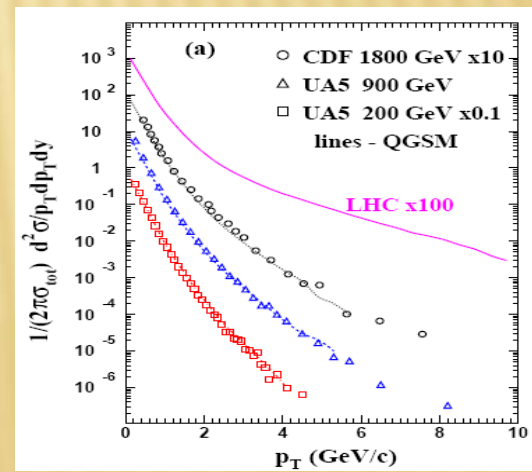

8. Flow in pp

9. Di-hadron azimuthal correl. …

Quark Gluon String Model
A.B. Kaidalov, K.A. Ter-Martirosyan,
A. Capella, Tran Than Van …

Regge poles in QCD.

Large distance phenomenon. Nonperturbative methods should be used.

- 1/N – expansion in QCD. H.t`Hooft, G.Veneziano

Expansion of amplitudes in terms of the small parameter 1/N, where $N=N_c \approx N_f$.

Diagrams are classified according to their topology.

The first term – planar diagrams.

Planar diagrams.

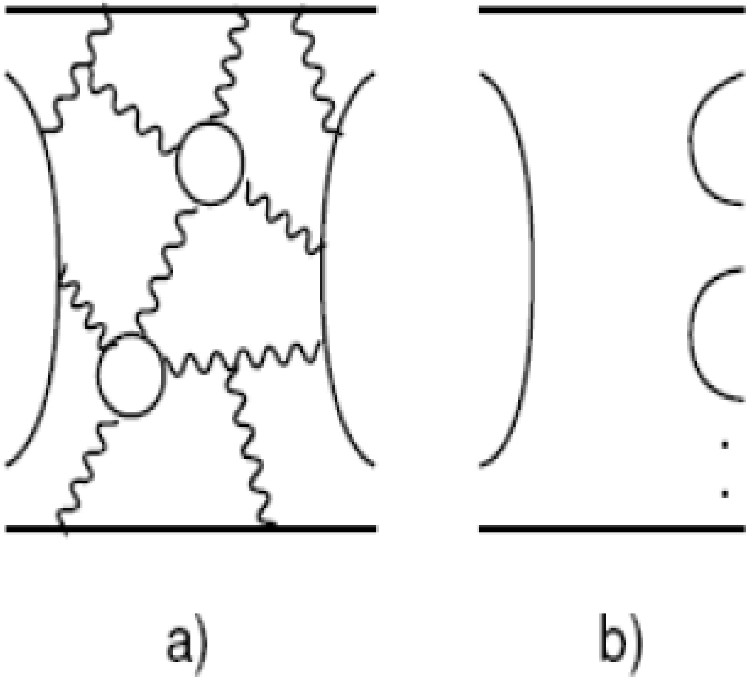

Exchange by valence quarks in the t-channel.

At large energies they correspond to ρ,ω,f,.. exchanges.

Contributions to total cross sections decrease as $s^{(\alpha_R(0)-1)} \approx 1/\sqrt{s}$

Pomeron in 1/N-expansion.

In 1/N-expansion the Pomeron corresponds to the cylinder-type diagrams.

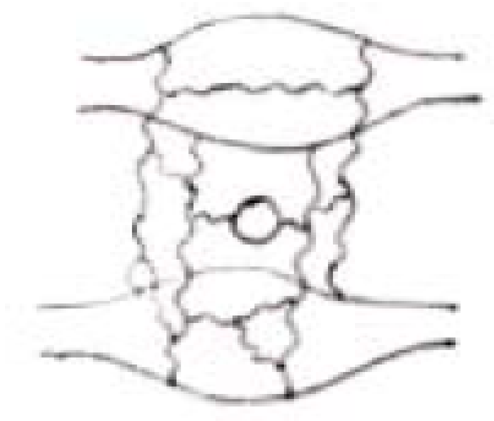

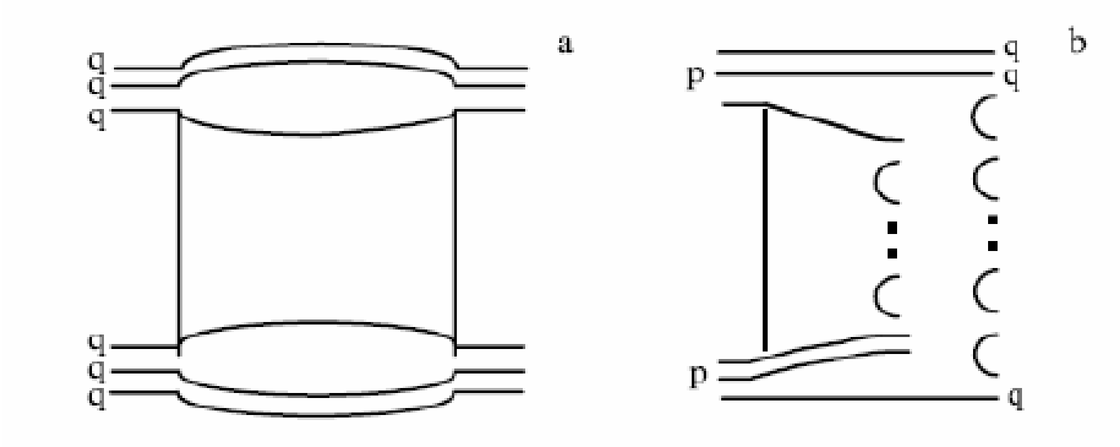

$T_{pl} \sim 1/N$

$T_{cyl} \sim 1/N^2$

$$T_{n_b,n_h} \sim \left(\frac{1}{N}\right)^{n_b+2n_h}$$

n_b - number of boundaries,

n_h – number of holes

Multiparticle production and topological expansion.

Cuttings of many pomerons in 1/N- expansion correspond to multi-chain configurations

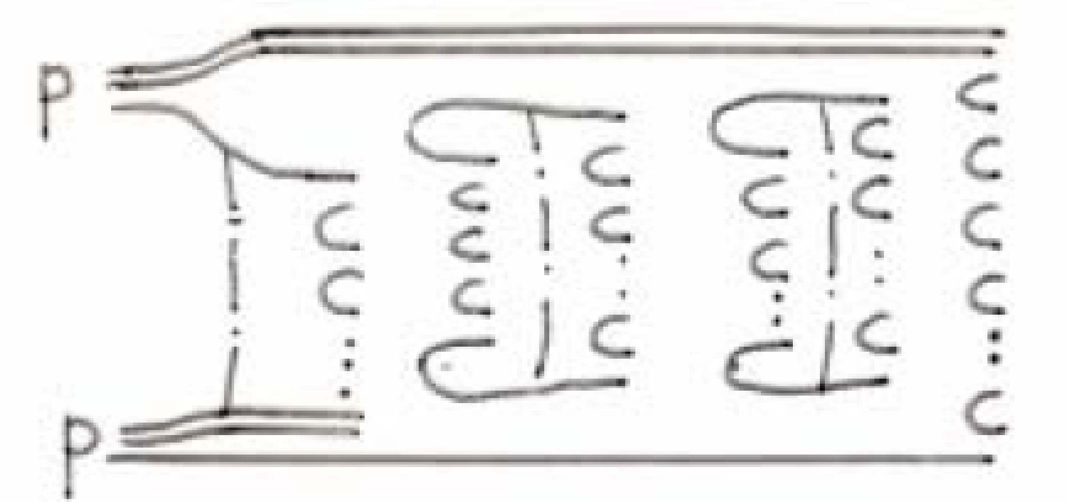

Extra chains due to sea-quarks or gluons in colliding hadrons

Quark-Gluon Strings Model.

Models of multi-particle production, based on reggeon calculus, 1/N-expansion and string dynamics:

Dual Parton Model (DPM) – Orsay,

Quark-Gluon Strings Model (QGSM) – ITEP

AGK-cutting rules determine the weights of 2k-chains configurations.

Rapidity and multiplicity distributions of final hadrons in chains can be determined theoretically.

Inclusive spectra

$$\frac{d\sigma^h}{dy} = \sum_{k=0}^{\infty} \sigma_k(\xi)\,\varphi_k^h(\xi, y) \quad ; \qquad \xi \equiv \ln\frac{s}{s_0}$$

σ_k cross section for 2k chains production

Multiplicity distribution (k=0 - diffraction)

$$\sigma_n(\xi) = \sum_{k=0}^{\infty} \sigma_k(\xi)\, W_n^k(\bar{n}_k(\xi))$$

Consider as an example $pp \to hX$

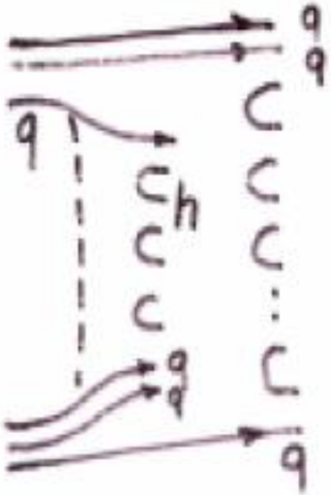

In the fragmentation region

$$\frac{x}{\sigma_2}\frac{d\sigma_2^h}{dx} = \int_x^1 dx_1\, f_p^{q(2)}(x_1)\, D_q^h\!\left(\frac{x}{x_1}\right)\frac{x}{x_1} +$$

+ contrib. from second chain

$x = 2p_{\parallel}/\sqrt{s} \equiv x_F$

$f_p^{q(2)}(x_1)$ determines how energy is devided between q and qq-chains

$$f_p^{qq(2)}(x_1) = f_p^{q(2)}(1-x_1)$$

Inclusive spectra of different hadrons are determined by the fragmentation functions $D_i^h(z)$. From planar diagrams:

$$z D_u^{\pi^+}(z) = \begin{cases} a^{\pi} , & z \to 0 \\ C^{\pi^+}(1-z)^{-\alpha_R + \lambda} , & z \to 1 \end{cases}$$

$$z D_u^{\pi^-}(z) = \begin{cases} a^{\pi} , & z \to 0 \\ C^{\pi^-}(1-z)^{-\alpha_R + \lambda + 1} , & z \to 1 \end{cases}$$

$2(1-\alpha_R(0))$

$\lambda = 2\alpha_R' \cdot \overline{p_{\perp\pi}^2} \approx 0.5$, $\alpha_R \equiv \alpha_R(0) = 0.5$

$(\tilde{D}_i^h(z) \equiv D_i^h(z)/a^h)$

Interpolation formulas for $D_i^h(z)$

e.g.

$$z D_u^{\pi^+}(z) = a^{\pi}(1-z)^{-\alpha_R+\lambda}$$

$$z D_u^{\pi^-}(z) = a^{\pi}(1-z)^{-\alpha_R+\lambda+1}$$

$$z D_u^{K^+}(z) = a^{K}(1-z)^{-\alpha_\varphi(0)+\lambda_K}\cdot(1+b_K z) \; ; \quad \alpha_\varphi(0) \simeq 0$$

$$z D_u^{\bar{D}^0}(z) = a^{D}(1-z)^{-\alpha_\psi(0)+\lambda_D}\cdot(1+b_D z)$$

Constants a^{π}, a^{K}, b_K can be determined theoretically.

$$a^{\pi} = 0.44$$

$$a^{K}/a^{\pi} \simeq 0.12$$

Constraints due to energy-momentum, S, B, Q,.. conservation allow one to fix parameters in many cases.

No free parameters!

The model has correct double ($x \rightarrow 0$) and triple ($x \rightarrow 1$) Regge limits.

Multiplicity distribution for a single cut Pomeron is of Poisson-type. Summary distribution is much broader.

QGSM PREDICTIONS FOR PP AT LHC

A.B. Kaidalov, K.A.Ter-Martirosyan, PLB 117 (1982)
N.S.Amelin, L.B., Sov.J.Nucl.Phys. 51 (1990) 133
N.S.Amelin, E.F.Staubo, L.P.Csernai, PRD 46 (1992) 4873

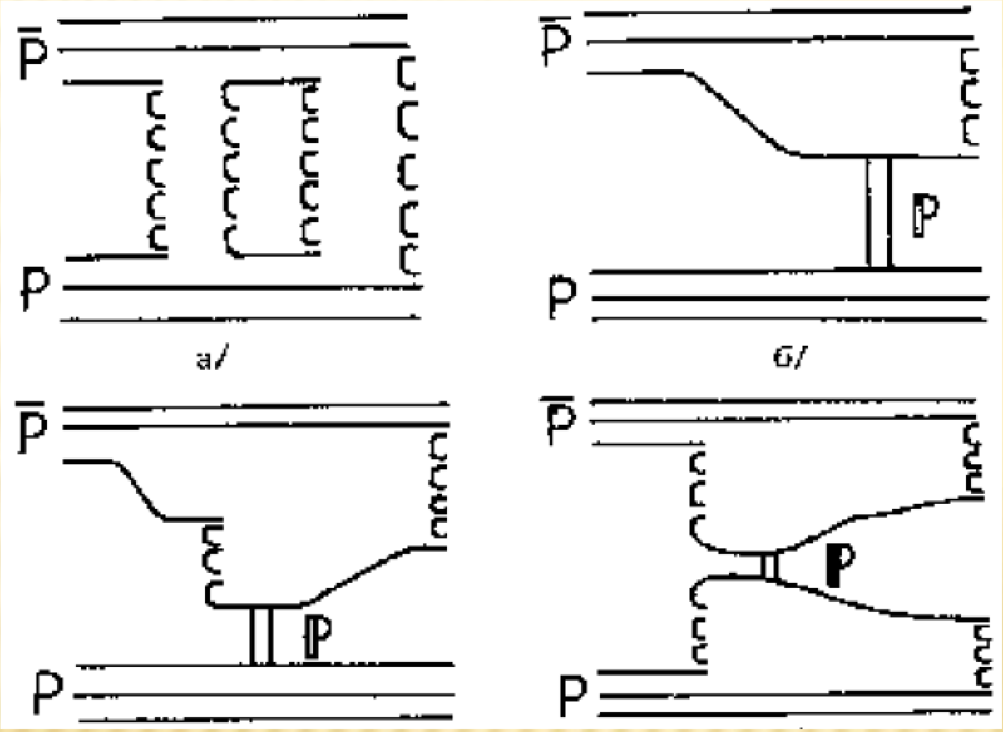

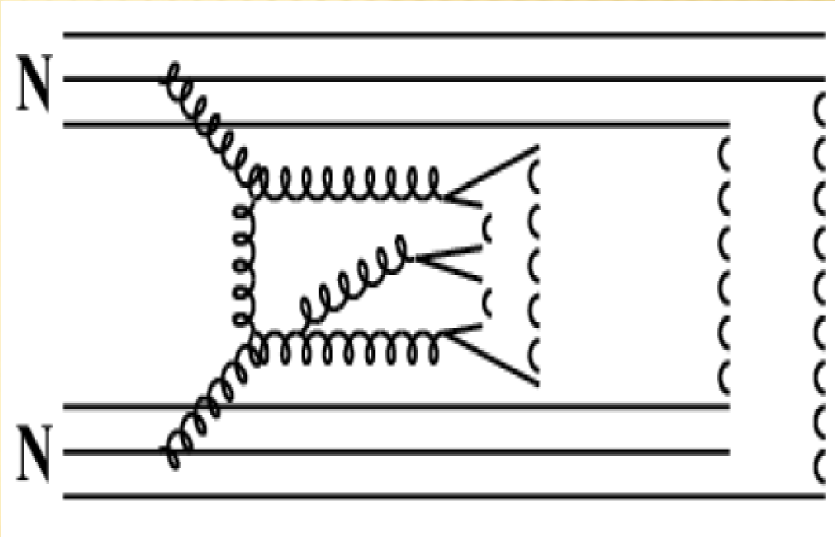

At ultra-relativistic energies: multi-Pomeron scattering, single and double diffraction, and jets (hard Pomeron exchange)

Gribov's Reggeon Calculus + string phenomenology

QGSM PREDICTIONS and RESULTS FOR LHC

Inelastic collisions **NSD collisions**

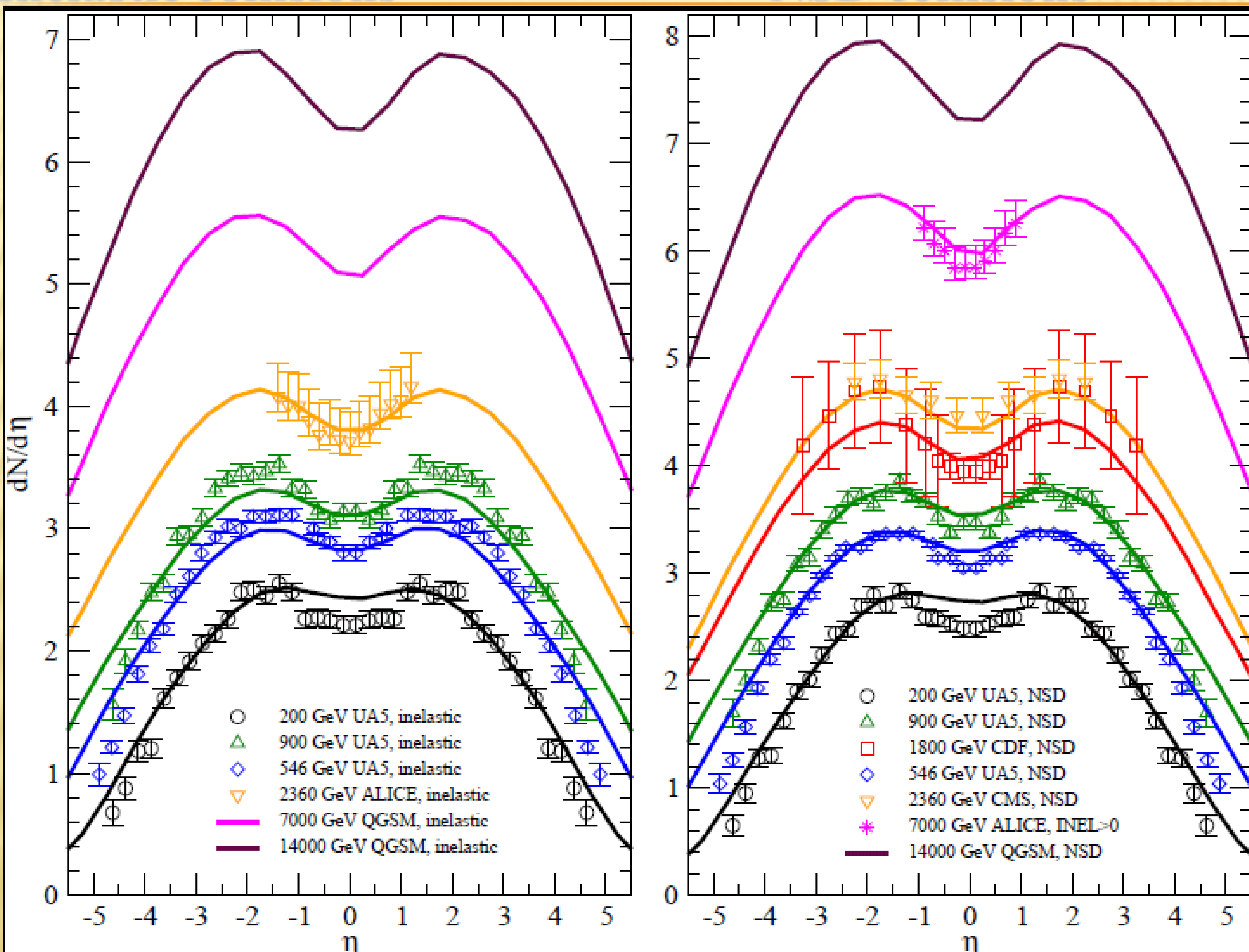

J.Bleibel. L.B. et al., (work in progress)

QGSM PREDICTIONS and RESULTS FOR LHC

Transverse momentum distributions

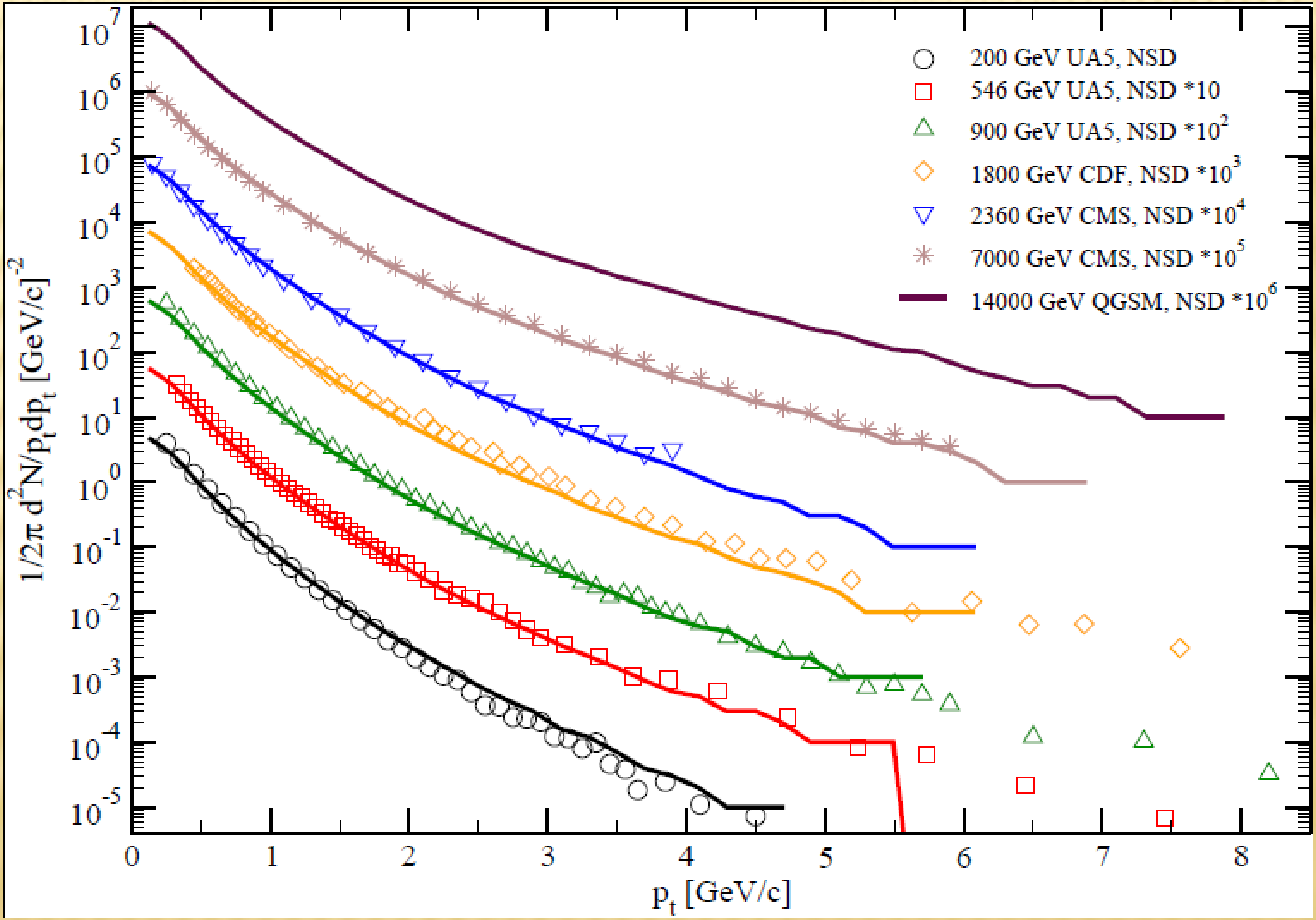

J.Bleibel, L.B. et al. (work in progress)

QGSM PREDICTIONS and RESULTS FOR LHC

Transverse momentum distributions

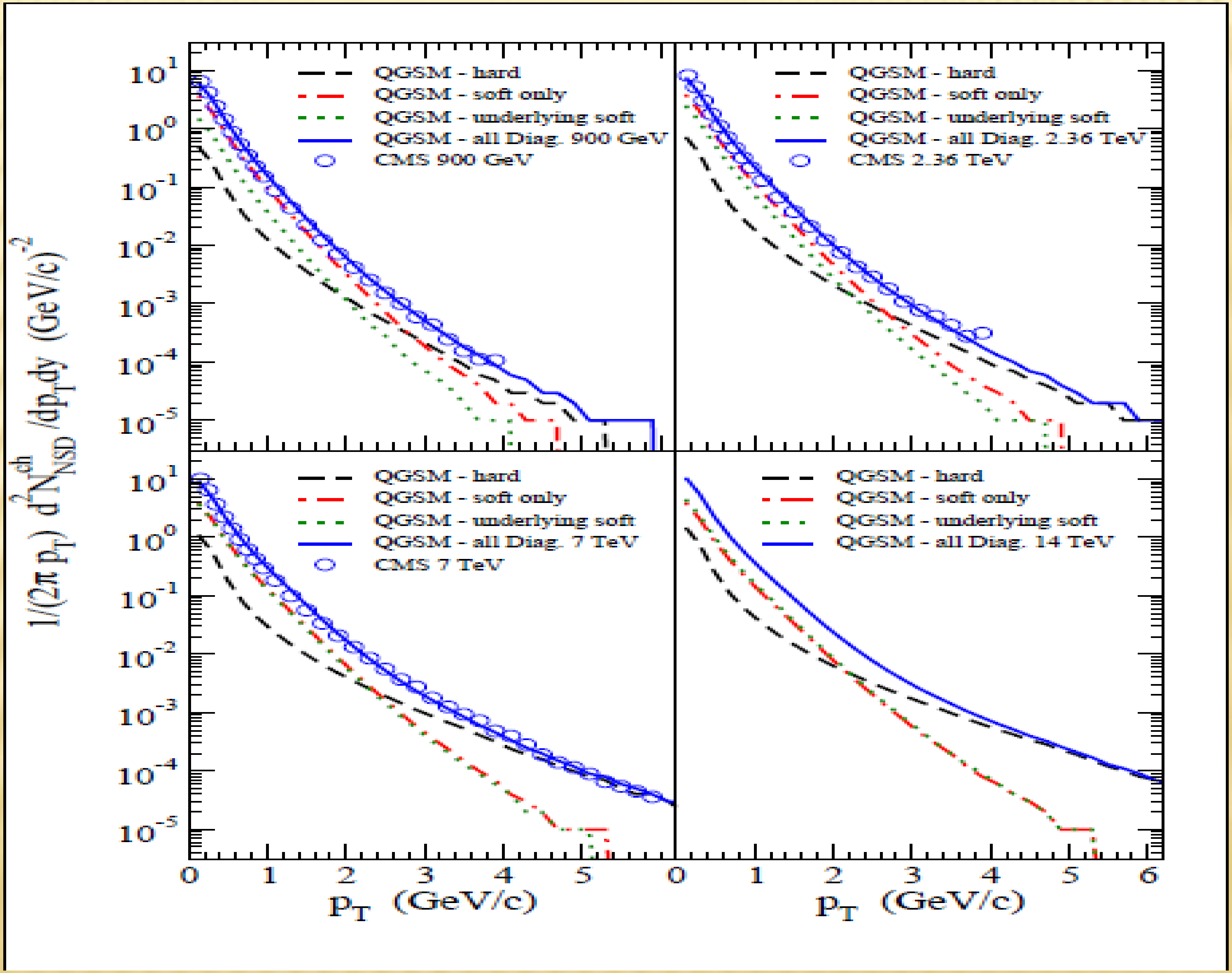

J.Bleibel, L.B. et al. (work in progress)

VIOLATION OF *Extended Longitudinal Scaling* IN HEAVY-ION COLLISIONS AT LHC?

J. Cleymans, J.Struempfer, L.Turko, PRC 78 (2008) 017901

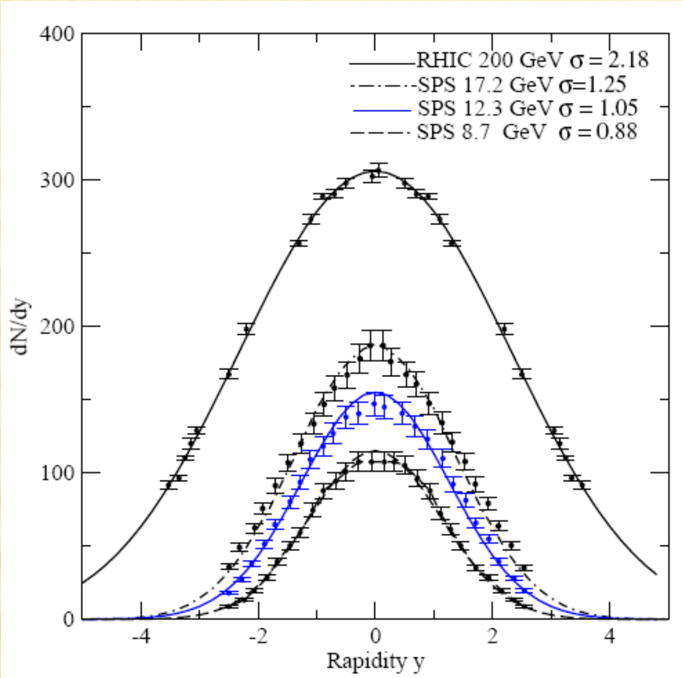

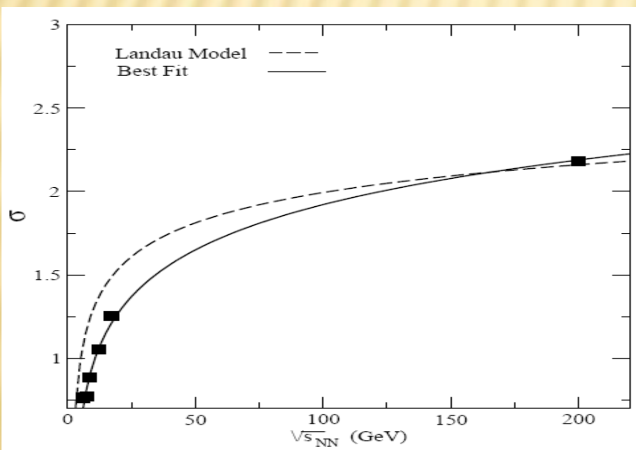

σ

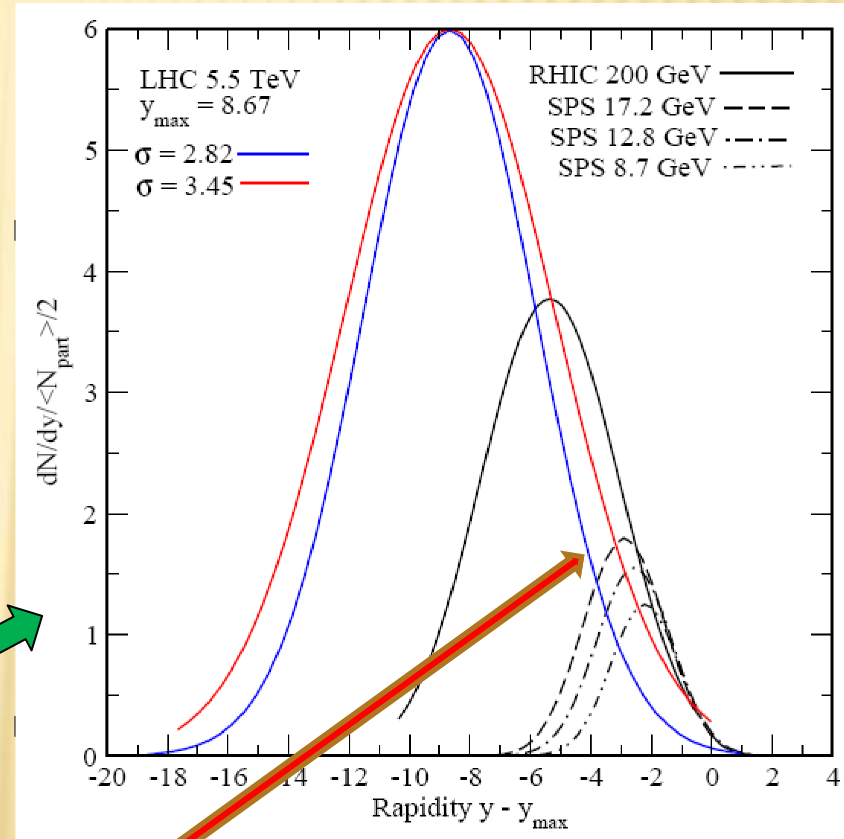

Statistical thermal model: ELS will be violated in A+A @ LHC. What about p+p ?

MOTIVATION: EXPERIMENTAL RESULTS

W. Busza, JPG 35 (2008) 044040

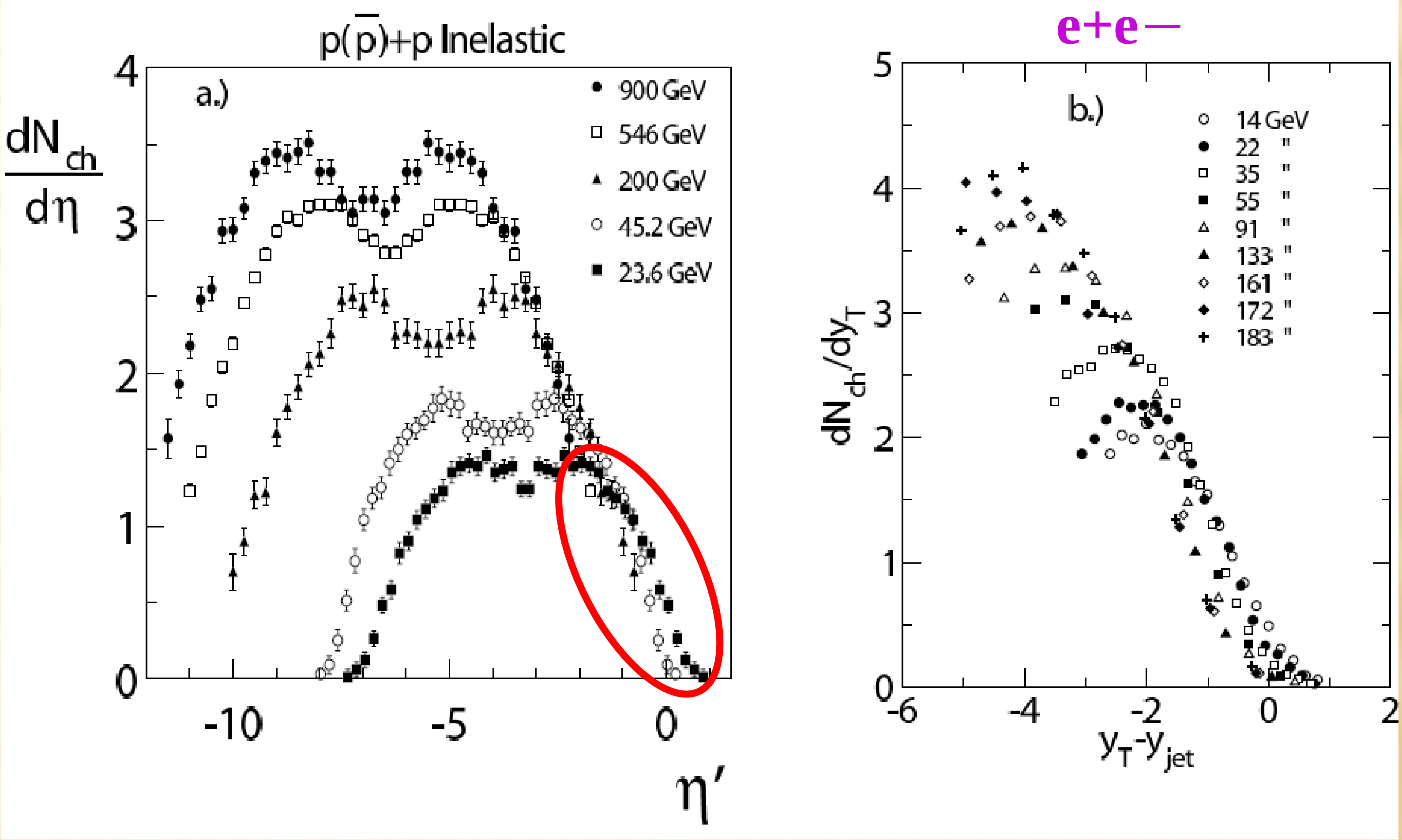

Example of extended longitudinal scaling in different reactions

PREDICTIONS FOR PP @ LHC

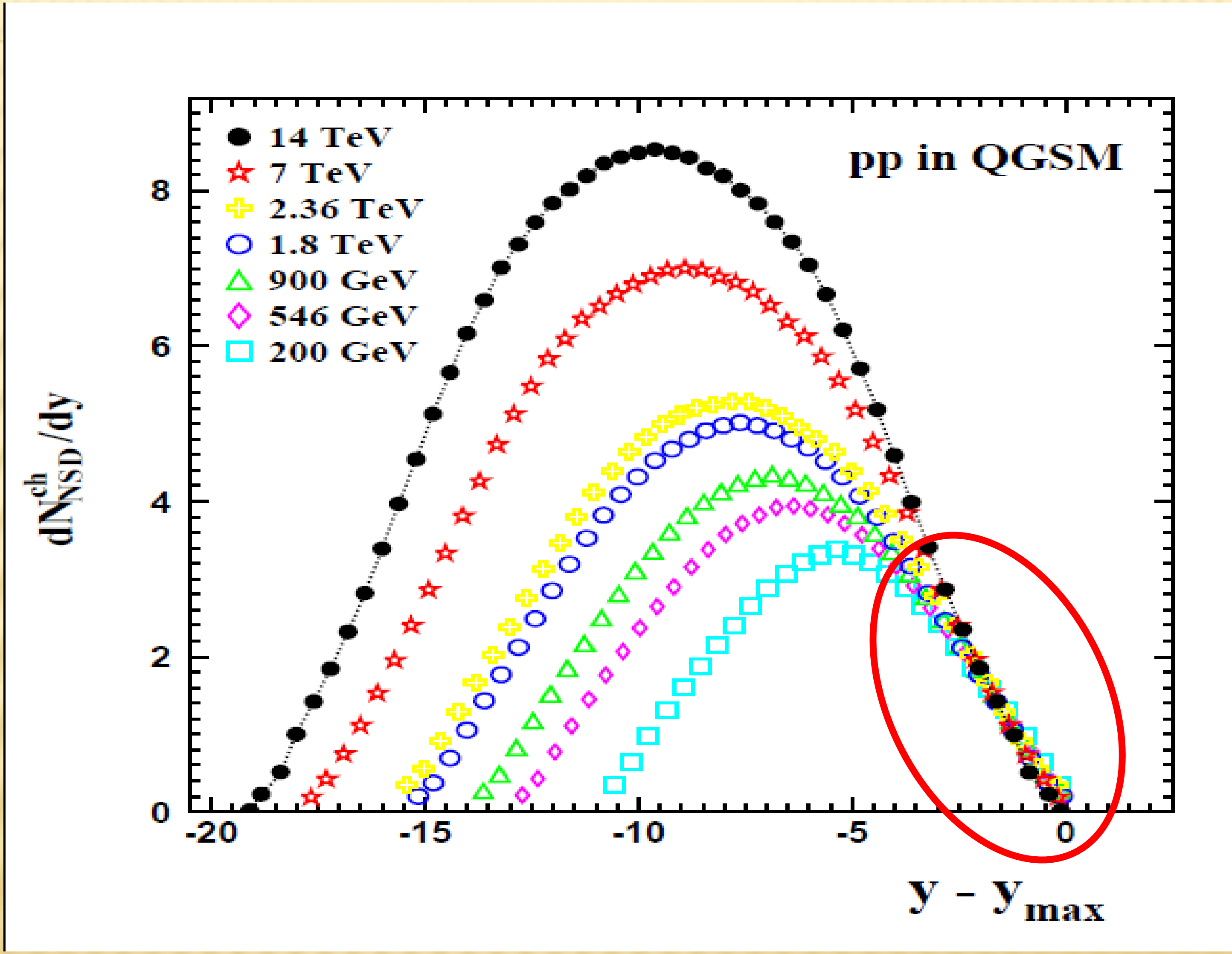

QGSM: extended longitudinal scaling in p+p collisions holds

QGSM PREDICTIONS and RESULTS FOR LHC

Multiplicity distributions

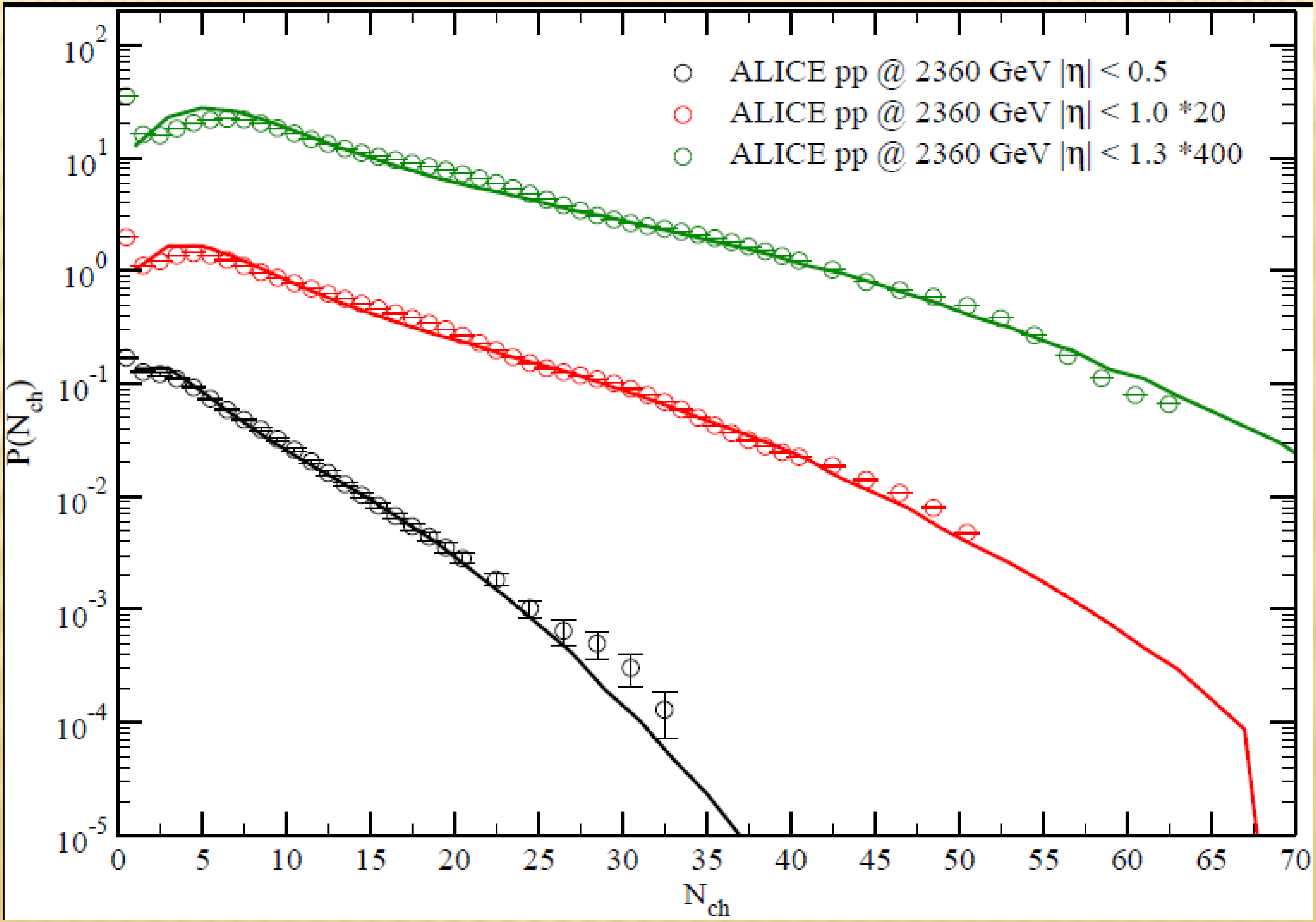

J.Bleibel, L.B. et al. (work in progress)

VIOLATION OF KNO SCALING AT LHC

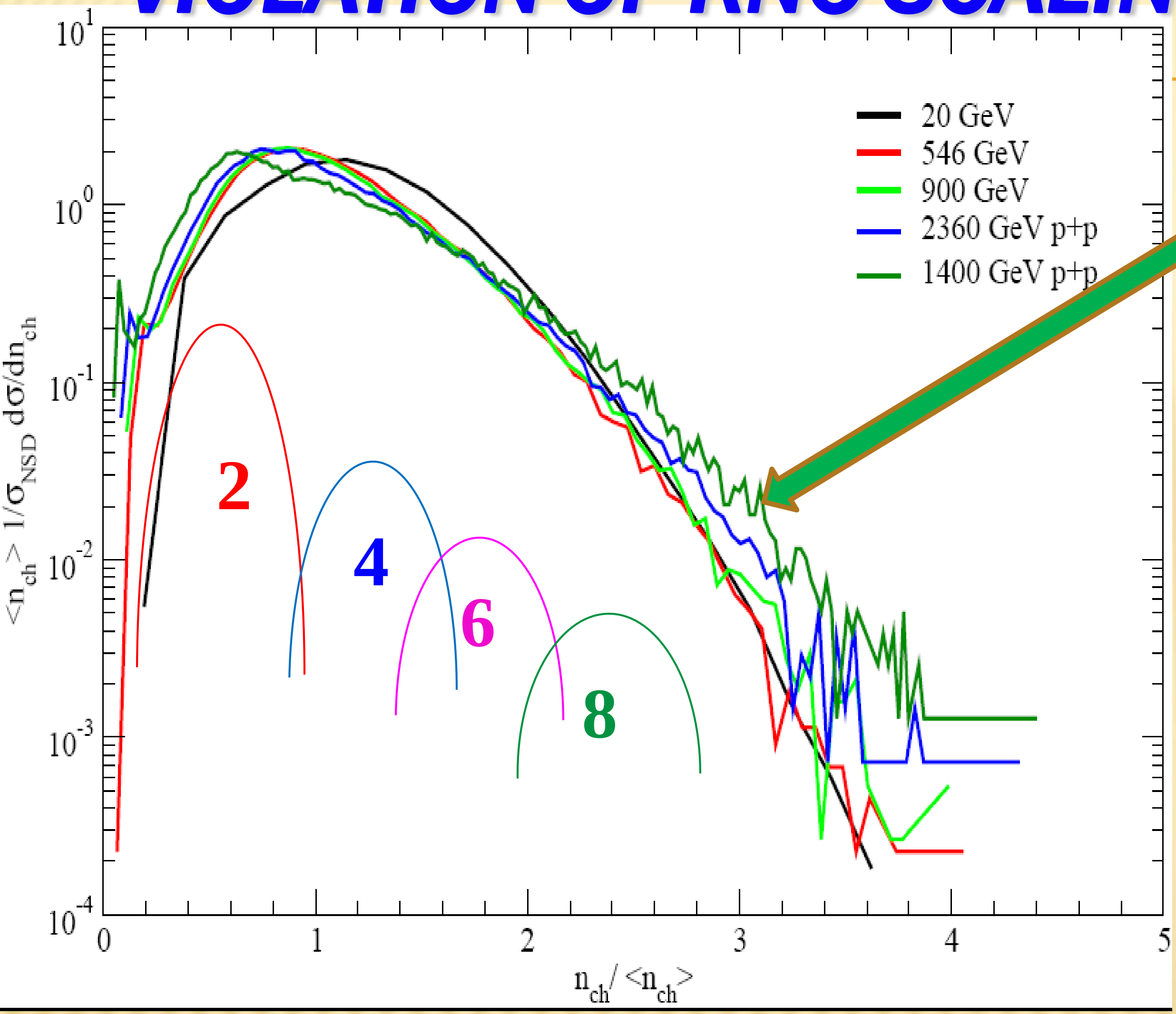

High-multiplicity tail is pushed up, whereas maximum of the distribution is shifted towards small values of z

At energies below 100 GeV different contributions overlap strongly, whereas at higher energies – more multi-string processes

=> Enhancement of high multiplicities

QGSM PREDICTIONS and RESULTS FOR LHC

Violation of KNO scaling at LHC

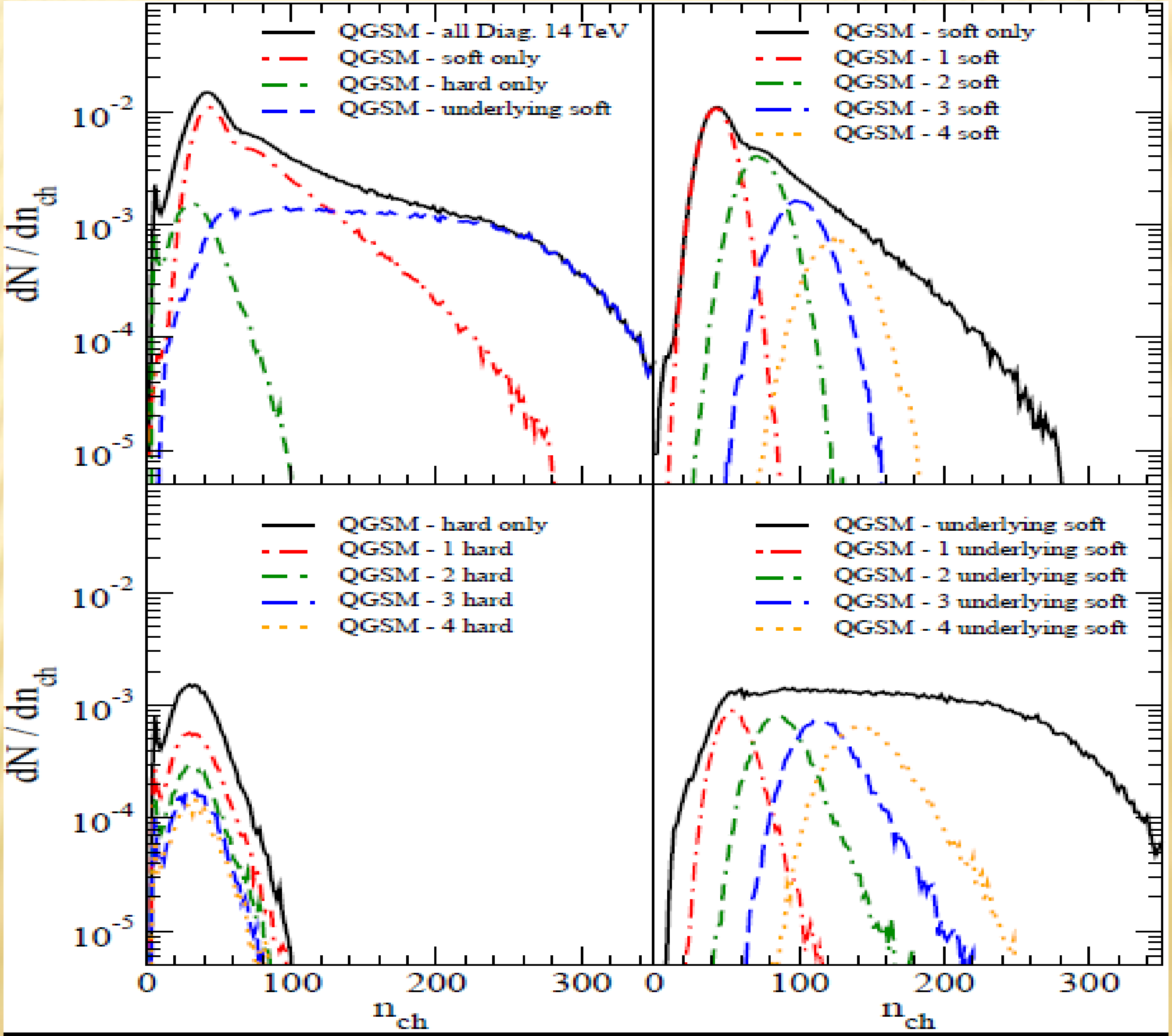

J.Bleibel, L.B. et al. (work in progress)

QGSM: Predictions for LHC. (14 TeV)

1.	$\sigma^{(tot)}$	103 mb	$(\sigma^{(tot)}(s) \sim \ln^2 \frac{s}{s_0})$
2.	$\sigma^{(el)}$	26 mb	$(\sigma^{(el)}(s) \sim \ln^2 \frac{s}{s_0})$
3.	$B(0)$	21.5 GeV^{-2}	$(B(0) \sim \ln^2 \frac{s}{s_0})$
4.	$\rho = \frac{Re\,T(0)}{Im\,T(0)}$	0.11	
5.	σ_{SD}	12÷13 mb	$(\sigma_{SD} \sim \sigma_{DD} \sim \ln \frac{s}{s_0})$
6.	σ_{DD}	11÷13 mb	

$$\sigma^{(el)} + \sigma_{SD} + \sigma_{DD} = 51\,mb \approx \frac{1}{2}\sigma^{(tot)}$$

QGSM: Predictions for LHC.

7. $\langle n_{ch} \rangle$ — $80 \div 100$

8. $\left.\frac{dn_{ch}}{dy}\right|_{y=0}$ — $5.5 \div 6.0$

9. Structures in σ_n

10. Strong long-range (in y) correlations

11. Large amount of minijets.

QGSM gives a unified description of:

$$\sigma^{(tot)}{}_{hp}(s), \quad \frac{d\sigma^{(el)}}{dt}, \quad E\frac{d^3\sigma}{d^3p}$$

for $\pi^{\pm}, K^{\pm}, K^0(\bar{K}^0), p, \bar{p}, \Lambda, \bar{\Lambda}, ..$

$\sigma_n(s)$, correlations,…

Substantial deviations from predictions of the model at superhigh energies would indicate to a new physics.

Important feature for (h)A+A collisions at ultrarelativistic energies - shadowing

THE GLAUBER MODEL

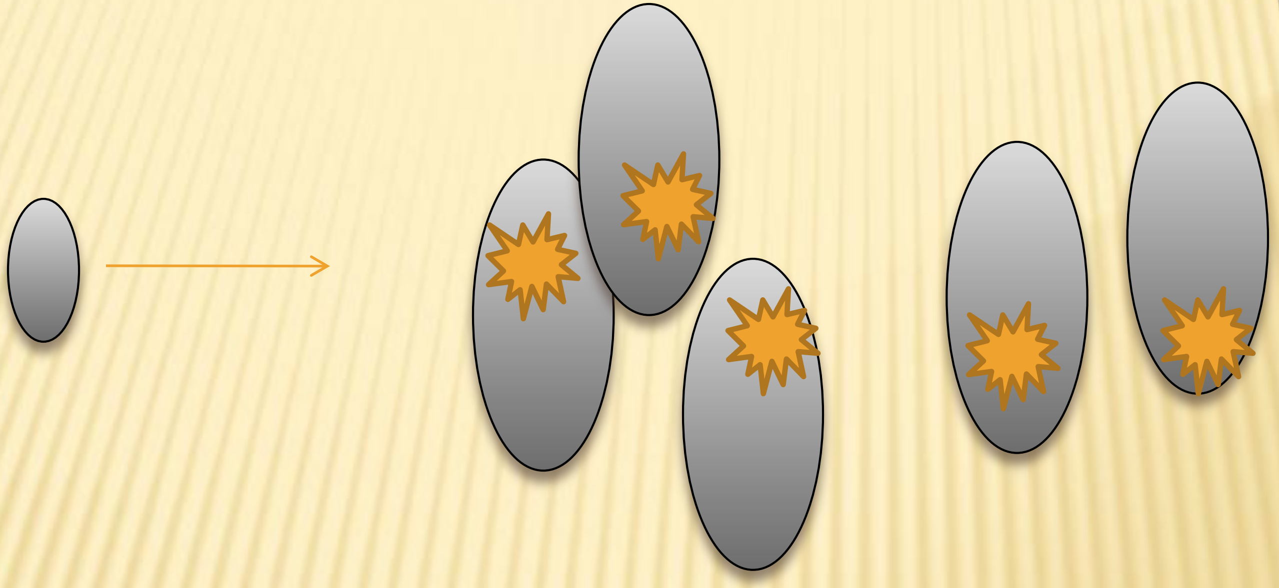

- heavy-ion collisions
- in each rescattering there is a certain probability for particle production

COHERENT INTERACTION

- **the projectile becomes large compared to the target**
- **interacts simultaneously with the whole system**
- effectively less interaction - **shadowing**
- **dramatic change of space-time picture**

FREEZE-OUT AT RHIC: QGSM

M.S. Nilsson (to be submitted)

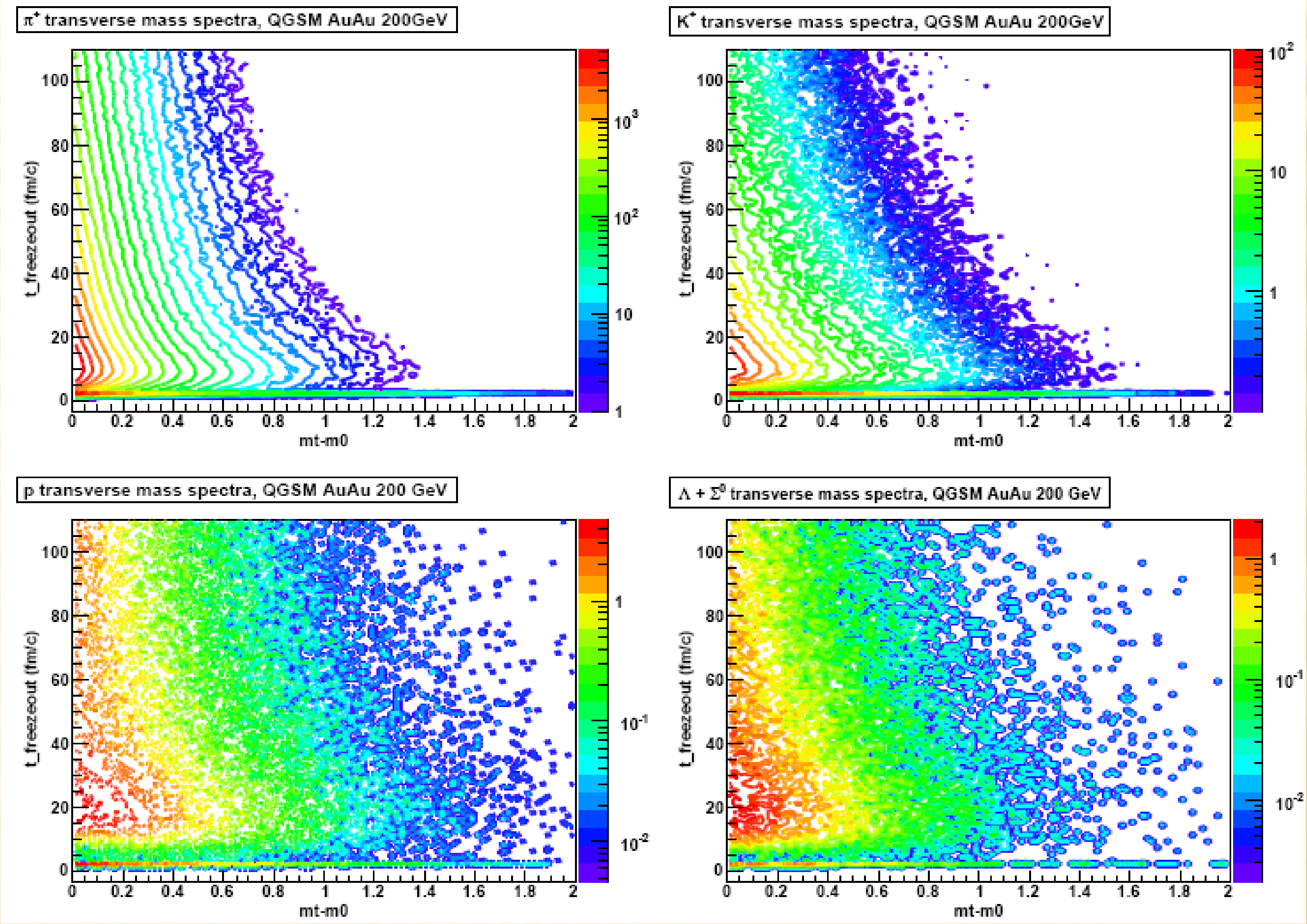

FREEZE-OUT AT RHIC: QGSM

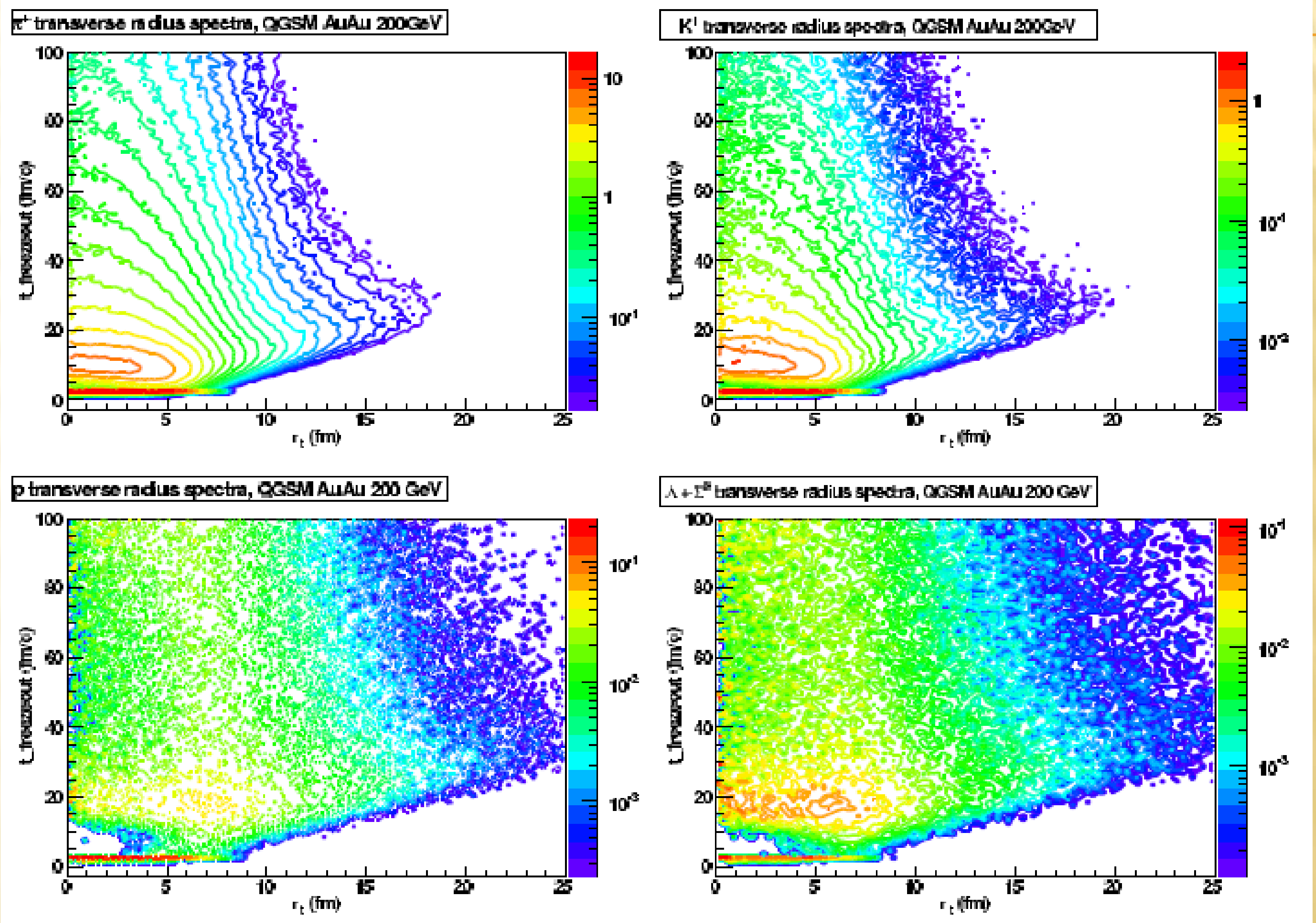

HANBURY-BROWN—TWISS CORRELATIONS

M.S. Nilsson , L. Malinina, L.B. et al. (to be submitted)

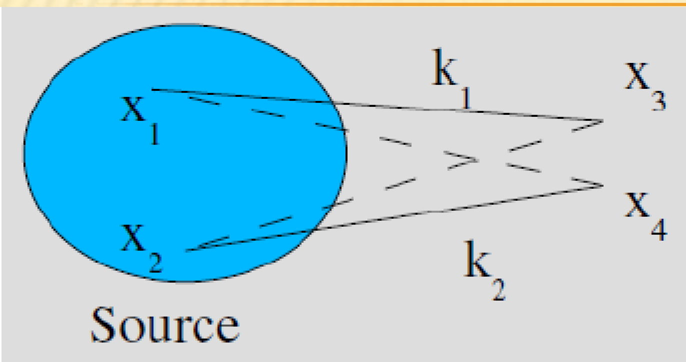

- We can consider two pions emitted from two spacetime points in the extended source.
- Correlations will then arise from exchange symmetry between identical particles.
- It is defined as the probability to measure both particles in coincidence, divided on the probability of measuring each separately.

$$C_2(k_1, k_2) = \frac{P(k_1, k_2)}{P(k_1)P(k_2)}$$

$$\mathbf{q} = \mathbf{p_1} - \mathbf{p_2}$$

$$C_2(q) = 1 + \lambda e^{-R^2_{out} q^2_{out} - R^2_{side} q^2_{side} - R^2_{long} q^2_{long} - R^2_{out,long} q_{out,long}}$$

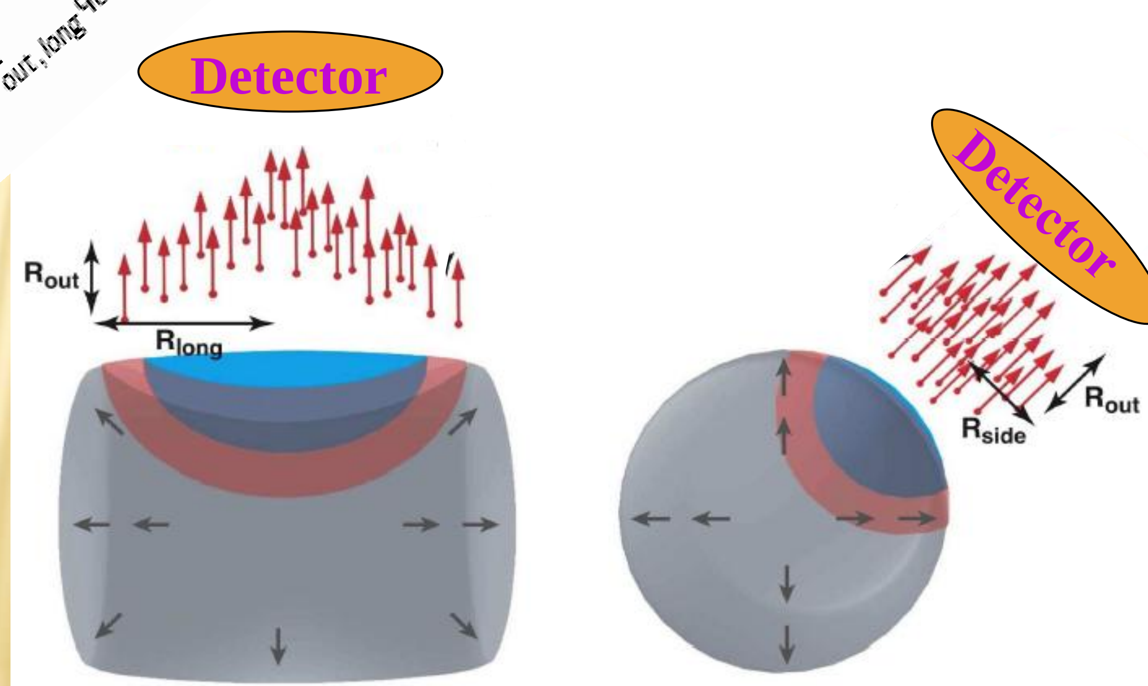

NON-IDENTICAL HBT CORRELATIONS

M.S. Nilsson , L. Malinina, L.B. et al. (to be submitted)

- Correlations between nonidentical particles arise not from exchange symmetry, but from final state Couloumb and strong interactions.
- These correlations contain information about which particle in the pair is emitted first.
- We have in the pair reference frame the parameter

$$r^*_{out} = \gamma_t(r_{out} - \beta_t \Delta t_{LCMS}) \quad (1)$$

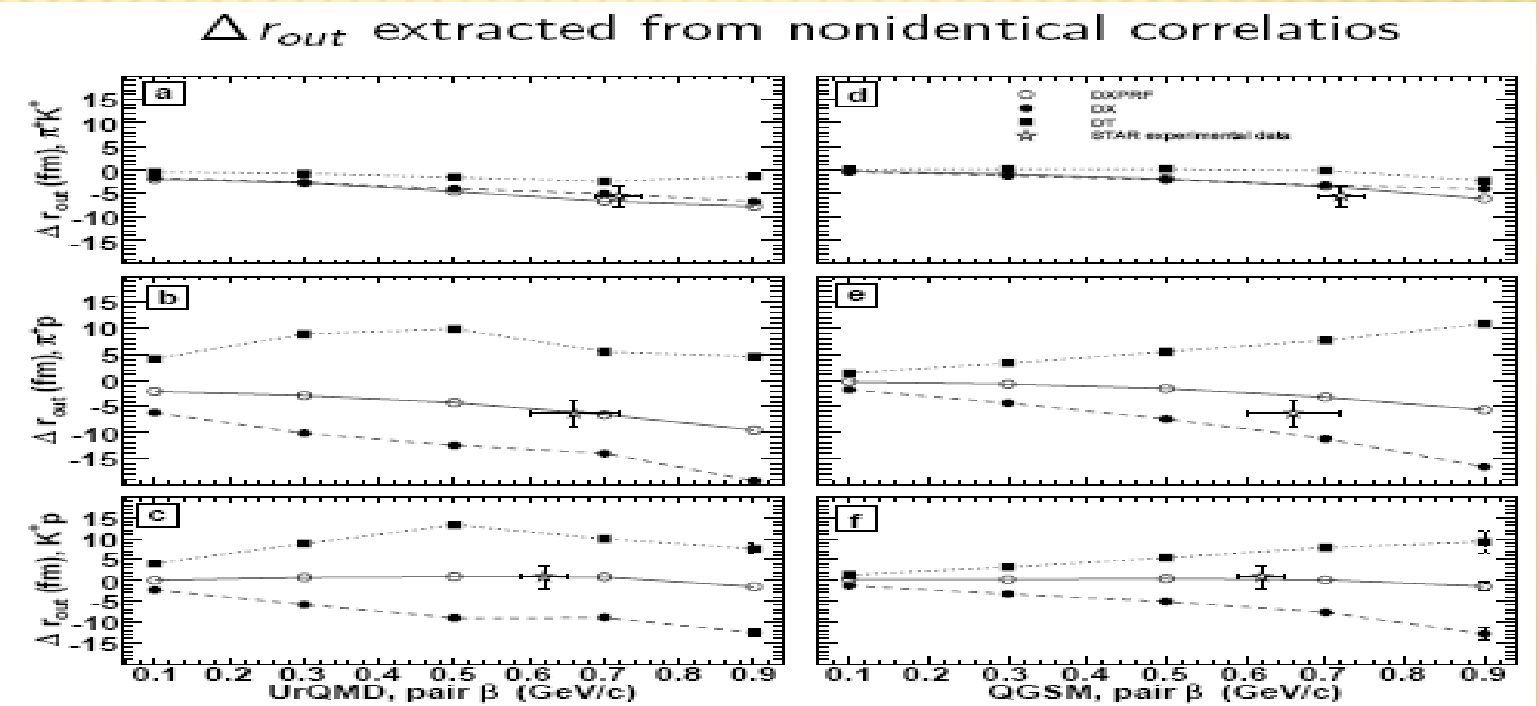

IDENTICAL HBT CORRELATIONS

M.S. Nilsson , L. Malinina, L.B. et al. (to be submitted)

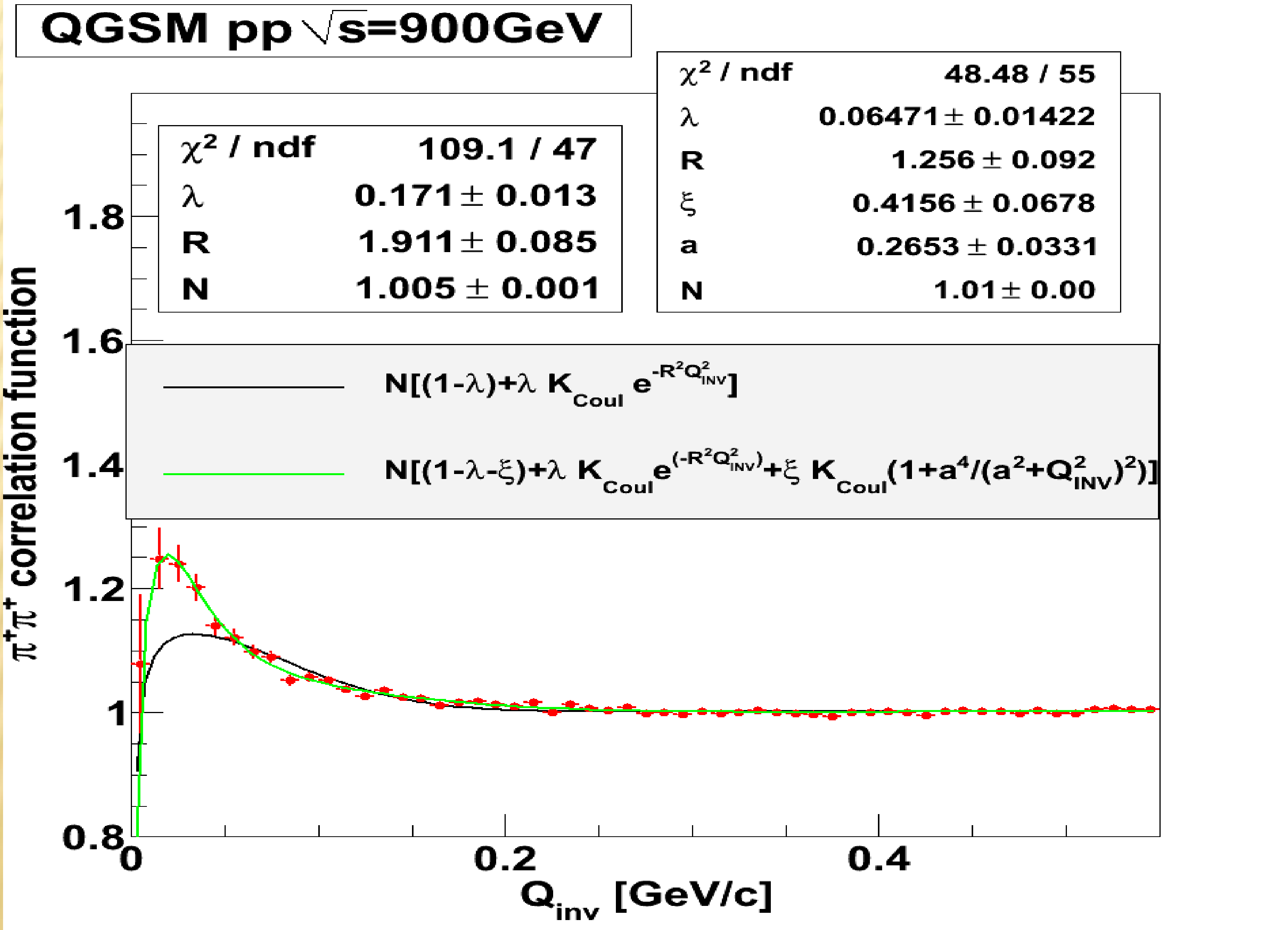

Femtoscopy in pp at 200 GeV (STAR data)

Mt dependence (“x-p” correlations) in very small systems (pp, e+e-) is usually attributed to:

-string fragmentation
-resonance contribution
-Heisenberg uncertainty
-jets

All Kt(mt) dependences of correlation radii observed by STAR scale with pp (!?) alghoght the expected origins driving these dependences are different.

ALICE didn't observed strong Kt dependence (!?)

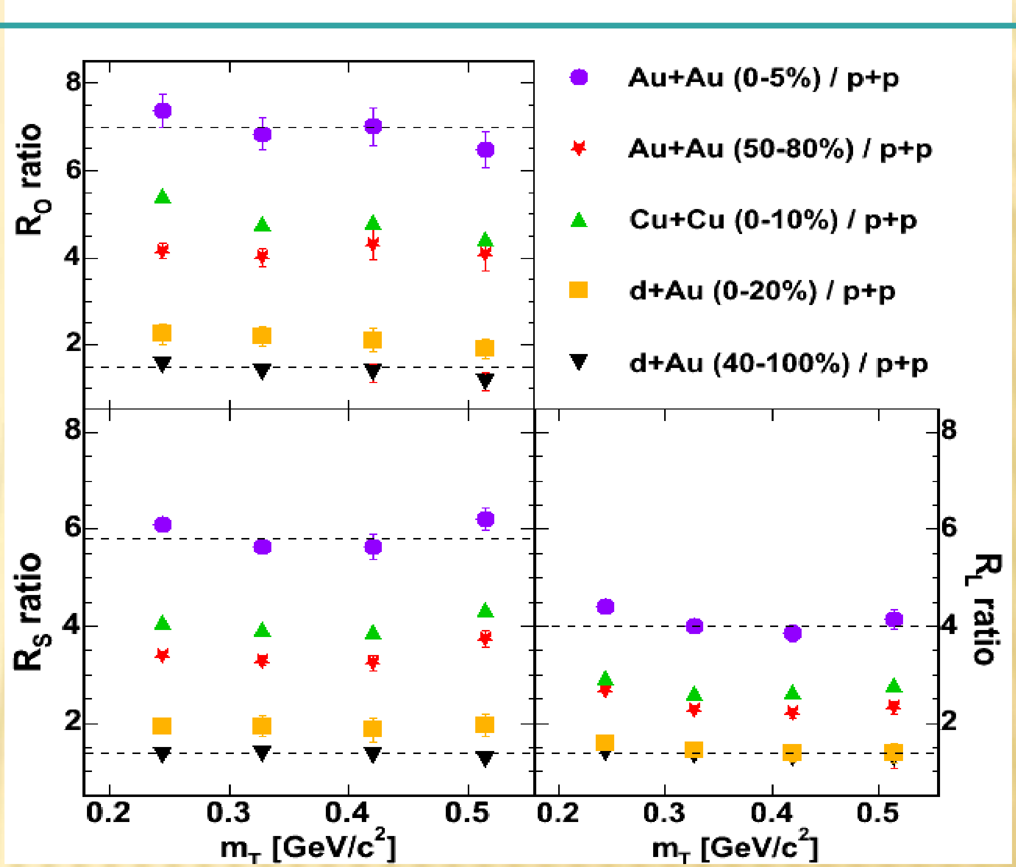

Kt-dependence of correlation radii pp at 200 GeV with QGSM

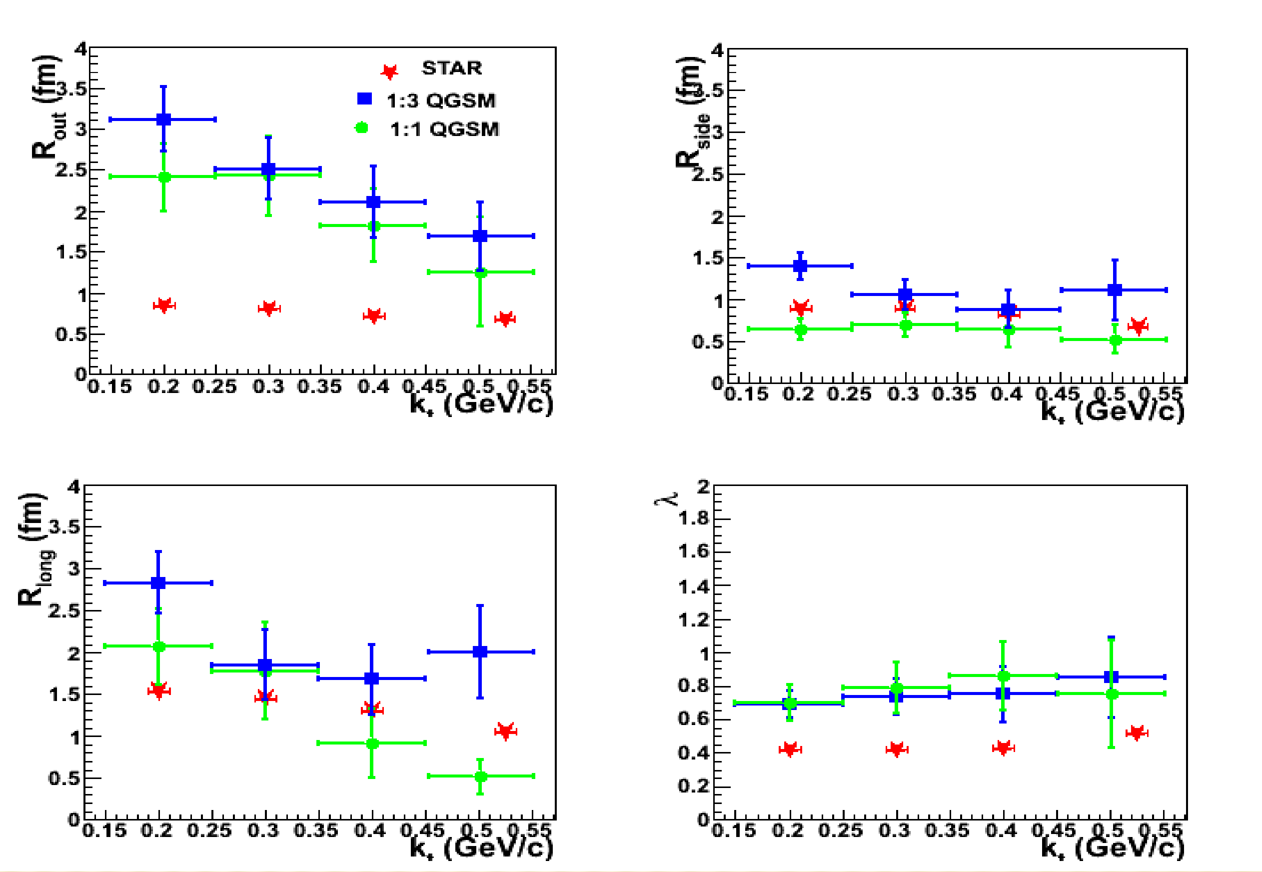

There is strong Kt dependence in QGSM.
What is it's origin ? Resonances ? String fragmentation ?

Source functions of ALL pions in different kT regions in QGSM pp 200 GeV

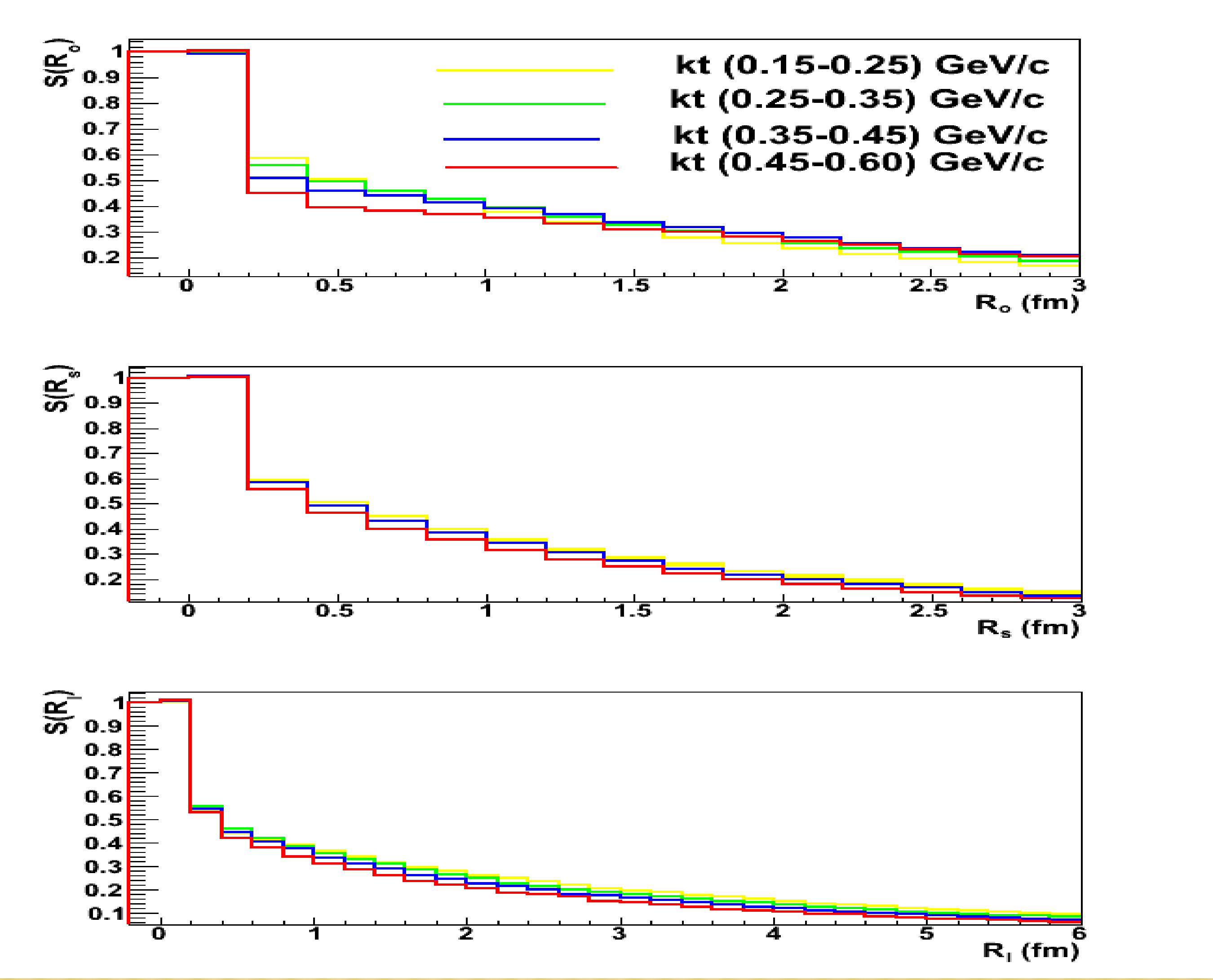

Source functions of direct pions and pions from different resonances in QGSM pp 200 GeV

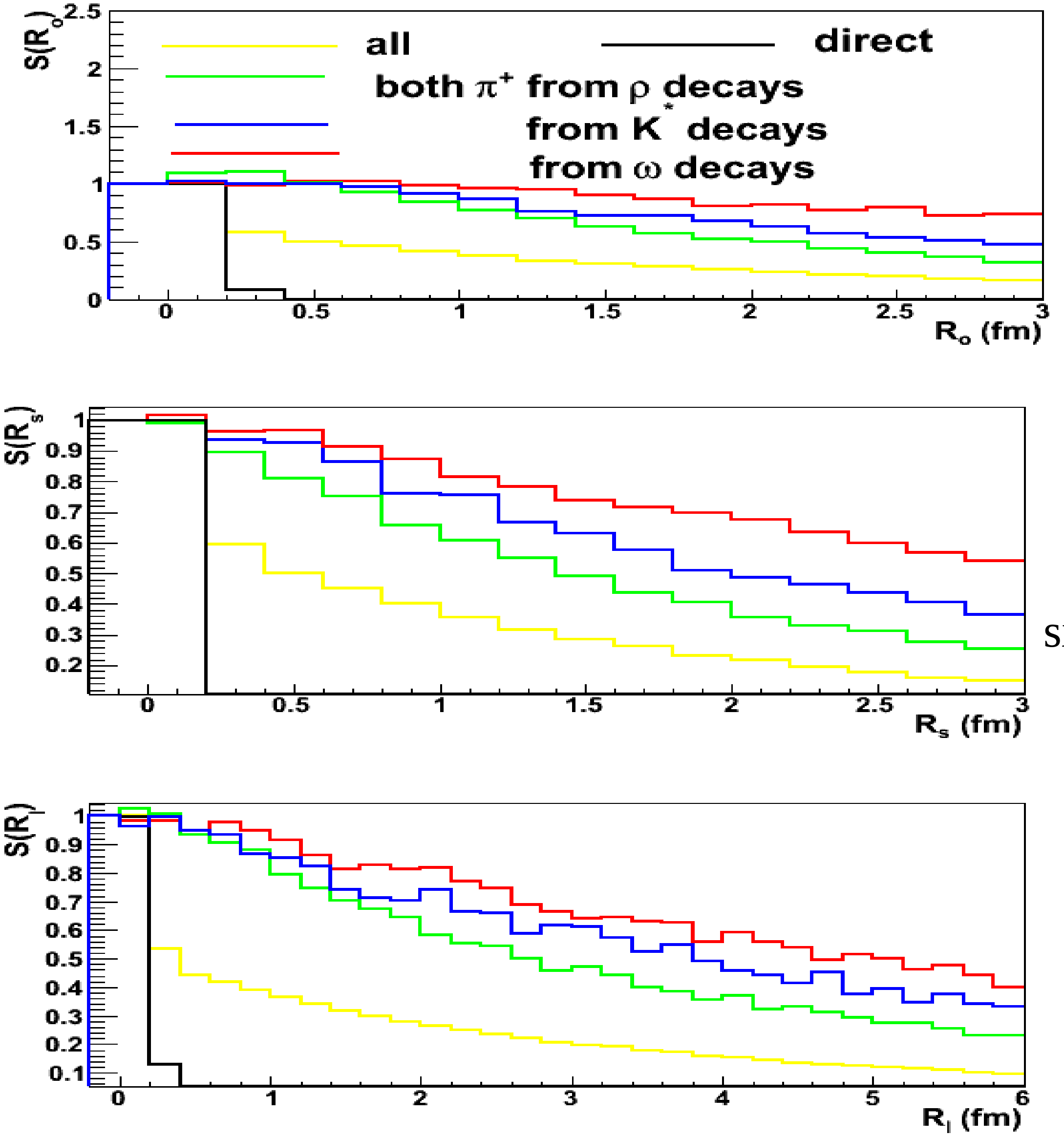

Kt ~(0.15-0.25) GeV/c

Direct pions source size < 0.5 fm

$\rho^0 \rightarrow \pi^-\pi^+$, $\rho^+ \rightarrow \pi^0\pi^+$

$K^{*+} \rightarrow K\pi^+$

$\omega \rightarrow \pi^-\pi^+\pi^0$ maximal source size

Interplay between contributions of different resonances and direct pions determine source size.

Relative contributions of direct pions and pions from different resonances QGSM (1:3)

Kt (GeV/c)	**(0.15-0.25)**	**(0.25-0.35)**	**(0.35-0.45)**	**(0.45-0.6)**
direct pion	26.0 %	26 %	26 %	28 %
$\rho^0 \to \pi^- \pi^+$, $\rho^+ \to \pi^0 \pi^+$	41.3 %	45.5 %	48.7 %	50.6 %
$K^{*+} \to K \pi^+$	12.8 %	12,0 %	10.9 %	9.6 %
$\omega \to \pi^- \pi^+ \pi^0$	12.3 %	10.5 %	8.9 %	7.5 %
$\eta \to \pi^- \pi^+ \pi^0$, $\eta' \to \eta \pi^- \pi^+$, $\Delta^{++} \to p \pi^+$	7.6 %	6.0 %	5.5 %	4.3 %

Relative contribution of pions from ρ increases with kt, when the relative contribution of ω, K* falls. It leads to decrease of correlation radii with kt. But the source size is too large (blue squares on slide 2) !

Relative contributions of direct pions and pions from different resonances QGSM (1:1)

Kt (GeV/c)	**(0.15-0.25)**	**(0.25-0.35)**	**(0.35-0.45)**	**(0.45-0.6)**
direct pion	39 .2 %	40.7 %	43.1 %	46.7 %
$\rho^0 \to \pi^- \pi^+$, $\rho^+ \to \pi^0 \pi^+$	33.7 %	36.0 %	37.3 %	37.1 %
$K^{*+} \to K \pi^+$	9.7%	8,9 %	7.9 %	6.8 %
$\omega \to \pi^- \pi^+ \pi^0$	10.3 %	8.7%	7.2 %	5.9 %
$\eta \to \pi^- \pi^+ \pi^0$, $\eta' \to \eta \pi^- \pi^+$, $\Delta^{++} \to p \pi^+$	7.1 %	5.7%	5.5 %	3.5 %

Relative contribution of direct and pions from ρ increases with kt, when the relative contribution of ω, K* falls. It leads to decrease of correlation radii with kt. Decrease of ratio "pions from ρ to direct pions" leads to requested decrease of the correlation radii (green circles on slide 2).

Kt-dependence of correlation radii pp at 200 GeV/c with QGSM

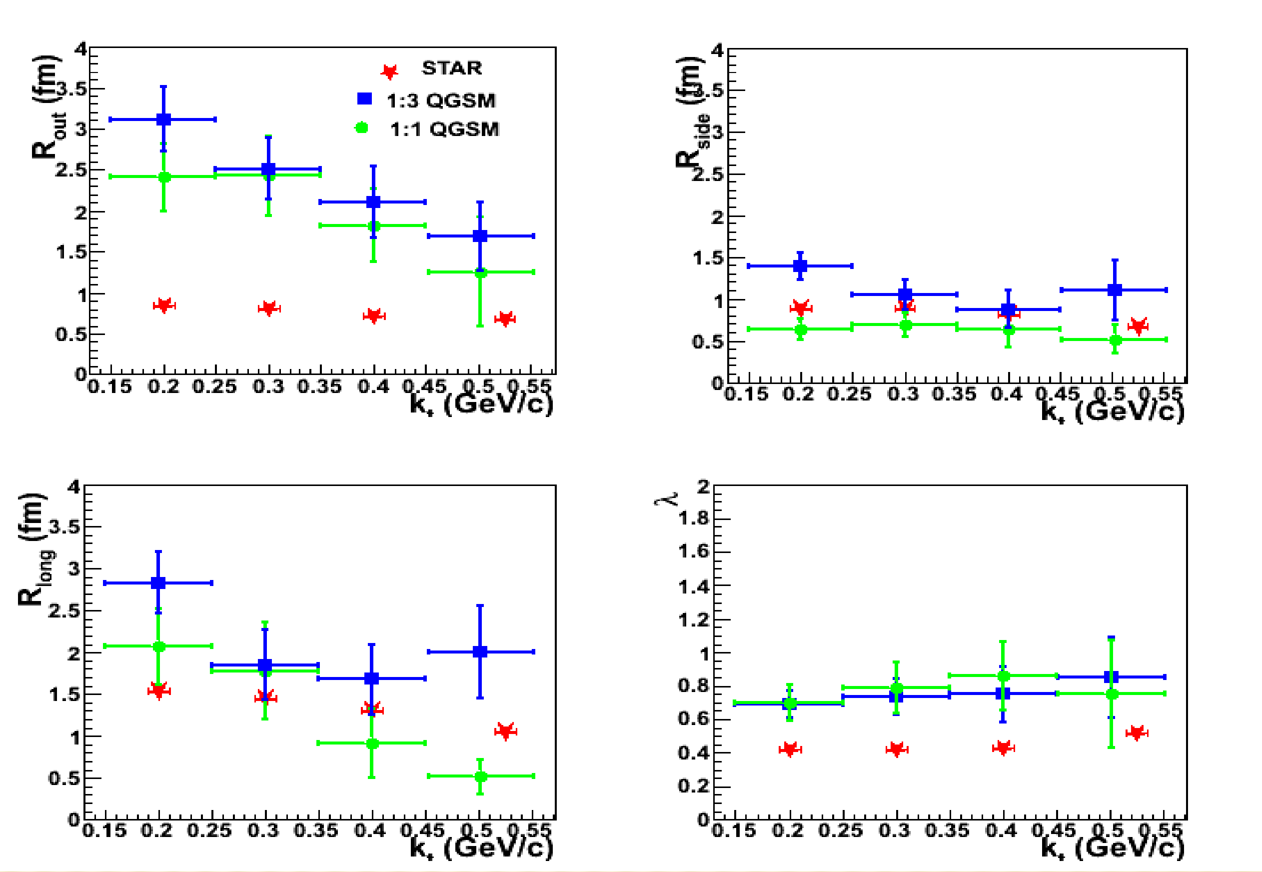

There is strong Kt dependence in QGSM.

One of it's origins are the resonances. String fragmenation ?

Example of source function of pions from different processes QGSM pp 200 GeV

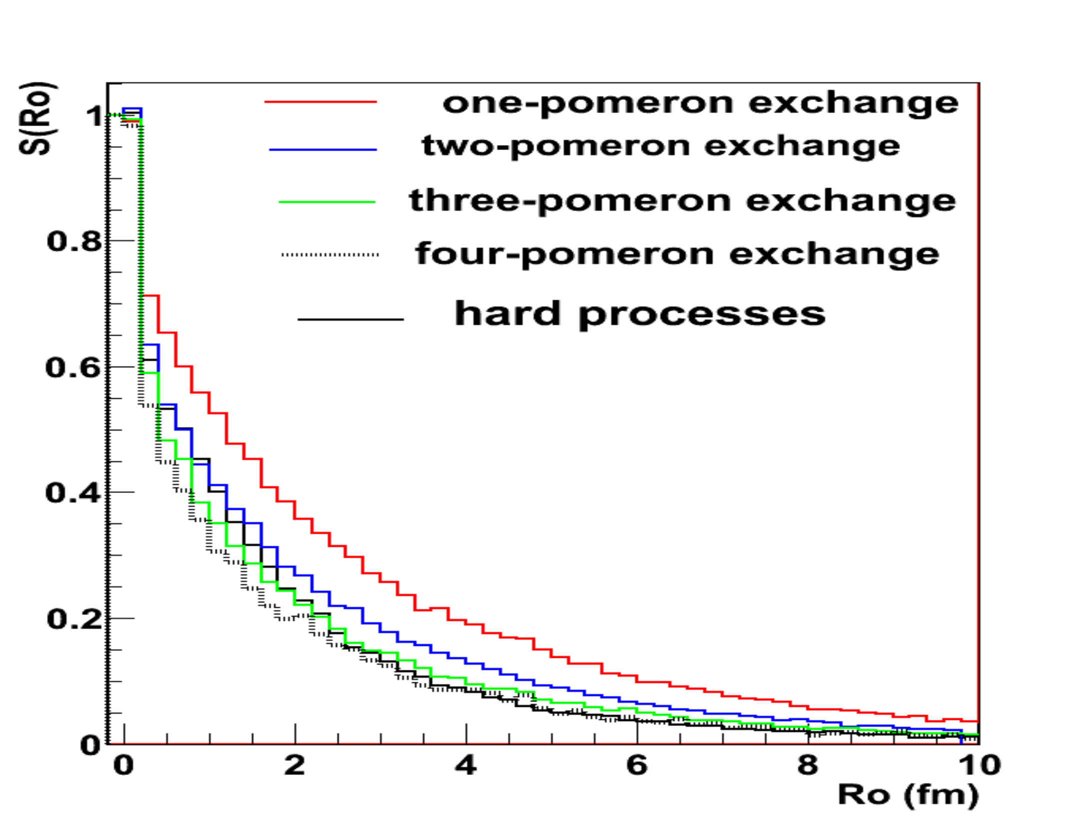

Relative contribution of pions from different processes determines the source size through the number of produced resonances. In one-pomeron exchange-process more resonances are produced, then in many-pomeron exchanges.

Correlation radii pp at 900 GeV/c with QGSM

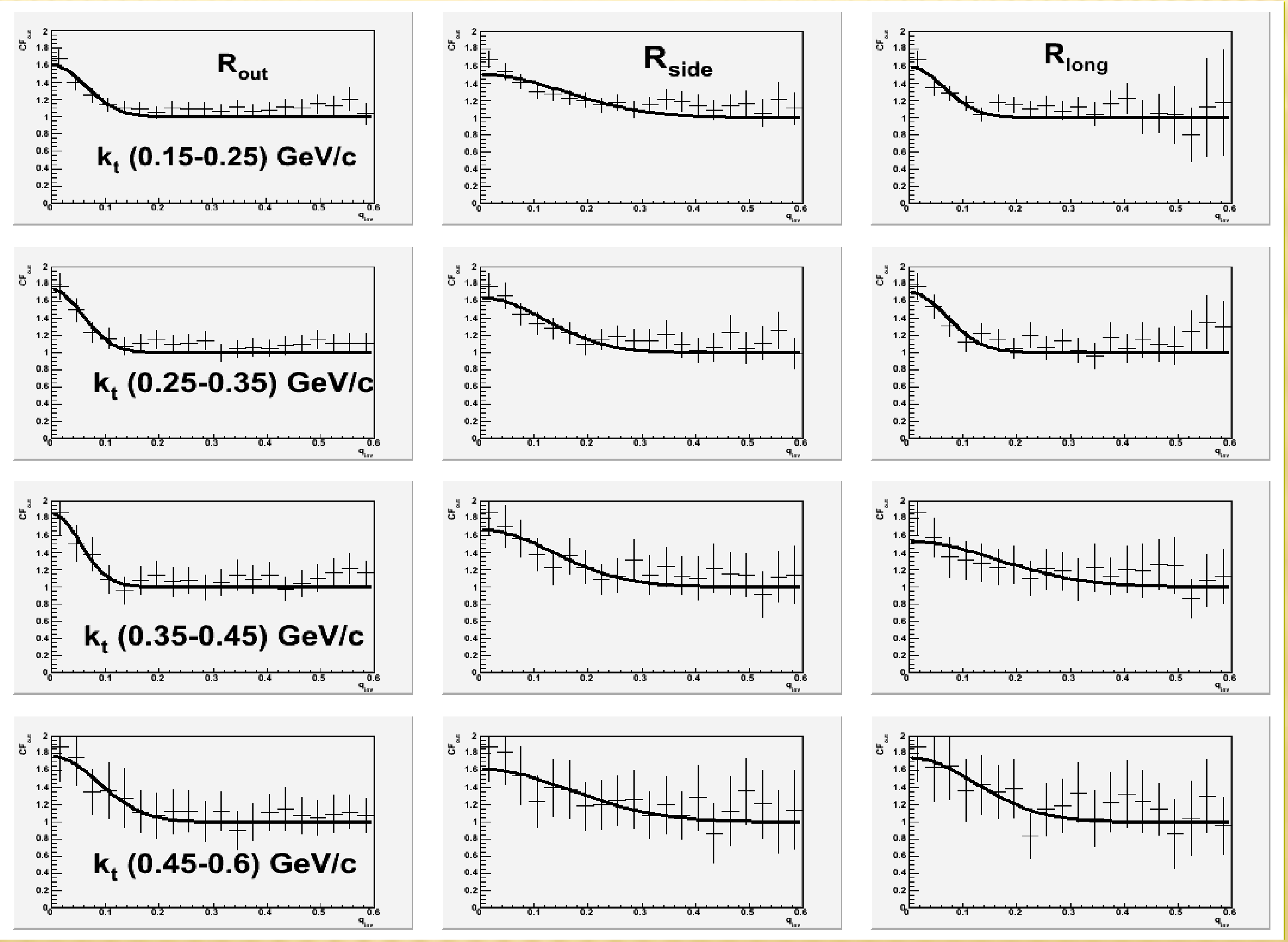

Kt-dependence of correlation radii pp at 900 GeV/c with QGSM

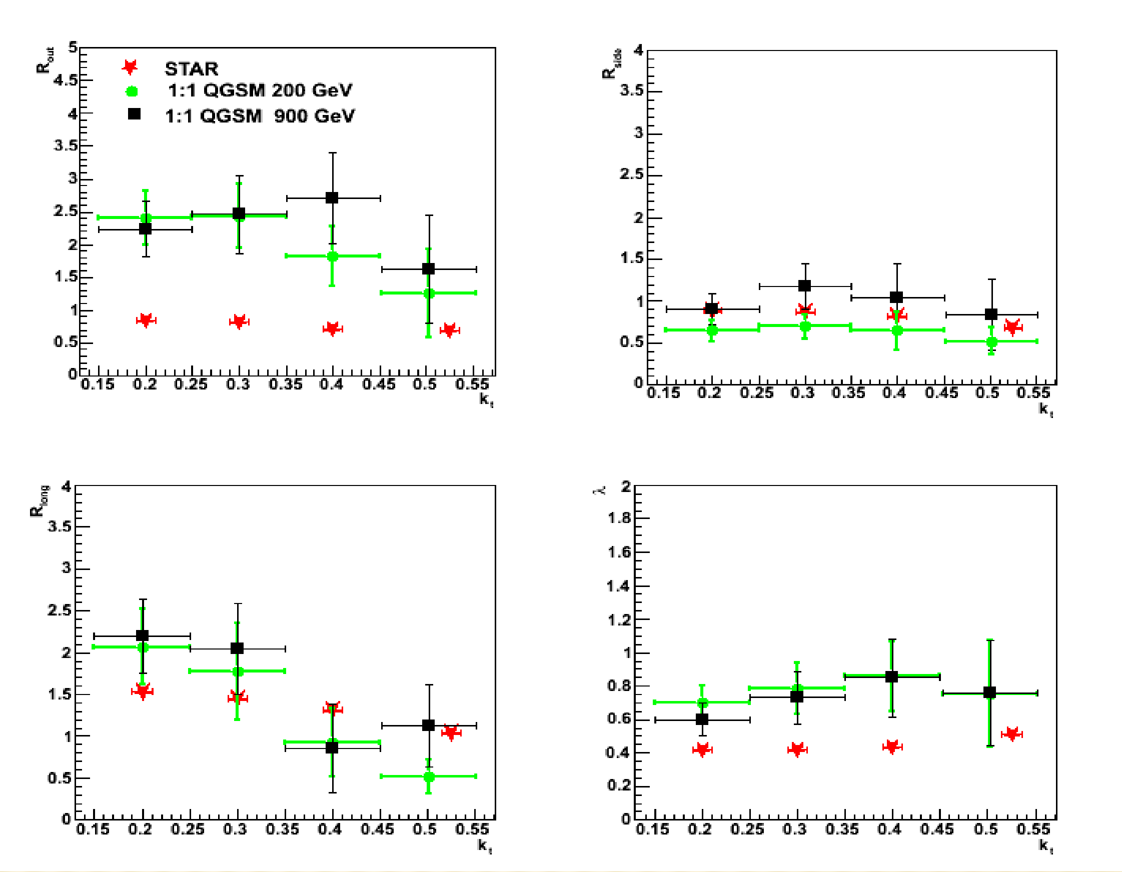

Radii are almost the same as at 200 GeV/c

Kt-dependence of correlation radii AuAu at 200 GeV/c with QGSM

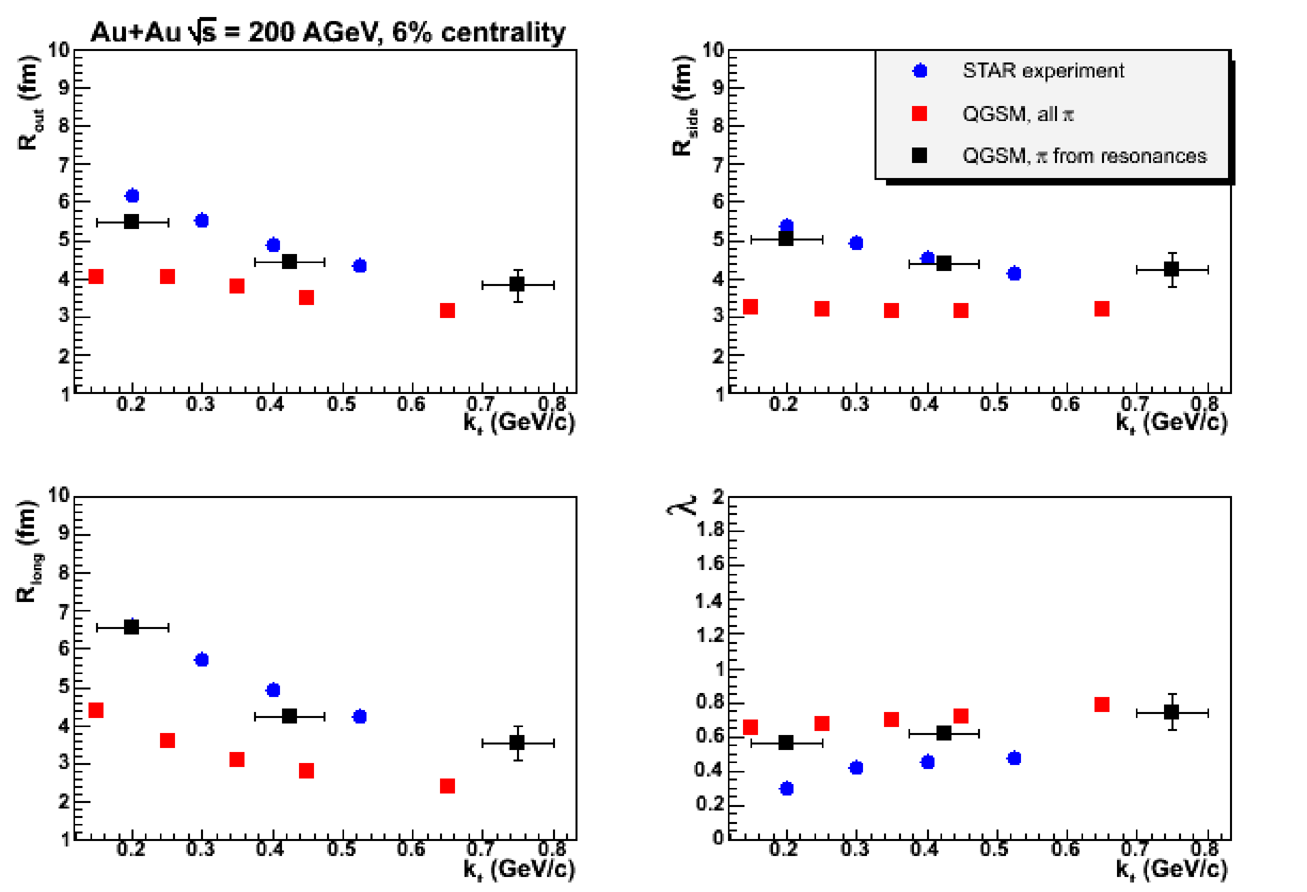

QGSM shows smaller correlation radii then in experiment (red squares).

What if we play with number of direct/rho here ?

If we take only pions from the inelastic secondary interations and resonance decays (black points) the correlation radii drastically increase and become close to STAR experimental data

Conclusions.

- The pomeron is the main building block of the reggeon approach. It has a rich dynamical structure in QCD.
- Many-pomeron exchanges are important for understanding high-energy interactions.
- Models based on reggeon calculus and 1/N –expansion in QCD give a good description of experimental data on interactions of hadrons, nuclei and small-x DIS.

Summary and outlook

- ***LHC is a discovery machine for both hard and soft physics in HI collisions***
- ***Event generators are an indispensable tool for planing the experiments and analysis of data***
- ***=> Further development of existing MC generators***
- ***HI theory groups in Oslo utilizes it to study : EOS, elliptic flow, particle freeze-out, HBT correlations of unlike particles, particle-jet correlations, heavy quark production in a large pT range, scaling properties …***

Back-up Slides

R. Lacey, QM'05 talk

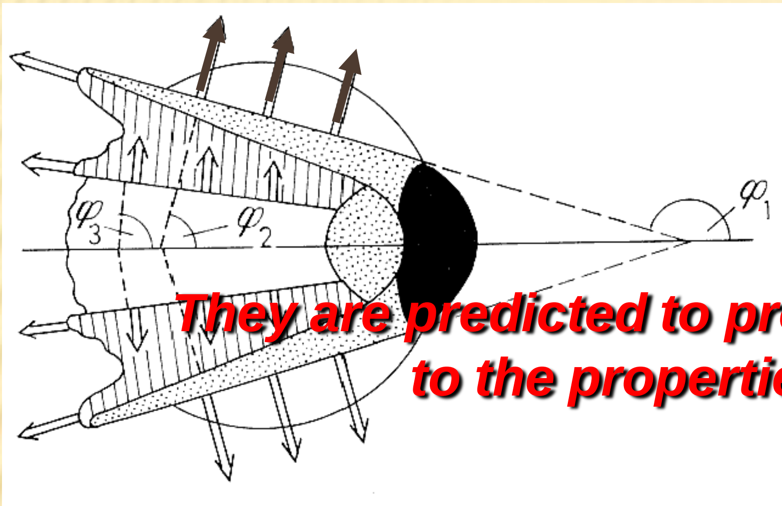

W. Scheid, H. Muller, and W. Greiner, PRL **32**, 741 (1974)

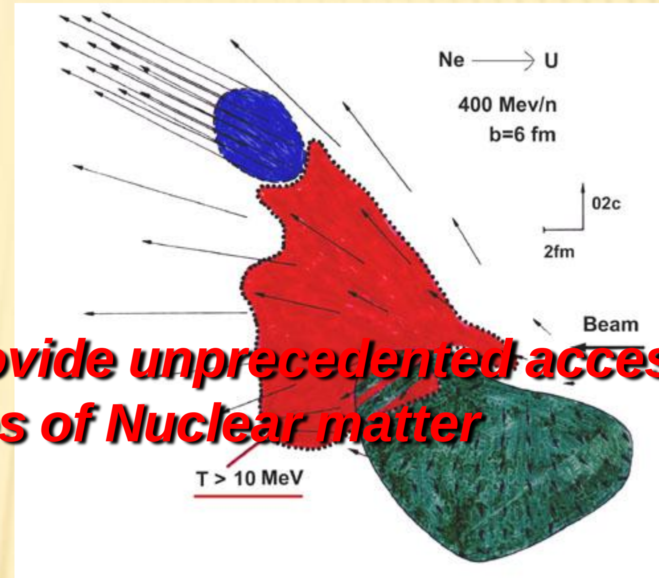

H. Stöcker, J.A. Maruhn, and W. Greiner, PRL **44**, 725 (1980)

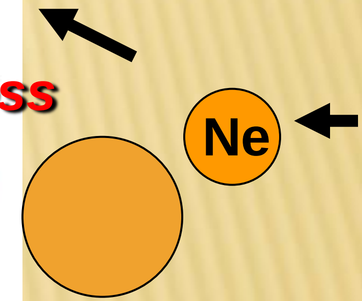

They are predicted to provide unprecedented access to the properties of Nuclear matter

M.I. Sobel, P.J. Siemens, J.P. Bondorf, an H.A. Bethe, Nucl. Phys. A251, 502 (1975)

G.F. Chapline, M.H. Johnson, E. Teller, and M.S. Weiss, PRD 8, 4302 (1973)

E. Glass Gold et al. Annals of Physics 6, 1 (1959)

The idea to use collective flow to Probe the properties of nuclear matter is long-standing

8. Anisotropic flow in pp

Azimuthal anisotropy in relativistic string fragmentation, I

Accepted picture for flow in heavy ion collisions – hydro expansion of QGP. Still, flow in *pp* and light AA is an open question:

- ? possible reasons for it
- ? magnitude
- ? possibility of observation

All the points are linked with each other

⇒ Importance of models as a test-ground for study of possible mechanisms.

Possibility of flow in DPM

- DPM: final particles come as fragments of *qg* strings, *N* of strings is defined via RFT.
- RFT study (K.Boreskov, A.Kaidalov, O.Kancheli) proposes asimuthal anisotropy.
- Model for $\mathbb{P}$ with transverse separation of its ends – *qg* string $\longrightarrow$ relativistic string with transverse separation of its ends.

8. Anisotropic flow in AA (and in pp)

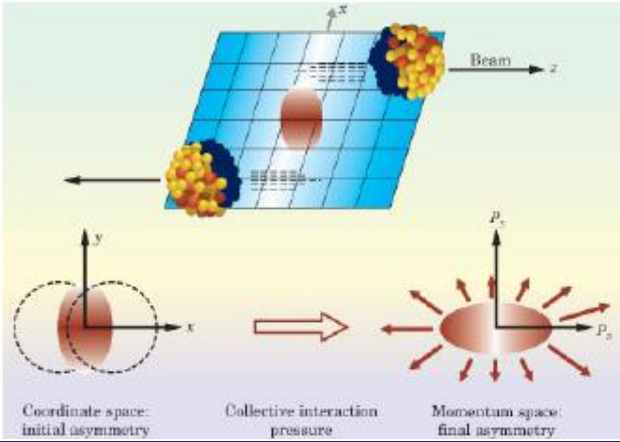

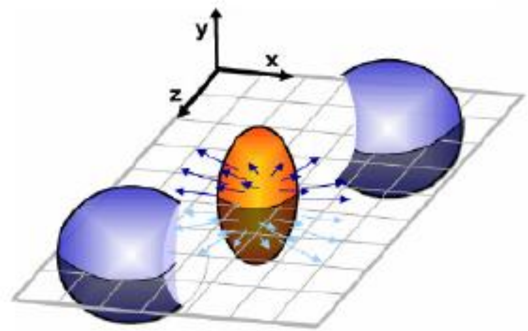

Ollitrault's suggestion (1992):

Finite impact parameter collisions => *anisotropic spatial density.*
Unequal pressure gradients (assuming thermalisation) produces an *anisotropic momentum distribution* of particles.

The strength of the anisotropy, and its systematic dependence on various parameters, provides *information on the equation of state*.

Fourie expansion of invariant cross section:

$$\frac{d^3N}{dp_t\,dy\,d\varphi} \propto 1 + 2v_1\cos(\varphi) + 2v_2\cos(2\varphi) + \ldots$$

Directed flow (v_1) — Elliptic flow (v_2)

$$v_2 = \left\langle \frac{p_x^2 - p_y^2}{p_x^2 + p_y^2} \right\rangle = \langle \cos(2\phi) \rangle$$

8. Anisotropic flow in AA

it depends on – energy, centrality,rapidity, pt, particle id:

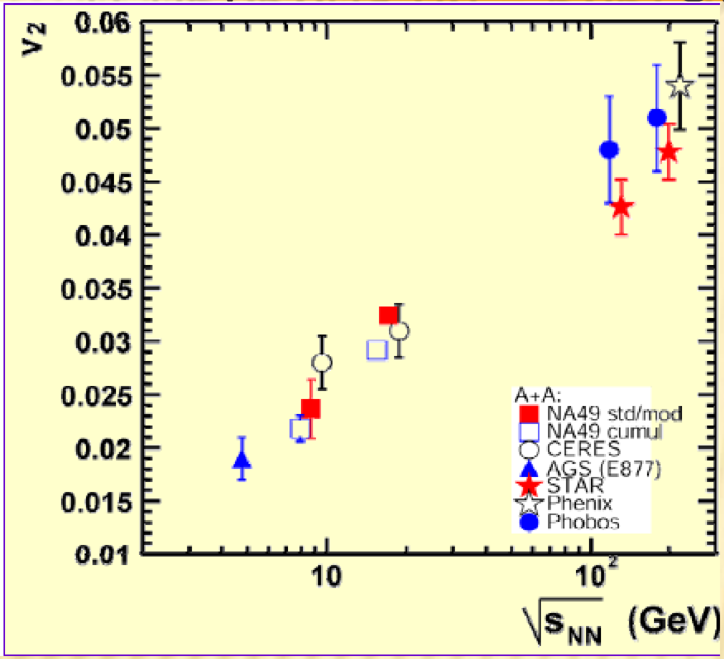

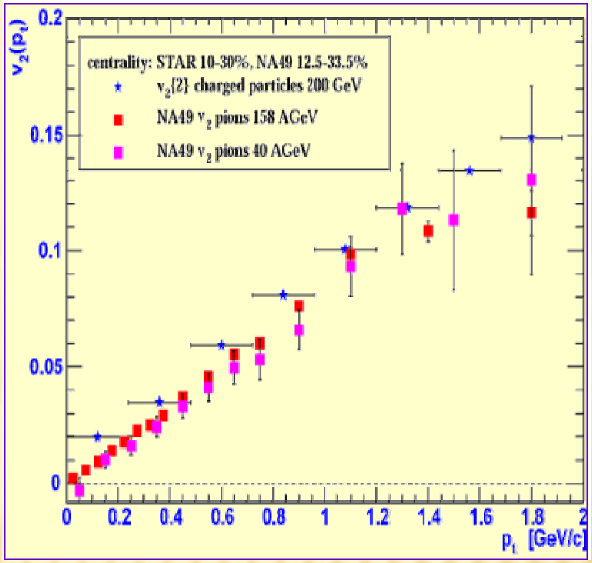

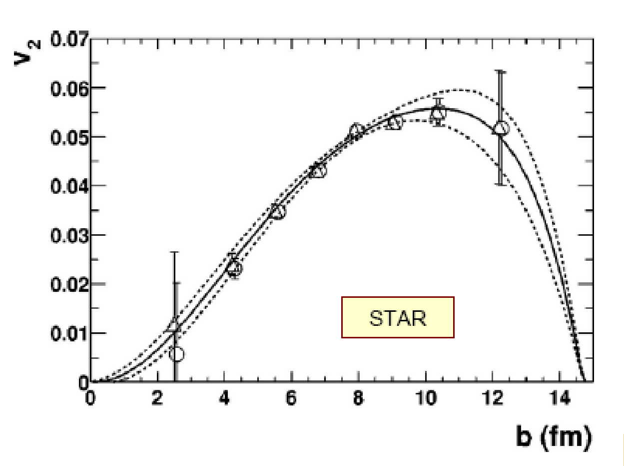

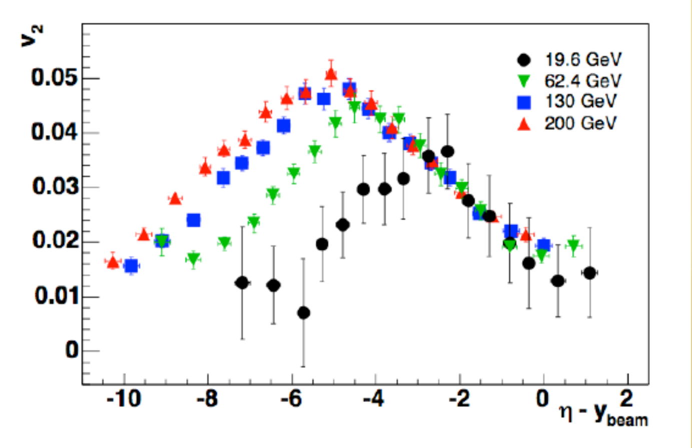

8. ANISOTROPIC FLOW IN PP

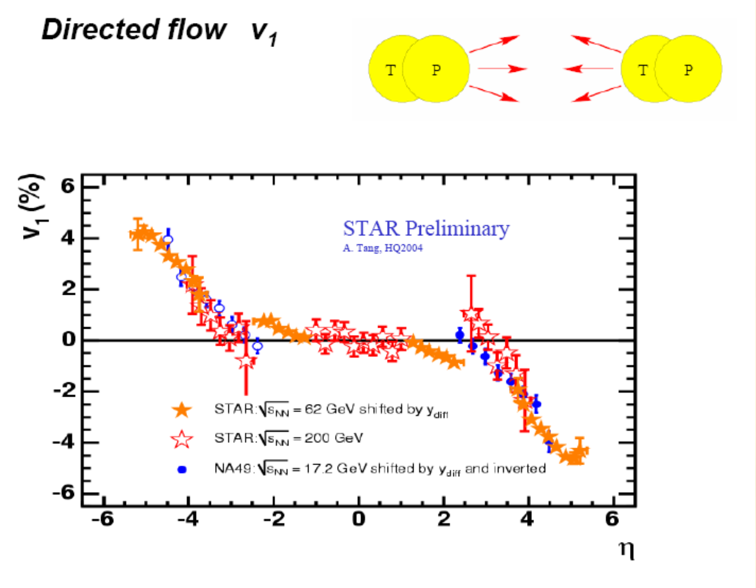

And connected with EOS and final state interactions.

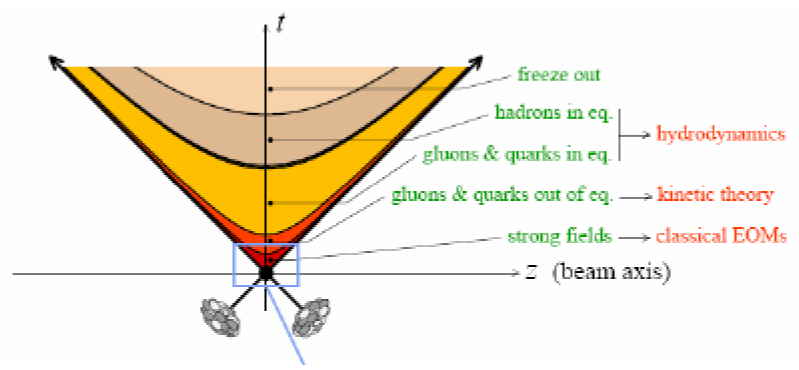

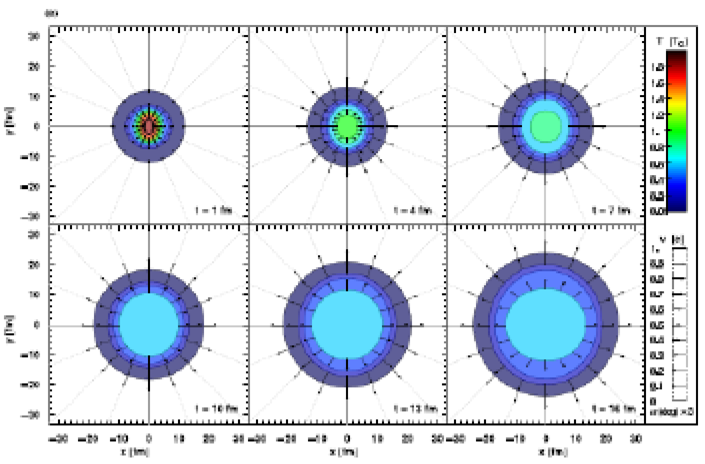

8. ANISOTROPIC FLOW IN PP

Anisotropic flows from initial state of a fast nucleus.
K.G. Boreskov, A.B. Kaidalov, O.V. Kancheli, Eur.Phys.J.C58:445-453,2008.

In Regge theory it appears as initial state effect and inversely proportional to the radius of the object: for pp it could be larger then for AA :

$$\Gamma(\vec{a},\vec{p}_t) \propto [1+\varepsilon p_{t,i} p_{t,j}\, \partial_i \partial_j]\delta^{(2)}(\vec{a})$$

Elliptic flow

$$v_2 = \varepsilon \frac{r_0^4\, T''_{overlap}(b^2)}{T_{overlap}}\left(r_0^2 p_t^2\right) = \frac{\varepsilon}{16}\frac{r_0^2}{R_A^2}\frac{b^2}{R_A^2}\left(r_0^2 p_t^2\right)$$

$$T_{overlap} = T_1 \otimes T_2$$

In Gauss approximation

Оценка:

$$A \sim 200;\; p_t \sim 1\, GeV/c;\; b \sim R_A;$$
$$r_0/R_A \sim 1/6;\quad r_0 p_t \sim 5$$

$$v_2 \sim 0.05\varepsilon$$

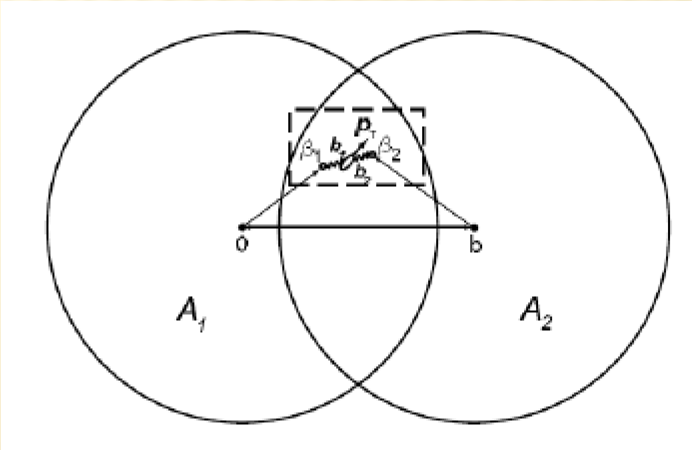

8. Anisotropic flow in pp

Azimuthal anisotropy in relativistic string fragmentation, II

Comparatively simple model, only one sort of particles("π-mesons").

But: explicitly observed string dynamics;
explicit energy-momentum conservation.

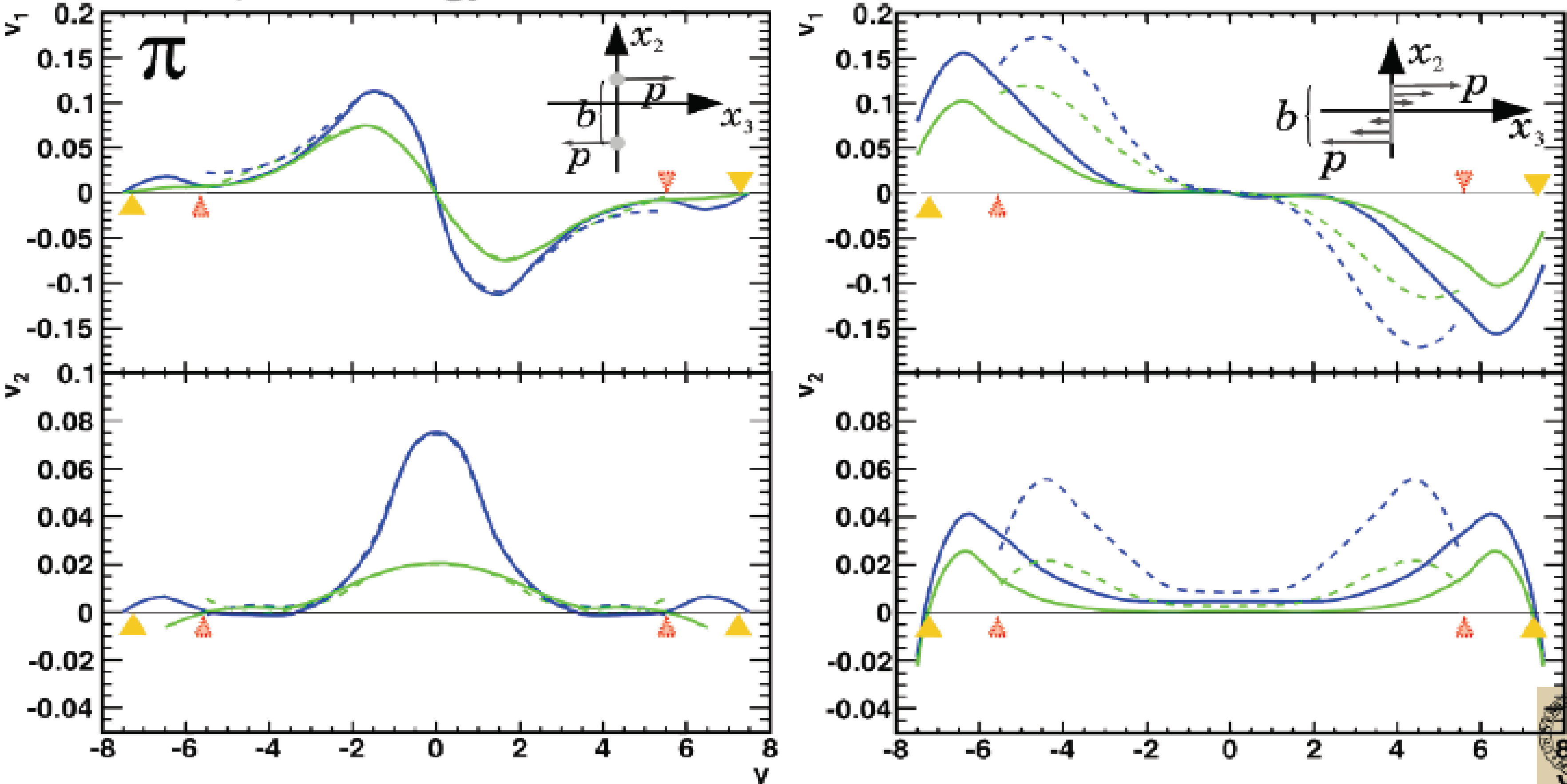

b = 0.5 fm, 1 fm; s^1/2 = 40 GeV , 200 GeV .

8. Anisotropic flow in pp

Estimates of hadron azimuthal anisotropy from multiparton interactions in proton-proton collisions at sqrt(s) = 14 TeV. D. d'Enterria , G.Kh. Eyyubova, et al Eur.Phys.J.C66:173,2010.

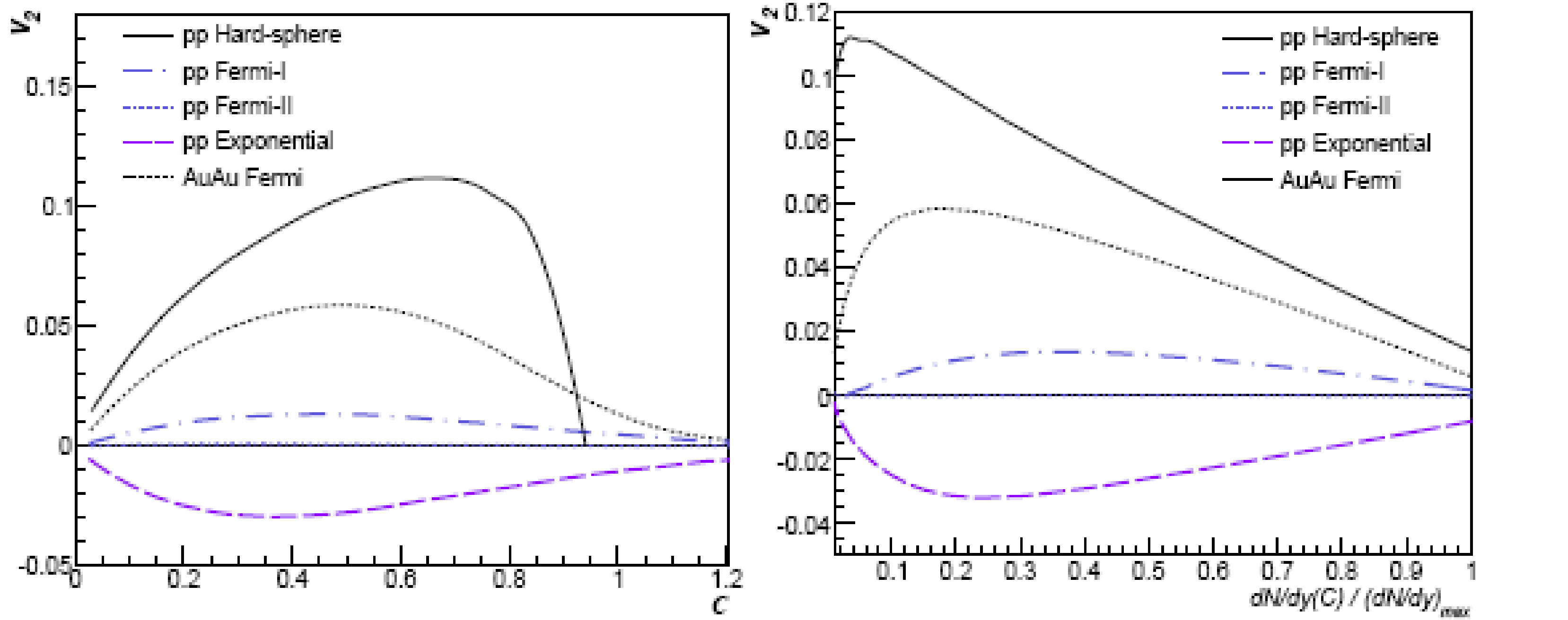

Fig. 8. Integrated elliptic flow v_2 parameter as function of centrality (left panel) and of normalised particle multiplicity (right panel) at midrapidity in p-p collisions at $\sqrt{s}$ = 14 TeV for the different proton density distributions considered in this work (Table 1). For comparison, the v_2 for Au-Au at RHIC energies is shown as a dotted line.

8. Anisotropic flow in pp

Azimuthal anisotropy in relativistic string fragmentation, III

RESULTS:

1. Both v_1 and v_2 present; positive v_2, v_1 comes with the same sign as v_1 in AuAu experiment.
2. Extreme sensitivity to the internal momentum distribution.

Paper R.Kolevatov "On azimuthal anisotropy in fragmentation of classical relativistic string " (arXiv:0912.5377v1 [hep-ph]); submitted to EPJC.

OUTLOOK:

1. Application to *pp* involve $2 \times n$ strings asymmetric in rapidity,
2. Need much deeper understanding of string formation within RFT (see p.2 of the results)

RFT – a theory of quasiparticle exchanges.

- Ladder (pole) exchange = building block of the apmlitude.
  - Ladder = Reggeon/Pomeron – quasiparticle in $(\vec{b}/\vec{q}_\perp) \times (y = \ln s/s_0)$ space
- A single Pomeron $(\alpha(0) = 1 + \Delta)$ exchange breaks unitarity
  - Unitarity is cured by multiP exchanges and R/P interactions

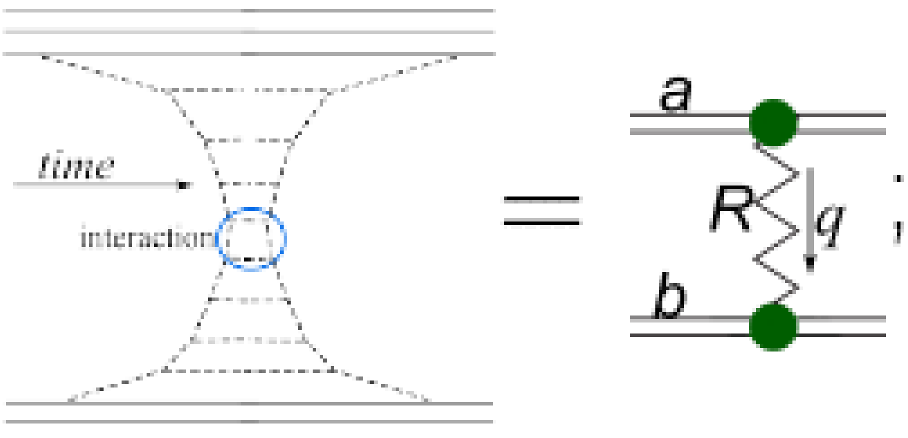

$$A = g_a^R(q^2) D_R(s, q^2) g_b^R(q^2);$$

$$D_R = \eta_R(q^2) \left(\frac{s}{s_0}\right)^{\alpha_R(q^2)}$$

The stochastic model.

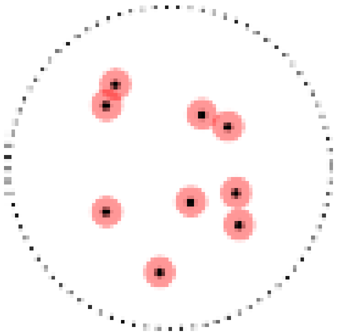

Consider a system of classic "partons" in the transverse plane with:

- Diffusion (chaotical movement) D;
- Splitting (λ – prob. per unit time)
- Death (m_1)
- Fusion ($\sigma_\nu \equiv \int d^2b\, \rho_\nu(b)$)
- Annihilation ($\sigma_{m_2} \equiv \int d^2b\, \rho_{m_2}(b)$)

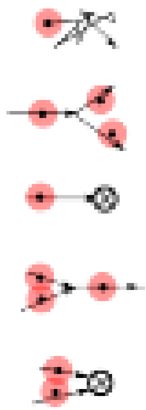

Parton number and positions are described in terms of

probability densities $\rho_N(y, \mathcal{B}_N)$ ($N = 0, 1, \ldots; \mathcal{B}_N \equiv \{b_1, \ldots, b_N\}$)

with normalization $\rho_N(y) \equiv \frac{1}{N!} \int \rho_N(y, \mathcal{B}_N) \prod d\mathcal{B}_N; \quad \sum_0^\infty \rho_N = 1.$

Correspondence RFT–Stochastic model

We use the simplest form of $g(b)$, $p_{m_2}(b)$ and $p_\nu(b)$:

$$p_{m_2}(\mathbf{b}) = m_2\,\theta(a - |\mathbf{b}|); \quad p_\nu(\mathbf{b}) = \nu\,\theta(a - |\mathbf{b}|);$$
$$g(\mathbf{b}) = \theta(a - |\mathbf{b}|);.$$

with a – some small scale; $\epsilon \equiv \pi a^2$.

RFT	stochastic model
Rapidity y	Evolution time y
Slope α'	Diffusion coefficient D
$\Delta = \alpha(0) - 1$	$\lambda - m_1$
Splitting vertex r_{3P}	$\lambda\sqrt{\epsilon}$
Fusion vertex r_{3P}	$(m_2 + \frac{1}{2}\nu)\sqrt{\epsilon}$
Quartic coupling χ	$\frac{1}{2}(m_2 + \nu)\epsilon$

Boost invariance ($\lambda = m_2 + \frac{\nu}{2}$) $\Leftrightarrow$ equality of fusion and splitting vertices

The effect of loops

Calculations with $\Delta = 0.12$:

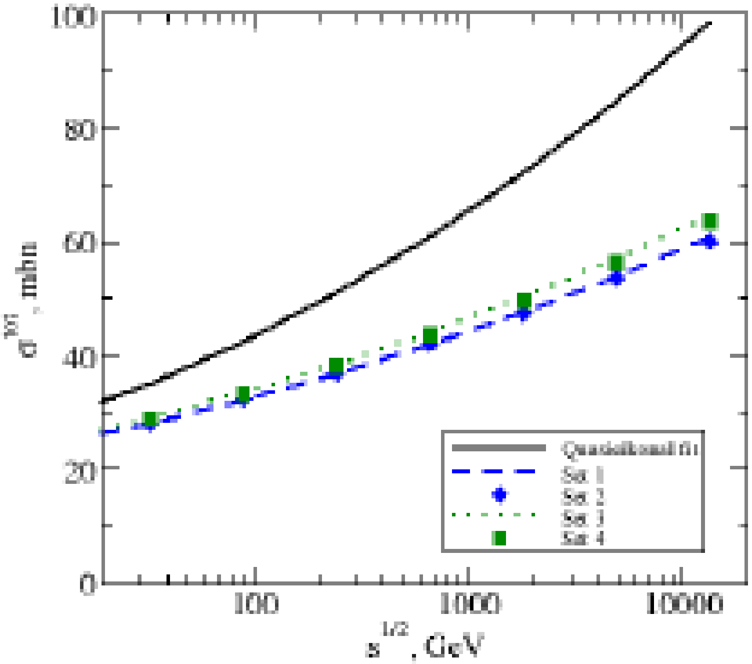

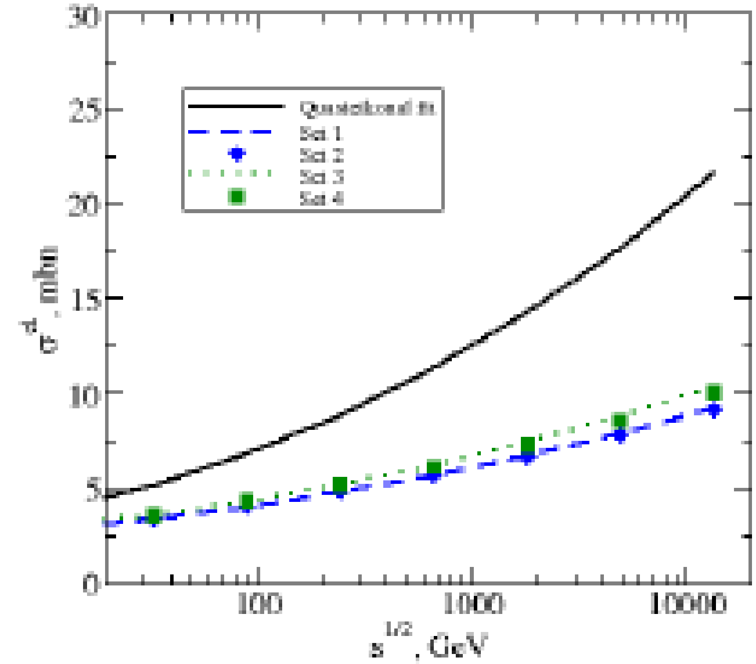

- The growth with $\sqrt{s}$ is suppressed compared to the eikonal.
- The role of $2 \to 2$ coupling is minor.

The effect of loops

Full calculation with $\Delta = 0.165$ and the same couplings vs the quasieikonal fit.

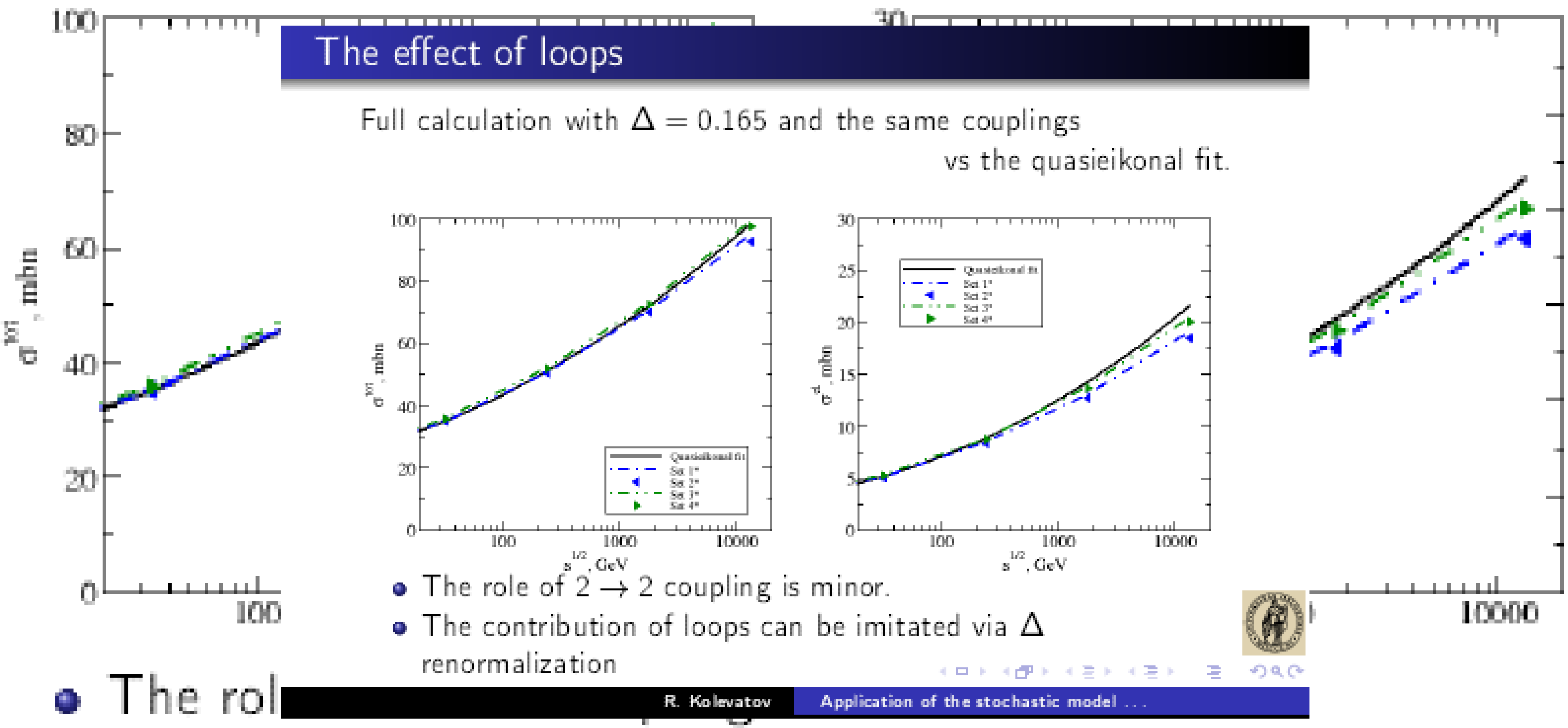

- The rol
- The contribution of loops can be imitated via Δ renormalization

MC realization: Correlations in double parton distributions at small x. Ch. Flensburg, G. Gustafson, L. Lonnblad, A. Ster JHEP 1106 (2011) 066 .1103.4320 [hep-ph]

VIOLATION OF FEYNMAN SCALING

UA5 Collab., Phys. Rep. 154 (1987) 247

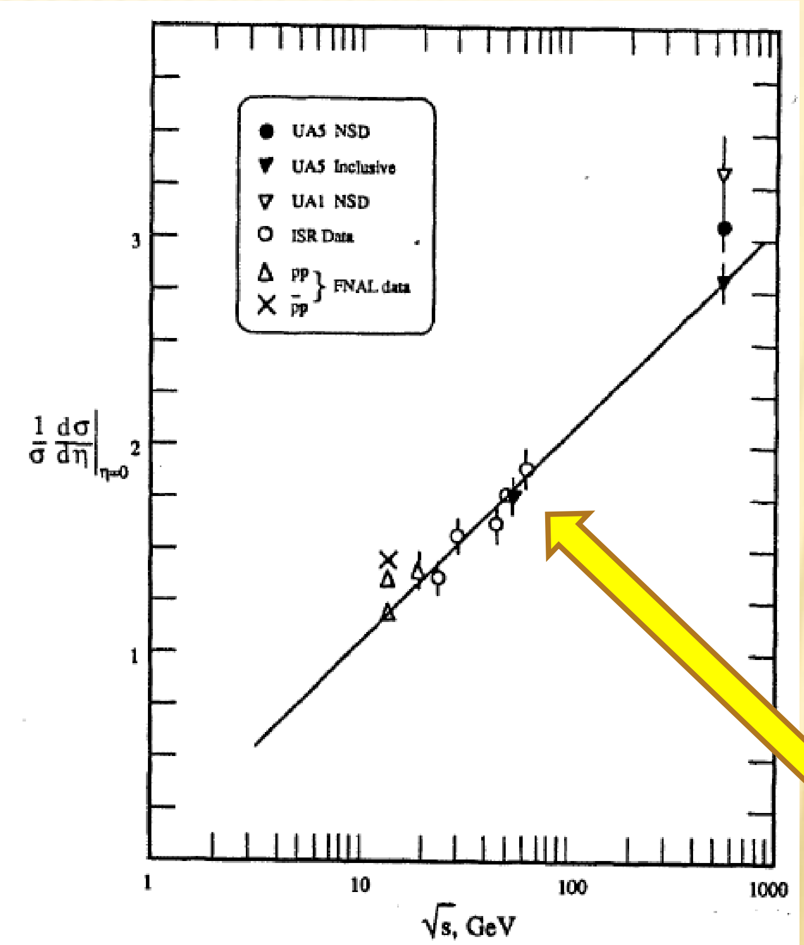

W. Busza, JPG 35 (2008) 044040

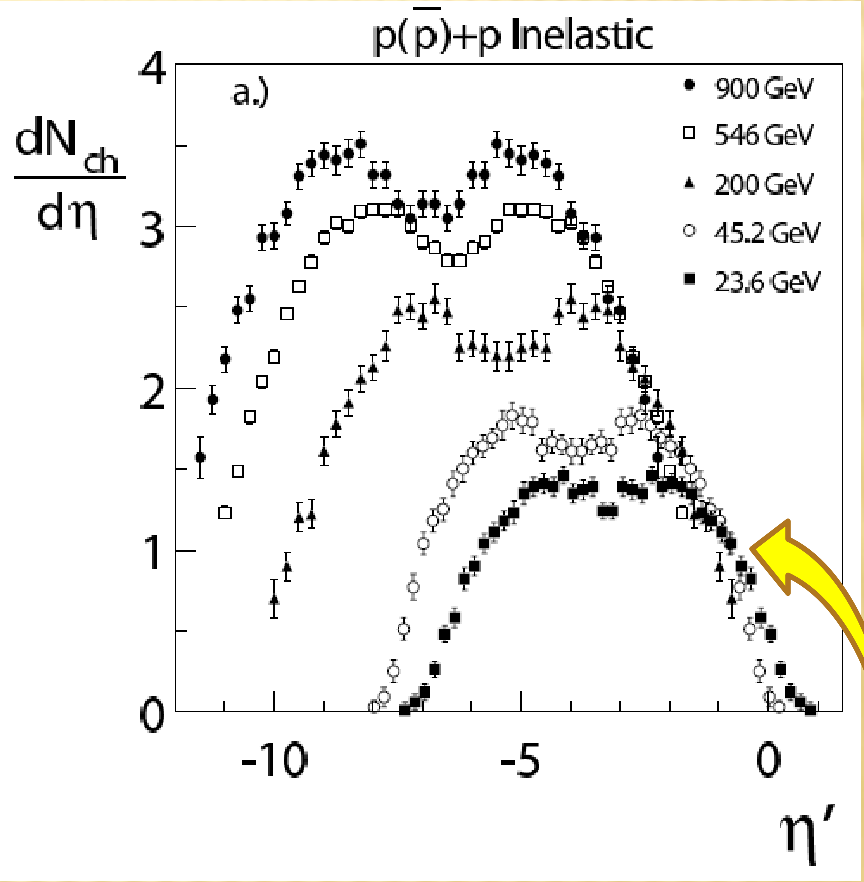

Charged particle pseudorapidity density at $\eta = 0$ as a function of $\sqrt{s}$

Violation of Feynman scaling, but ext. long. scaling holds?!

WHY SCALING HOLDS IN THE MODEL?

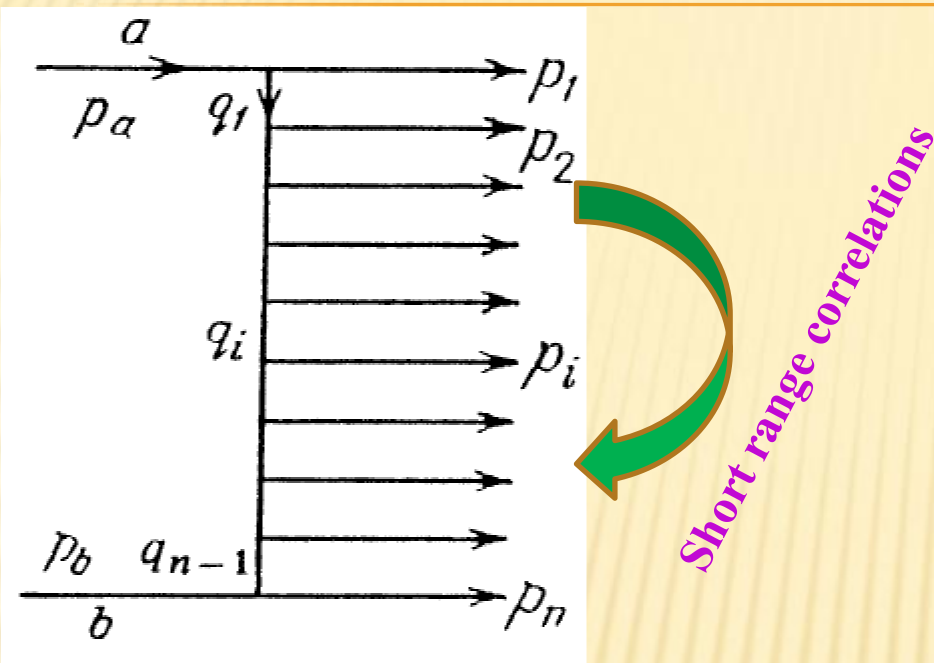

Correlation function

$$C(y_i, y_j) \propto \exp\{-\lambda(y_i - y_j)\}$$

Particles are uncorrelated if

$$y_i - y_j \equiv \Delta y \gg 1$$

Consider now inclusive process

$$1 + 2 \rightarrow i + X$$

Particle inclusive cross section

$$f_i = \frac{d^2\sigma(y_1 - y_i, y_i - y_2, p_{iT}^2)}{dy_i d^2 p_{iT}}$$

In the fragmentation region of particle 1

$$y_1 - y_i \approx 1,\; y_i - y_2 \approx y_1 - y_2 \gg 1$$

Inclusive density

$$x_F^{(i)} \equiv \frac{p_{i\|}}{p_{\|}^{\max}} \approx \exp\{-(y_1 - y_i)\}$$

therefore

$$n_i = \psi(x_F^{(i)}, p_{iT}^2) \quad \longleftrightarrow \quad \mathrm{n}_i = f_i / \sigma_{inel} = \phi(y_1 - y_i, p_{iT}^2)$$

In string models both FS and ELS holds in the fragmentation regions

VIOLATION OF KNO SCALING

A.B.Kaidalov, K.A.Ter-Martirosyan, PLB 117 (1982) 247
UA5 Collaboration, Phys. Rep. 154 (1987) 247
N.S.Amelin, L.V.Bravina, Sov.J.Nucl.Phys. 51 (1990) 133

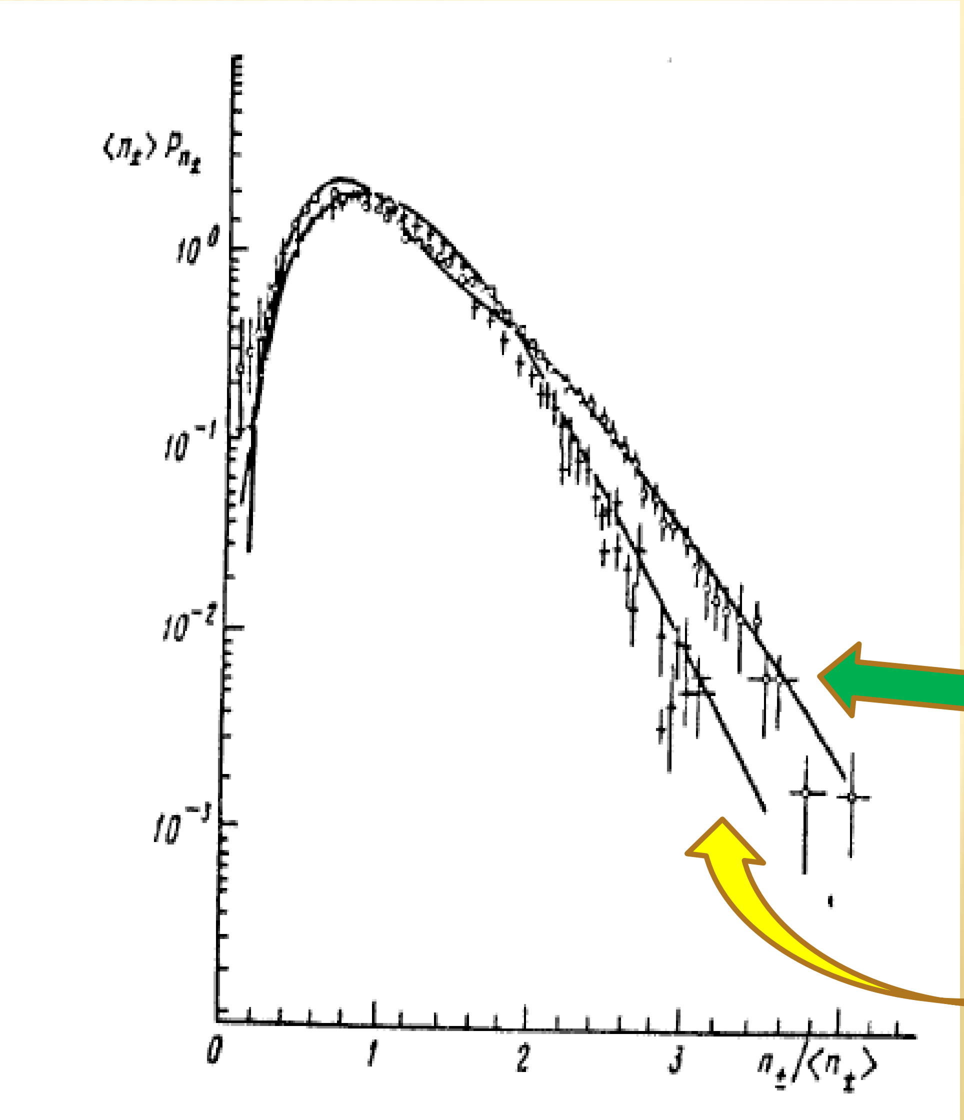

Charged-particle multiplicity distributions in the KNO variables in nondiffractive antiproton-proton collisions at $\sqrt{s}$ = 546 GeV and 53 GeV